Large-Scale Structure and Dynamics of the Magnetotails of Mercury, Earth, Jupiter and Saturn

**C.M. Jackman · C.S. Arridge · N. André · F. Bagenal · J. Birn · M.P. Freeman · X. Jia ·
A. Kidder · S.E. Milan · A. Radioti · J.A. Slavin · M.F. Vogt · M. Volwerk · A.P. Walsh**

Abstract Spacecraft observations have established that all known planets with an internal magnetic field, as part of their interaction with the solar wind, possess well-developed mag-

C.M. Jackman (✉)
Department of Physics and Astronomy, University College London, Gower Place, London, WC1E 6BT,
UK
e-mail: c.jackman@soton.ac.uk

C.M. Jackman · C.S. Arridge
Centre for Planetary Sciences at UCL/Birkbeck, London, WC1E 6BT, UK

C.M. Jackman
Department of Physics and Astronomy, University of Southampton, Southampton, SO17 1BJ, UK

C.S. Arridge
Mullard Space Science Laboratory, University College London, Holmbury St. Mary, RH5 6NT, UK

N. André
Institut de Recherche en Astrophysique et Planétologie, Université Paul Sabatier, Toulouse, France

N. André
CNRS, Institut de Recherche en Astrophysique et Planétologie, Toulouse, France

F. Bagenal
Laboratory for Atmospheric and Space Physics, University of Colorado at Boulder, Boulder, CO, USA

J. Birn
Space Science Institute, Boulder, CO, USA

J. Birn
Los Alamos National Laboratory, Los Alamos, NM, USA

M.P. Freeman
British Antarctic Survey, Madingley Road, High Cross, Cambridge, CB3 0ET, UK

X. Jia · J.A. Slavin
Dept. of Atmospheric, Oceanic and Space Sciences, University of Michigan, Ann Arbor, USA

netic tails, stretching vast distances on the nightside of the planets. In this review paper we focus on the magnetotails of Mercury, Earth, Jupiter and Saturn, four planets which possess well-developed tails and which have been visited by several spacecraft over the years. The fundamental physical processes of reconnection, convection, and charged particle acceleration are common to the magnetic tails of Mercury, Earth, Jupiter and Saturn. The great differences in solar wind conditions, planetary rotation rates, internal plasma sources, ionospheric properties, and physical dimensions from Mercury's small magnetosphere to the giant magnetospheres of Jupiter and Saturn provide an outstanding opportunity to extend our understanding of the influence of such factors on basic processes. In this review article, we study the four planetary environments of Mercury, Earth, Jupiter and Saturn, comparing their common features and contrasting their unique dynamics.

Keywords Magnetotail · Mercury · Earth · Jupiter · Saturn · Magnetosphere

1 Introduction

A planetary magnetosphere is the region which contains the planet's magnetic field and where this magnetic field has the dominant effect on the motion of charged particles (e.g. Gold 1959). Six of the planets in our solar system are known to possess significant internal magnetic fields. The magnetospheres of the smaller and slower rotating terrestrial planets (i.e. Mercury and Earth) exhibit very different features from those of the fast-rotating, natural satellite-rich, gas giant planets (i.e. Jupiter and Saturn) and the highly asymmetric, tilted ones of Uranus and Neptune. We refer the reader to Bagenal (1992, 2009), Russell (2001) and Kivelson (2007) for examples of comprehensive reviews of planetary magnetospheres. The reader is referred to Arridge (2014) for a recent review of the magnetotails of Uranus and Neptune. Here we focus on Mercury, Earth, Jupiter and Saturn due to the new results available from not only the Cassini and MESSENGER missions, but also continuing analysis of measurements from the Galileo mission to Jupiter and terrestrial missions such as Geotail, Cluster and THEMIS. Figure 1 shows the approximate relative sizes of their planetary magnetospheres (Fig. 1a is absolute size, Fig. 1b is scaled to the dipole magnetopause). Throughout this paper, we have generally ordered our discussion with Earth first, followed

A. Kidder
Department of Earth and Space Sciences, University of Washington, Seattle, WA, USA

S.E. Milan · M.F. Vogt
Department of Physics and Astronomy, University of Leicester, Leicester, LE1 7RH, UK

A. Radioti
Laboratoire de Physique Atmospherique et Planetaire, Institut d'Astrophysique et de Geophysique, Universite de Liege, Liege, Belgium

M.F. Vogt
Center for Space Physics, Boston University, Boston, USA

M. Volwerk
Space Research Institute, Austrian Academy of Sciences, Graz, Austria

A.P. Walsh
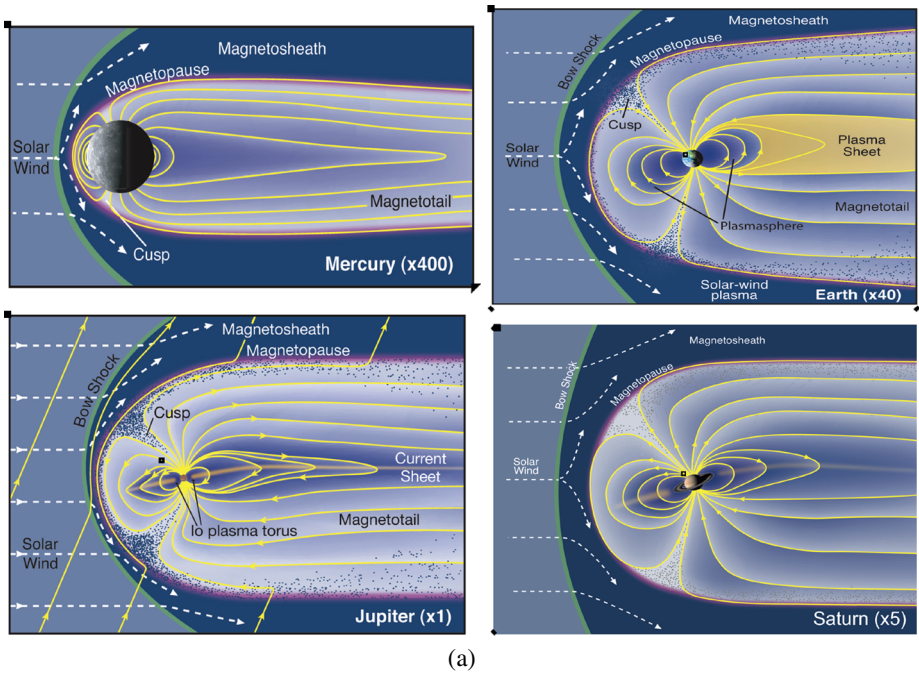ESTEC, ESA, Keplerlaan 1, 2201 AZ Noordwiik ZH, The Netherlands

Fig. 1 Schematic comparison of the magnetospheres of Mercury, Earth, Saturn and Jupiter. The Sun is to the left with the solar wind blowing from left to right across the diagrams. (**a**) Absolute scales, (**b**) scaled to the subsolar magnetopause distance for a simple dipole. Jupiter's and Saturn's nominal magnetopause positions are somewhat larger than this dipole approximation due to substantial internal plasma pressures. Credit: Fran Bagenal and Steve Bartlett

by Jupiter, Saturn and finally Mercury. The reasons for this ordering are partly historical and partly based on the relative amounts of available data for each planet.

In this paper, we focus on the specific region of a planetary magnetosphere known as the magnetotail. The magnetotail is the name given to the region of extended magnetic fields that stretches in an anti-sunward direction on the nightside of a planet. It is shaped by the solar wind and interplanetary magnetic field (IMF) flowing past the magnetosphere. Magnetotails are important because they are the sites of plasma and energy build up and explosive release. At the centre of a planetary magnetotail lies a current sheet and plasma sheet of high-beta plasma (where beta is the ratio of thermal to magnetic pressure), separating the northern and southern tail lobes. The lobes house the 'open' magnetic flux stored in the tail, where one end of a field line magnetically connects to the northern (or southern) polar cap, with the other end of the field line extending far downstream and generally believed to connect to the solar wind. Closed magnetic field lines, with both ends connected to the planet at lower latitudes, contain plasma of planetary and/or solar wind origin.

The Earth's magnetotail is by far the most extensively sampled of all planetary magnetotails. Its existence was first established in the 1960s (Parker 1958a; Piddington 1960; Dessler 1964; Axford et al. 1965; Ness 1965; Behannon 1968), and since then it has been explored by a host of spacecraft, including the IMP and ISEE satellites, Geotail, Cluster and THEMIS missions, to name but a few. One of the defining topics of terrestrial magnetotail research has been the study of the phenomenon called the substorm (Akasofu 1964, 1968) which involves reconfiguration of the magnetotail structure and the release of mass and en-

Fig. 1 (*Continued*)
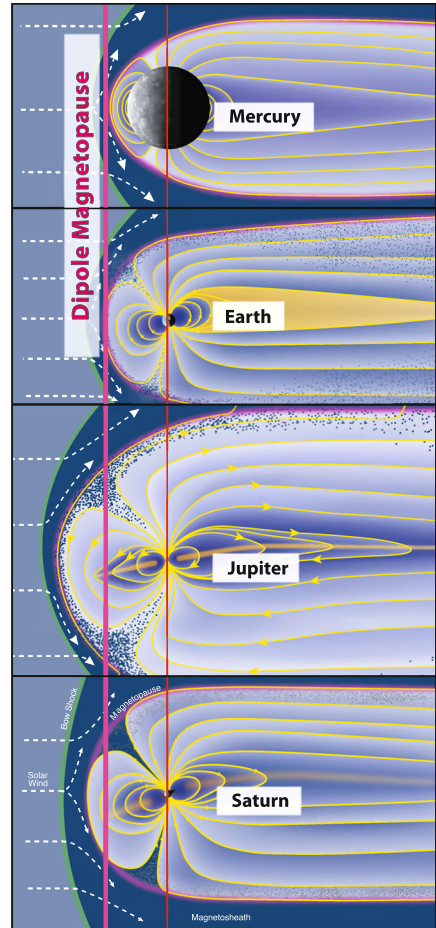
(b)

ergy through magnetic reconnection (discussed in more detail in Sect. 4 below). See Sharma et al. (2008) for a comprehensive review of dynamics in Earth's magnetotail.

In contrast to the dynamics of the Earth's magnetosphere which is largely driven by the solar wind, Jupiter's magnetospheric dynamics are dominated by the rapid planetary rotation and the strong internal mass loading from the volcanic moon Io. Jupiter has been visited by a total of eight spacecraft in the last 40 years, but only a few have sampled the magnetotail in any detail. The Voyager 2 spacecraft flew by in 1979, and sampled the magnetotail to several hundred R_J behind the planet, then encountered the magnetotail again at a distance of ∼9,000 R_J or ∼5 AU (1 Astronomical Unit, AU = 1.496×10^8 km) (Kurth et al. 1982; Lepping et al. 1983), while the Galileo spacecraft orbited between 1995–2003 and is the source of a great deal of our current knowledge about the Jovian system (see Bagenal et al. 2004). Most recently (2006–2007), the New Horizons spacecraft traversed the Jovian tail to distances greater than 2500 R_J, and the dataset can tell us about the structure of the very distant regions, as well as the evolution of plasmoids (McComas et al. 2007; McNutt et al. 2007). Our next chance to explore Jupiter will be with the arrival of the Juno mission in 2016 (Bolton 2010) followed by the JUICE mission in 2030 (Grasset et al. 2013).

Saturn has often been described as intermediate between Earth and Jupiter in terms of its magnetospheric dynamics, and we will address some of these features throughout this review. The Pioneer 11 (1979), Voyager 1 (1980) and Voyager 2 (1981) spacecraft glimpsed the Kronian magnetotail on their flybys, but the Cassini mission's exploration of Saturn (2004–2017, as currently planned) has shed huge light on the dynamics of this complex environment (see "Saturn from Cassini-Huygens" eds. Dougherty, Esposito, Krimigis, 2009).

Finally Mercury, a small, rocky planet with an average orbit ∼0.38 AU from the Sun, presents a very different environment for study (Ness et al. 1974; Ogilvie et al. 1974; Slavin et al. 2007; Anderson et al. 2008; Raines et al. 2008; Zurbuchen et al. 2008). The solar wind influence at Mercury dominates the magnetospheric dynamics, and in this review we compare and contrast the timescales and nature of plasma processes here with those of the other planets. The first spacecraft to visit Mercury was Mariner 10 which executed three flybys in 1974–1975 (see reviews by Ness 1979; Russell et al. 1988; Slavin 2004). More recently, the MESSENGER mission (Solomon et al. 2001) executed three flybys before successful orbit insertion on March 18th 2011. These flybys provided observations of the magnetotail to downstream distances of ∼3.25 R_M (Slavin et al. 2012a). At the time of writing this mission is scheduled to continue until 2016. The BepiColombo mission (Benkhoff et al. 2010; Milillo et al. 2010), which is scheduled to be launched in 2016 and arrive at Mercury in 2024, will consist of two spacecraft, one of which (Mercury Planetary Orbiter, MPO) will sample Mercury's tail at distances comparable to MESSENGER, while a second higher apoapsis orbiter (Mercury Magnetospheric Orbiter, MMO) will investigate Mercury's tail at approximately twice the downstream distance reached by MESSENGER.

1.1 Magnetotail Formation

Magnetotails are regions shaped by the solar wind, where magnetic field lines can stretch out in the direction of the solar wind flow to very long distances downstream of the planet. Magnetotails result more specifically from the tangential stress exerted by the solar wind in its interaction with the magnetosphere. Two main mechanisms have been proposed for the formation of planetary tails at slow rotating terrestrial-type magnetospheres, derived from the reconnection-driven (Dungey 1961, 1963), and the viscous interaction driven (Axford and Hines 1961; Axford 1964) solar wind interaction models, respectively.

The Dungey-type solar wind interaction can drive magnetic flux and plasma circulation within the magnetosphere. It involves magnetic reconnection, a key process in which field lines break and merge to form new field lines. Magnetic reconnection at the dayside magnetopause opens magnetic flux, and the solar wind interaction carries these open magnetic field lines from dayside to nightside, where they are stretched out to form the tail lobes (here we define the lobe as the open field line region, while noting that centrifugal confinement of plasma to the equator in rapidly rotating systems can alter this picture somewhat (e.g. Hill and Michel 1976; Ray et al. 2009)). As they are stretched out down-tail, open field lines sink in towards the centre plane of the tail, where they reconnect again, closing the flux that was opened on the dayside. The "Dungey cycle timescale" refers to the length of time from the opening of the field lines at the dayside to the closing of the field lines on the nightside. Figure 2 shows the stages involved in the Dungey cycle for the case of Earth (but may also be applicable to other magnetospheres). The Dungey cycle time at Earth is ∼1 hour (Cowley 1982), but at Mercury it is only ∼1–2 minutes (Siscoe et al. 1975; Slavin et al. 2012a). When active at Jupiter, the Dungey cycle timescale is estimated to be of order several weeks (Kennel 1973; Badman and Cowley 2007), whereas the timescale is ∼ 1 week or more at Saturn (Jackman et al. 2004).
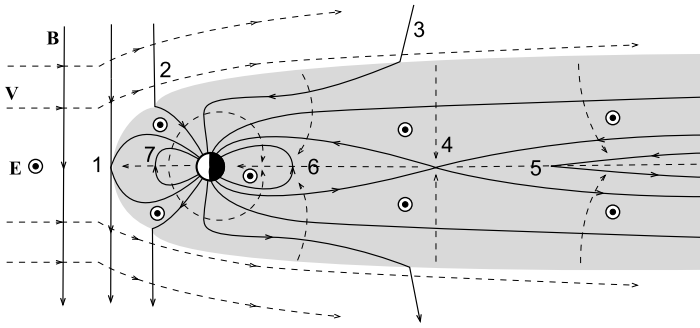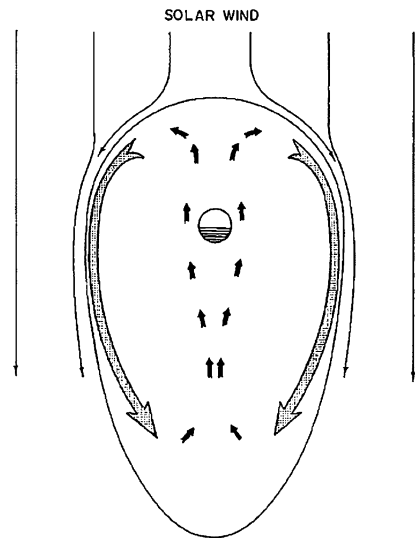
Fig. 2 Schematic diagram showing the stages of the Dungey cycle for the case of Earth's magnetosphere (courtesy Steve Milan)

Fig. 3 Schematic of the viscous cycle (from Axford and Hines 1961). This is a view down on to the equatorial plane with the solar wind blowing from top to bottom of the diagram

The viscous cycle also involves momentum transfer from the solar wind to the magnetotail via quasi-viscous interaction, particularly at the low-latitude magnetopause. It is illustrated schematically in Fig. 3. This cycle can drive circulation within a closed magnetosphere, provided an appropriate tangential-drag mechanism exists. A widely-discussed mechanism to enable this interaction is the Kelvin-Helmholtz instability, driven by flow shear at the magnetopause, which may also be coupled with magnetic reconnection (e.g. Hasegawa et al. 2004; Nykyri et al. 2006). Figure 4 illustrates the combination of the Dungey and viscous-cycle flows in the Earth's ionosphere.

For the rapidly rotating magnetospheres of the outer planets with their large amounts of moon-derived plasma, the "planetary wind" or "Vasyliunas cycle" is of critical importance (Hill et al. 1974; Michel and Sturrock 1974; Vasyliunas 1983). This Vasyliunas cycle is driven not by the solar wind, but by the energy transferred to internally generated plasma by the fast rotation of these planets. The plasma created deep inside the magnetosphere is accelerated by magnetic stresses from the ionosphere, gains energy, and moves outward from the planet. Centrifugal forces cause the field lines to stretch. These stretched field lines can form a thin current sheet, across which the closed field lines reconnect. This reconnection

Fig. 4 Northern high-latitude ionospheric flow associated with a combination of Dungey and viscous cycle (after Cowley 1982). The *hatched region* indicates convection driven by the boundary layers in which magnetic flux tubes remain closed during the cycle, while the remainder of the flow is associated with the reconnection process
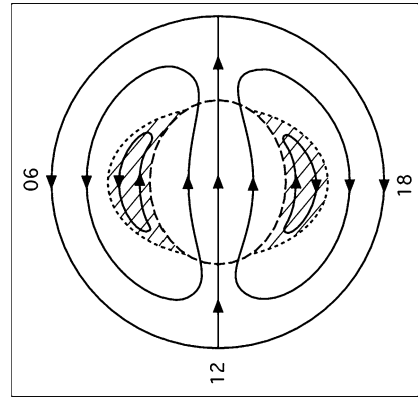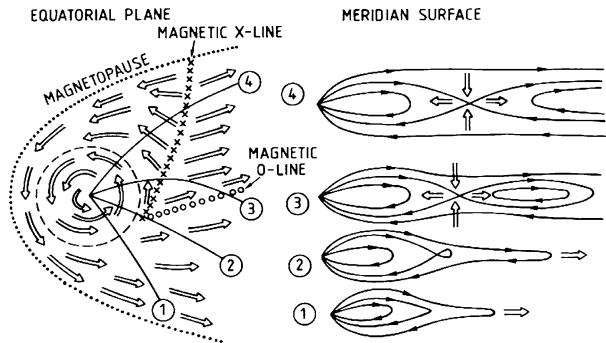
Fig. 5 Flow pattern (*left*) and field configuration (*right*) expected for a steady-state planetary wind, first proposed for Jupiter by Vasyliunas (1983)

simultaneously shortens the field line and (like the Dungey cycle), releases plasma down the tail in the form of a "plasmoid". The stages of this cycle, as viewed in an inertial frame of reference, are illustrated in Fig. 5, the picture originally put forward by Vasyliunas (1983).

1.2 Upstream Solar Wind Conditions

While the topic of this review concerns the dynamics of planetary magnetotails, it is important to consider the properties of the solar wind and interplanetary magnetic field upstream of the various planets, and how these shape and control the magnetospheres they impact. We note at the outset that the Earth's magnetosphere is the only one for which the upstream solar wind conditions are routinely sampled by a dedicated upstream monitor. One of the key features of the IMF as it evolves with increasing heliocentric distance is its spiral shape. The field lines become increasingly tightly wound due to the field lines being frozen both to the rotating solar surface and to the outflowing solar wind. Such a winding was first postulated by Parker (1958b) and, as can be seen from Table 1, the average angle that the interplanetary field lines make with respect to the radial direction increases from ∼20° at Mercury's orbital distance of ∼0.4 AU (Kabin et al. 2000) to ∼83° at Saturn's orbital distance of ∼9 AU (Jackman et al. 2008a).

In addition to predicting the spiral shape, the Parker model also predicted that the strength of the radial component of the IMF would decrease approximately as r^{-2}. There are of course smaller-scale variations on timescales of less than a solar rotation, where the IMF is structured by corotating interaction regions and coronal mass ejections, but overall the

Table 1 List of planetary and magnetospheric parameters, organised by increasing distance from the Sun

	Mercury	Earth	Jupiter	Saturn
Average distance from the Sun (AU)	0.38	1	5.2	9.54
Equatorial planetary radius, R_P (km)	2440	6371	71492	60268
Surface field strength (nT)	195	31000	420000	21084
Dipole moment (A m^2)	4.9×10^{19}	8.3×10^{22}	1.5×10^{27}	4.6×10^{25}
Planetary field direction at the equator	North	North	South	South
Dipole tilt (°)	<0.8 (offset 0.2)[a]	10.5	9.6	<1
Sidereal rotation rate (hh:mm)	1407:30	23:56	09:55	~10:48
Average solar wind P_{dyn} (nPa)	20	2	0.08	0.03
Average IMF strength (nT)	30	8	1	0.6
Average IMF spiral angle (°)	20	45	80	83
Asymptotic tail radius (R_P)	2–3[b]	30	150	60
Tail lobe flux content (GWb)	0.003	0.2–1	100 s	~15–50
Average subsolar magnetopause distance (R_P)	1.4	10	~60–90	~22–27
SW transit time to tail (min)	2.8	5.3	360	120

[a]Anderson et al. (2012)

[b]Winslow et al. (2013)

expected trend has been reported from analysis of data collected between 0.46–5 AU (e.g. Smith 1974; Behannon 1978; Slavin et al. 1984a) and beyond the orbit of Saturn by the Pioneer 11 and Voyager spacecraft (Kurth et al. 1982; Lepping et al. 1983; Goldstein et al. 1985). Thus, for example, the IMF at Mercury is much stronger than at Saturn (Burlaga 2001), and this has implications for solar wind-magnetosphere coupling. Indeed, DiBraccio et al. (2013) confirm the strong reconnection initially reported by Slavin et al. (2009), but also go on to show that the reconnection rate is not dependent on IMF direction but rather is affected mostly by magnetosheath plasma beta.

Changes in solar wind velocity (and hence dynamic pressure) also directly impact magnetospheres by altering the location of their bow shocks and magnetopauses. Despite the fact that the solar wind velocity is largely independent of heliocentric distance, transient features in the solar wind such as CMEs can cause short-term changes in the velocity, with dramatic consequences for solar wind-magnetosphere coupling. A final factor to consider is the orientation of the component of the IMF parallel to the planet's magnetic dipole moment, which determines the efficiency of magnetic reconnection at the dayside magnetopause, with highest efficiency for anti-parallel IMF and planetary field (see Appendix for co-ordinate system definitions).

The varying upstream conditions, planetary field strengths and planetary rotation rates lead to very different magnetospheric characteristics at Mercury, Earth, Jupiter and Saturn. In this paper we focus on the similarities and differences between the four planets. Section 2 focuses on magnetospheric size and large-scale magnetospheric structure. Section 3 discusses basic mass, flux, and energy transport, storage and release, Sect. 4 describes in situ observations of magnetospheric dynamics, while Sect. 5 explores remote observations. We conclude in Sect. 6 with a brief summary.

2 Magnetospheric Size and Structure

Under quiescent conditions, magnetosphere and magnetotail sizes and structures are controlled primarily by the force balance between the interior pressure forces, dominated by magnetic pressure in the lobes and plasma pressure in the low-latitude regions, and the solar wind pressure forces in the magnetosheath, dominated by the dynamic pressure. In Sect. 2.1 we explore characteristic dimensions of magnetospheres. Planetary magnetotails are not homogeneous. All magnetotails that have been measured in situ have been shown to vary both spatially and temporally and display structure within them. Characteristic variations with latitude are discussed in Sect. 2.2, and longitudinal structure explored in Sect. 2.3.

2.1 Basic Magnetospheric Dimensions

2.1.1 Subsolar Magnetopause Distance

One characteristic scale of a planetary magnetosphere is the distance from the planet to the subsolar point of the magnetopause, a scale determined by pressure balance between the interior of the magnetosphere and the magnetosheath. For a magnetosphere whose outer region is characterized by low beta, the pressure interior to the magnetosphere, P_{msph}, is given by:

$$P_{msph} = B^2/2\mu_0 = \left(f B_0^2/2\mu_0\right)r^{-6}, \tag{1}$$

where $B = B_0/r^3$ is the magnetic field strength in the magnetosphere with B_0 equal to the equatorial surface field strength at the planet, μ_0 is the permeability of free space, and r is the planetocentric distance measured in units of planetary radii. Because the field due to the Chapman-Ferraro currents provides additional field pressure the dipole magnetic field pressure $(B_0^2/2\mu_0)r^{-6}$ is amplified by a factor f. Thus, the subsolar magnetopause distance can be obtained from the following pressure balance condition:

$$k P_{dyn} = \left(f B_0^2/2\mu_0\right)r^{-6} \tag{2}$$

leading to

$$r = \left(f B_0^2/2k\mu_0\right)^{1/6} P_{dyn}^{-1/6}, \tag{3}$$

where P_{dyn} is the dynamic pressure of the upstream solar wind, and k is a factor to account for the conversion of dynamic to thermal stagnation pressure along the stagnation streamline, and equals 0.881 as the upstream sonic Mach number tends to infinity. Hence the subsolar magnetopause distance decreases with the 1/6 power of the solar wind dynamic pressure and increases with planetary surface field strength. When this "vacuum dipole" approximation is applied to Mercury, Earth, Jupiter and Saturn we obtain the dipole subsolar magnetopause distances of 1.4 R_M, 11 R_E, 45 R_J, and 21 R_S. This 1/6 power law has been confirmed from observations and modelling of the terrestrial (e.g., Shue et al. 1997) and hermean (e.g. Winslow et al. 2013) magnetopause. However, Mercury's internal dynamo could have a strong interaction with the solar wind magnetic field (Glassmeier et al. 2007), stiffening (i.e. decreasing the exponent) the magnetosphere under certain conditions.

The vacuum dipole approximation breaks down for the Jovian and Kronian magnetospheres where the plasma beta is $\sim$1–10 (e.g., McNutt 1983; Kanani et al. 2010). Observations of the location of the magnetopause show that it is displaced outwards from the dipole prediction. Modelling of the magnetopause location also shows that it responds more dramatically to changes in solar wind dynamic pressure with power laws
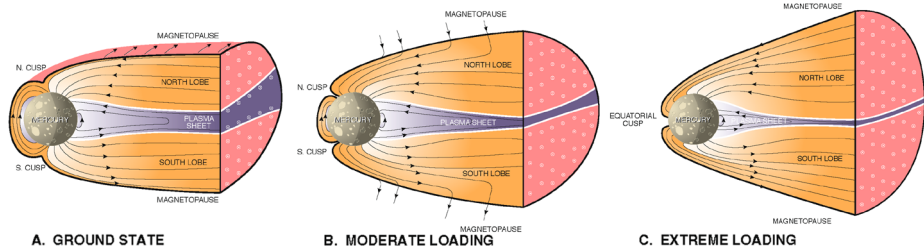
Fig. 6 Illustration of erosion of dayside magnetopause by dayside reconnection (from Slavin et al. 2010)

between 1/4 and 1/5 (Slavin et al. 1985a; Huddleston et al. 1998; Arridge et al. 2006; Kanani et al. 2010). This effect is often attributed to the effect of hot plasma pressure inside the magnetosphere, although Bunce et al. (2007) demonstrated that at Saturn centrifugal stresses inside the ring current increase strongly with the subsolar magnetopause distance resulting in the ring current magnetic moment increasing with the subsolar magnetopause distance. This increase in the magnetic moment leads to a more compressible magnetosphere and a shallower power law. The average magnetopause subsolar magnetopause distances for Mercury, Earth, Jupiter and Saturn are presented in Table 1. The subsolar magnetopause distance is also known to be bimodal at Jupiter (Joy et al. 2002), and Saturn (Achilleos et al. 2008), such that the magnetospheres of these planets tend to be in either compressed or expanded states. Joy et al. (2002) attributed the two subsolar magnetopause distances at Jupiter in-part to bimodal variations in the solar wind dynamic pressure during the interval analysed, whereas the analysis for Saturn by Achilleos et al. (2008) found no such bimodal distribution in solar wind dynamic pressure, and instead attributed the variation to changes in internal mass content of the magnetosphere.

Magnetopause reconnection also changes the subsolar position of the terrestrial magnetopause by eroding magnetic flux on the dayside under anti-parallel IMF orientations thus allowing the magnetopause to move inwards by ∼10–20 % during a typical interval of southward IMF (Aubry et al. 1970; Holzer and Slavin 1978, 1979; Sibeck et al. 1991; Roelof and Sibeck 1993; Shue et al. 1997; Volwerk et al. 2011). Similar effects have been observed at Jupiter (Kivelson and Southwood 2003). The case at Saturn is less clear, with conflicting arguments as to the importance of dayside reconnection as a flux transfer process (Scurry and Russell 1991; Grocott et al. 2009), although the dayside magnetopause does not appear to exhibit evidence of erosion (Lai et al. 2012). At Mercury, tail loading-unloading events during MESSENGER's third fly-by were of such large amplitude that it was suggested that all of the magnetic flux in the dayside magnetosphere might have reconnected (Slavin et al. 2010); however, analysis of such a possible situation (and in particular the role of inductive effects) is left to future work. In such an event, the northern and southern cusps would come together and merge to form a single cusp (see Fig. 6 taken from Slavin et al. 2010).

2.1.2 Tail Flaring

The tail magnetopause is also subject to a similar pressure balance, between the lobe magnetic pressure in the magnetosphere and the magnetosheath thermal, magnetic and dynamic pressure. The terrestrial tail magnetopause is known to flare, i.e. the tail radius is a function of distance along the magnetotail and increases up to some asymptotic value at some asymptotic distance along the tail. Tail flaring can be seen as a requirement by considering

the lobe magnetic pressure that is required to balance the thermal and magnetic pressure in the magnetosheath (e.g., Coroniti and Kennel 1972). A flared magnetotail can also be seen in models of the magnetopause (e.g., Shue et al. 1997). Estimates for the asymptotic tail radius for various planets can be found in Table 1.

Flaring of the magnetopause changes with changing dynamic pressure and the orientation of the IMF, with the magnetopause flaring out significantly with increasingly negative values of IMF B_z and moderately with increasing dynamic pressure, from the model of Shue et al. (1997). Mercury's tail magnetopause exhibits very little flaring beyond a few subsolar magnetopause distances downtail from the planet in stark contrast to Earth where the asymptotic distance is more than 100 R_E (∼10 subsolar magnetopause distances). Also Mercury's tail does not flare more with increasing solar wind dynamic pressure.

There are very few observations of the tail magnetopause at the giant planets and so our understanding of flaring at the giant planets is limited to modelling (e.g., Macek et al. 1992). The flaring behaviour of Saturn's tail as a function of solar wind dynamic pressure is not well established, presumably due to the dayside bias in the distribution of magnetopause crossings (Arridge et al. 2006; Kanani et al. 2010). However, it should be noted that increases in tail flaring due to dayside reconnection and open flux production might be entirely masked by changes due to increased solar wind pressure due to the time scales required to accumulate sufficient flux to affect tail flaring (e.g., Arridge et al. 2006).

2.1.3 The Length of an Open Magnetic Tail

In this section we consider the length of the tail of an open magnetosphere, such as that at Earth. There are two definitions of this length: the length of the "connected tail", the longest open magnetic field line connected to the Earth, and the length of the "disconnected tail", that distance downstream of the Earth where field lines released from the magnetotail by reconnection form a structured wake (Cowley 1991; Milan 2004). In 2-d equilibrium models of the magnetotail (Coroniti and Kennel 1972; Birn et al. 1975; Birn 1991) the main parameters that influence the length of a tail are the Mach number of the solar wind and the magnetic flux content of the open field regions (defined here as the lobes). Open (lobe) fields, however, may extend much farther out than the last closed field line, for a distance that cannot be determined within static models. In three dimensions the relationship between cessation of flaring and pressure minimum need no longer be exact, due to possible differences between flaring in the dawn-dusk (y) and the north-south direction (z) and the fact that the internal field flaring in the y direction may be different from a boundary flaring (Birn 2005). These properties are closely related to the plasma pressure distribution on closed field lines and its dawn-dusk variation, which are influenced by dayside and nightside reconnection rates (see below). The characteristic feature of such quasi-static models (e.g. Wiechen and Schindler 1988) is that the closed field line region ends at a finite distance at a Y shaped neutral line and that open field lines continue in a 1D fashion for an undetermined distance, separated by a current sheet. Pressure balance requires that the pressure within this current sheet must be finite to balance the magnetic pressure in the lobes. The thickness of this current sheet is also finite, as confirmed by observations (Pulkkinen et al. 1993). Stability requires that it be thicker than a typical ion inertial length (Sects. 2.2.2 and 4.3).

The Earth's magnetotail lobes are formed by open magnetic field lines stretched antisunwards by the flow of the solar wind. As calculated by Dungey (1965), if the field lines remain open for 4 hours from the time that they are formed by dayside reconnection to disconnection in the tail, then they are stretched (at a solar wind speed of 450 km/s) to a
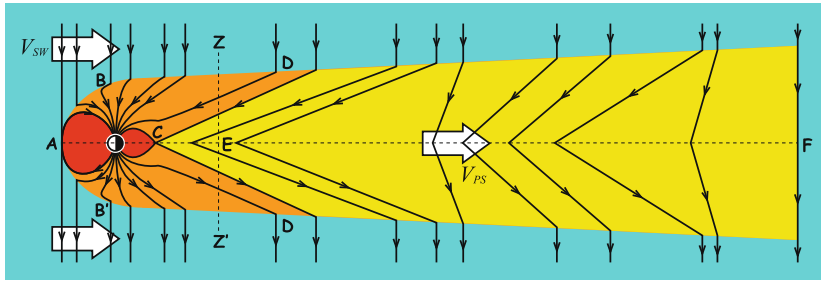
Fig. 7 A schematic sketch of the Earth's magnetosphere in the X–Z plane illustrating the regions of connected and disconnected tail field lines. The markings point to: (A) the low-latitude magnetopause reconnection site, (B) potential lobe reconnection sites, (C) the tail reconnection site, (D) field lines crossing the tail magnetopause, (E) field lines crossing the current sheet, (F) the end of the disconnected tail. Note that distances are not to scale, as the near-Earth X-line is expected to be around 20 R_E, whereas the length of the connected tail is ∼1000 R_E and the disconnected tail ∼5000 R_E. Adapted from Milan (2004)

length of ∼1000 R_E. Indeed, the Earth's tail has been studied in detail by ISEE 3 (Slavin et al. 1985b) and Geotail (Nishida et al. 1998) up to 240 R_E downstream with sporadic tail encounters at distances out to 500–800 R_E (e.g. Scarf et al. 1970) and maybe as far as 3100 R_E (Intriligator et al. 1979). Once the field lines are disconnected by reconnection in the magnetotail, they are expected to be highly stretched and kinked: the tail reconnection X-line is located at perhaps 20 R_E downtail, but the field lines are stretched to a length near 1000 R_E. Cowley (1991) speculated that these disconnected field lines form a structured wake downstream of the planet, remaining tail-like until they straighten, a distance that could be up to five times longer than the connected tail. Figure 7 shows a schematic picture of the connected vs. disconnected tail at Earth.

The quasi-static picture applies best to cases without significant dayside or nightside reconnection. For anti-parallel IMF and planetary field, however, one has to account for both dayside and nightside reconnection and the fact that an imbalance between the two leads to temporal changes. Milan (2004) assessed the variability of the length and open flux content of the tail, determining the instantaneous magnitude of open flux in the tail lobes from knowledge of the current polar cap open flux content and the history of the dayside reconnection rate (see also Sect. 5.1). The amount of open flux in the lobe decreases with down-tail distance as field lines cross the magnetopause to interconnect with the IMF. At a given down-tail distance, the rate at which field lines leave the tail lobe across the magnetopause is related to the dayside reconnection rate at the time that those field lines were opened; the greater the down-tail distance being considered, the further back in time the reconnection rate must be known. Periods of nightside reconnection disconnect the oldest (longest) open field lines from the Earth and the tail rapidly shortens.

These considerations indicate that during prolonged periods of strong dayside reconnection the terrestrial magnetotail lobes are expected to be short (100s R_E), as all the open field lines must be relatively young. By contrast, during periods of low dayside reconnection, open field lines have been connected to the Earth for many hours and have been stretched to great lengths (1000s R_E).

Milan and Slavin (2011) applied the same idea to the magnetotail of Mercury. In that study it was shown that when the IMF is directed southwards the reconnection rate at Mercury is expected to be very large compared to the open flux content of the magnetosphere, such that the polar cap "refresh" time (i.e. the Dungey cycle timescale) is of the order of minutes (not hours, as is the case at Earth). During such periods, the tail is expected to be only

10s of R_M of length. On the other hand, when the IMF is directed northwards, the dayside reconnection rate is low and the tail may be stretched to many 100s R_M. The characteristic duration of periods of northwards- and southwards-directed IMF in the solar wind at Mercury (1 to 2 hours) dictates an almost bimodal tail structure. During periods of southwards IMF the tail flux cycles rapidly and the maximum tail length depends on the cycle time of open flux, while during periods of northwards IMF the tail gets longer, with its maximum length associated with the duration before the next southward turning.

This picture must be modified for magnetospheres in which the polar cap refresh time is long compared to the rotation period of the planet. Milan et al. (2005) considered the case of Saturn, where the polar cap refresh time is expected to be many days (e.g. Badman et al. 2005), but the planetary rotation period is ∼10–11 hours. In such cases the magnetotail lobes are thought to become twisted by a rotational torque applied to the ionospheric ends of the open field lines (e.g. Isbell et al. 1984). Milan et al. (2005) argued that the Earth is an open flux first-in-first-out system, in which it is the oldest open field lines that are first disconnected by reconnection in the tail; in contrast, Saturn is a last-in-first-out system, in which it is recently opened field lines that are the first closed in the tail, due to the imposed twist. This implies that the lobes contain a core of old open field lines that can be stretched to incredible lengths (significant fractions of an AU), and that disconnected flux produces bundles wrapped around this inner core—inside-out plasmoids.

At Jupiter, as we shall explore in more detail later, the Vasyliunas cycle is thought to dominate, and so calculations of tail length based on open field lines residence times as shown above are not applicable. The New Horizons spacecraft has sampled the coherent Jovian magnetotail *in situ* to distances from 1600 R_J (McNutt et al. 2007) to 2500 R_J (McComas et al. 2007). However, observations from the Voyager spacecraft suggest that the Jovian tail can stretch beyond ∼9000 R_J (Lepping et al. 1983), and indeed even as far as the orbit of Saturn (e.g. Kurth et al. 1982; Scarf et al. 1982; Goldstein et al. 1985), which would make the Jovian magnetosphere by far the largest coherent structure in our solar system.

2.2 Latitudinal Structure

Planetary magnetotails display structure that varies with latitude. In the case of the terrestrial magnetotail, the latitudinal structure is illustrated in Fig. 8, which shows a cut through the noon-midnight meridian in northern hemisphere summer. We describe the various regions in the sections below.

2.2.1 Plasma Sheet

The region of highest measured plasma flux is the magnetotail plasma sheet, located closest to the equatorial plane of the magnetotail. The plasma sheet exists on closed magnetic field lines and has embedded in it the magnetotail current sheet, which separates the northern and southern hemispheres (lobes) with their oppositely-directed magnetic fields (see Sect. 2.2.2 for a discussion of the current sheet itself). The plasma sheet is the region of a planetary magnetotail where the internal, i.e. thermal, plasma pressure balances the magnetic pressure in the lobes, implying high plasma beta.

The Earth's mid-tail (i.e. anti-sunward distance of 15–30 R_E) plasma sheet has an average proton number density of 0.4 cm^{-3} and proton temperature of 5×10^7 K (equivalent to 4.3 keV via $k_B T$) (Baumjohann et al. 1989). The electrons in the plasma sheet are generally of lower temperature than the protons and the electron temperature is related to the proton temperature by $T_p = 11 T_e^{0.62}$ (Artemyev et al. 2011). Earlier estimates (Baumjohann et al.

Fig. 8 Schematic of the latitudinal structure of the terrestrial magnetotail
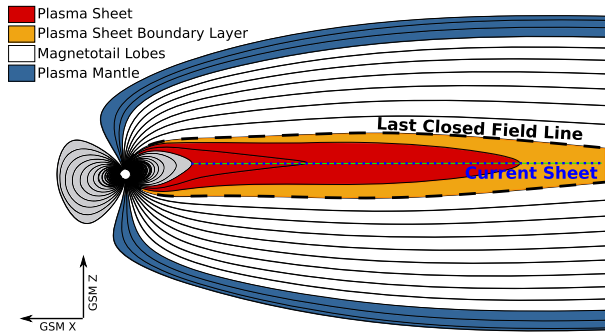
1989) of a constant proton to electron temperature ratio of $\sim$7 are valid for $T_e < 2 \times 10^7$ K (1.7 keV). Plasma sheet densities and temperatures are variable, however, and tend to be correlated with solar wind density, temperature and dynamic pressure (Borovsky et al. 1998). Proton distributions in the terrestrial plasma sheet are generally quite isotropic (Parks et al. 1984; Runov et al. 2010), except for periods of activity, which are characterized by current sheet thinning, flow bursts, and rapid field changes (Sect. 4). Electron distributions have been shown to have anisotropy such that there is excess flux in the (anti-) field-aligned directions, particularly at sub-keV energies (Walsh and Forsyth 2011). Closer to Earth both ion and electron distributions become anisotropic; the isotropy boundaries provide an important remote diagnostic for identification of the source region of auroral features (e.g., Sergeev et al. 2012a). Fast (field-aligned) flows and anisotropies are also commonly found near the plasma sheet—lobe interface, in the "plasma sheet boundary layer (PSBL)" discussed in Sect. 2.2.3. Plasma sheet particles tend to become more energetic with decreasing distance from Earth, particularly inside of about 15 R_E (Walsh and Forsyth 2011). This can be understood as adiabatic heating.

The plasma in the Jovian plasma sheet is composed of protons and heavy ions separated into two distinct populations; a lower-energy population and a population of energetic particles. This latter group are minor in terms of number density but provide almost all the particle pressure inside the plasma sheet. Voyager and Galileo observations presented by Kane et al. (1995, 1999) found two populations of energetic ions, a light group assumed to be protons, and a heavy group, assumed to be sulphur. The number densities were typically 10^{-3} cm^{-3} with the sulphur number density about three times that of protons. The temperatures were 10 keV for protons 30 keV for sulphur at 70 R_J, with the sulphur showing a modest increase with radial distance. Flow speeds for these ions were roughly 500 km s^{-1}. The plasma beta ranged between 1 and 10. Frank et al. (2002) presented the most complete survey of "thermal" plasma in Jupiter's magnetotail, detecting a cool population of protons with a temperature of 0.01 keV and a warmer population of heavy ions composed of O$^+$, O^{2+}, S^{2+} and S^{3+} with a temperature of 0.5 keV. The plasma flows were typically in the direction of corotation but with significant outward flows, and at 100 R_J a significant anti-sunward flow of 200 km s^{-1} was reported, perhaps supporting the idea of a planetary wind. Near 100 R_J the densities were typically several times 10^{-2} cm^{-3} with a plasma beta of 10–100 in the current sheet. Magnetotail electrons have been most comprehensively studied by Scudder et al. (1981) based on Voyager observations. They found a hot component with a temperature of around 1 keV and cooler component in the plasma sheet of $\sim$0.01 keV and they suggested these two components had very different temporal histories.

In the case of Saturn, electron distributions in the plasma sheet have been observed to have three states: A quiet plasma sheet characterised by electrons with energies of 0.1 keV;

a disturbed plasma sheet with energies ∼1 keV and a state in which bimodal electron distributions containing both of the above components are observed as well as bimodal distributions with a cold ∼0.01 keV component (Arridge et al. 2009). Arridge et al. (2009) also defined a central and an outer plasma sheet for Saturn with densities of 0.001–0.1 and 0.0001–0.01 cm^{-3}, respectively. The temperatures of the central plasma sheet and outer plasma sheet were found to be 0.06–0.2 keV and 0.1–0.2 keV, respectively. The electron distribution function for all populations was found to be best described by a Kappa distribution. McAndrews et al. (2009) have presented the most comprehensive study of plasma ions at Saturn. Ion flows are typically 150–200 km s^{-1} and predominantly in the corotational direction out to 30 R_S, with some outward flow beyond this distance. Ion temperatures were found to be ∼1 keV for heavy W$^+$ ions and ∼0.1 keV for protons. Ion densities fall from 1 cm^{-3} near 20 R_S to 0.1 cm^{-3} near 45 R_S. The composition is variable, with the observed number density ratio n_{W+}/n_p varying between 1 and >10, but typically 2–3. The plasma pressure in the plasma sheet appears to have roughly equal contributions from thermal plasma and energetic particles, although a comprehensive study of pressure partitioning and the plasma beta has not yet been carried out.

At Mercury the plasma electron measurements from Mariner 10 showed the presence of a plasma sheet containing electrons of energy ∼0.1 keV during "quiet" times, and in excess of 1 keV during "disturbed" intervals thought to be associated with the Hermean analogue of substorms (Ogilvie et al. 1977; Siscoe and Christopher 1975). More recently observations made during MESSENGER flybys of Mercury have confirmed the existence of a plasma sheet population of protons with a density of ∼4–5 cm^{-3} and temperature of $T_p \sim 4 \times 10^6$ K (0.35 keV) for the northward IMF quiet first Mercury flyby and ∼8 × 10^6 K (0.7 keV) for the southward IMF second flyby (Raines et al. 2011). These plasma measurements are generally consistent with the plasma beta values of ∼2–5 inferred for the plasma sheet using the MESSENGER average magnetic field measurements and the assumption of pressure balance between the tail lobes and plasma sheet (Slavin et al. 2012a; Korth et al. 2011). However, Slavin et al. (2012a) inferred plasma beta values up to ∼200 for individual plasmoids in the plasma sheet that could not be resolved by the plasma measurements and indicative of strong plasma heating by reconnection. Magnetospheric scaling arguments (Ogilvie et al. 1977) suggest the Mariner 10 electron observations show broadly equivalent electron populations to those expected at the equivalent locations in the terrestrial magnetotail.

2.2.2 Current Sheet

The canonical picture of a magnetotail consists of two semicylinders of oppositely directed magnetic field, which are separated by a current layer well described to lowest order by Harris (1962). This is the so-called cross-tail current which flows in the dawn-dusk direction (at Earth). In its simplest form the magnetic field and current can be described as:

$$B_x = B_0 \tanh\left(\frac{z}{L}\right), \tag{4}$$

$$j_y = \frac{B_0}{L} \operatorname{sech}^2\left(\frac{z}{L}\right), \tag{5}$$

where B_0 is the field strength of the magnetotail lobes, and L is the half-thickness of the current sheet. Using the measurement of the four Cluster spacecraft in Earth's magnetosphere, the magnetic field at four places can be obtained and from that electric current can be calculated. This can be compared with the model of Runov et al. (2005a). More sophisticated

current sheet models include a normal magnetic field component B_z. Force balance in x then requires a pressure gradient in x, which balances the Lorentz force $j_y B_z$. This can be accomplished by generalising the Harris model to include x variations of B_0 and L (Schindler 1972; Birn et al. 1975). The central part of the current sheet, where the X-component of the magnetic field goes through zero, is often called the neutral sheet. The current sheet itself is embedded in the plasma sheet; under quiescent conditions the plasma pressure varies on the same scale L as the current density as given by Eq. (5) (see Fig. 8).

While the Harris model is often a very appropriate description for the terrestrial current sheet (e.g. Zhang et al. 2006), evidence for bifurcation of the current sheet has been presented by a number of authors (Hoshino et al. 1996; Nakamura et al. 2002; Sergeev et al. 2003; Runov et al. 2003a; Asano et al. 2004). Crossings through bifurcated currents sheets show multiple reversals of the radial field component and multiple maxima (usually double) in the current density profile when the spacecraft cross from one hemisphere into the other. An example of this was presented by Runov et al. (2003a) who found evidence of a cross-tail current located in two sheets separated by an extended region of almost uniform weak magnetic field. Bifurcation has been linked with magnetotail reconnection processes (e.g. Sergeev et al. 1993). A statistical survey (Asano et al. 2005) showed that for thin current sheets (thickness <1500 km), off-equatorial current density maxima were often found during times of fast flows.

Another common feature is that of embedded current sheets, where the current sheet does not look Harris-like, but rather displays a strong thin current sheet at the centre, surrounded by a much thicker current sheet of lower current. Based on a survey of Cluster current sheet crossings, Petrukovich et al. (2011) found that the embedded current sheet thickness is on the order of the proton Larmor radius R_0 determined by the field strength B_0 at the boundary of the thin embedded current sheet which is located at a distance z_0 from the centre of the current sheet. This indicates a kinetic structure of embedded current sheets (Sitnov et al. 2000; Schindler and Birn 2002; Zelenyi et al. 2004; Artemyev and Zelenyi 2013).

The shape of the terrestrial magnetotail current sheet depends on the orientation of the IMF, dynamic pressure and the orientation of the dipole with respect to the Sun and is found to be warped and twisted (e.g., Tsyganenko and Fairfield 2004). Twisting of the current sheet causes the current sheet to rotate around the tail axis and is associated with IMF B_y. Warping occurs both with distance down the tail, where the tail "hinges" to become parallel to the solar wind flow over a characteristic distance known as the hinging distance, and transverse to the tail such that the tail current sheet curves towards the flanks of the tail. Significant IMF B_y rotates the current sheet along the tail axis, an effect which becomes much stronger under northward IMF. An increase in solar wind dynamic pressure reduces the hinging distance of the tail but also increases the magnitude of its transverse warping (Tsyganenko and Fairfield 2004).

The first observations of the Jovian current sheet were discussed by Ness et al. (1981) with respect to Voyager 1 and 2 data. They found that the Jovian magnetotail was 300–400 R_J wide and that the tail plasma sheet was relatively thin at ∼2 R_J. A longer discussion of these data was presented by Behannon et al. (1981), who state that the current sheet of the Jovian tail consists of a plasma sheet with a neutral sheet embedded, similar to the Earth's magnetotail, with the difference that at Jupiter the current sheet is an extension of the current disk in the inner magnetosphere. Israelevich and Ershkovich (2006) and Israelevich et al. (2007) found evidence of bifurcation from the Voyager 2 and Galileo crossings of the Jovian current sheet. However, they concluded that it is a relatively rare phenomenon at Jupiter. Khurana (2001) made an estimate of the strength of the cross-tail current, and found it to vary from ∼6 MA/R_J at 15 R_J to about ∼1 MA/R_J at 75 R_J.

The shape of Jupiter's magnetospheric current sheet is controlled by two principal effects: the oscillation of the Jovian magnetic equator due to Jupiter's significant dipole tilt, and warping by the solar wind at large ($\gtrsim 30\ R_J$) distances. This warping becomes significant beyond the hinging point. Current sheet crossings are found to be delayed with increasing radial distance due to the bend-back of the magnetic field, and propagation effects associated with communicating the tilt of the dipole via Alfvén waves in the presence of plasma outflow. The most comprehensive study of the time-dependent shape of Jupiter's magnetospheric current sheet was presented by Khurana and Schwarzl (2005) using all available magnetic field data from Pioneer 10 and 11, Voyager 1 and 2, Ulysses, and Galileo. They improved on the already existing models of the bend-back of the magnetic field and delays due to Alfvén wave delay and outflow by introducing local-time dependence. They also estimated a hinging point of $x_{\mathrm{JSO}} = -47\ R_J$, slightly larger than previous studies (where JSO is Jovicentric Solar Orbital coordinates, explained in Appendix).

Similar to the case of Jupiter, the current sheet in the tail region of Saturn's magnetosphere is an extension of the magnetospheric current sheet with an inner edge near 6 R_S (Connerney et al. 1983; Arridge et al. 2008a). At large distances in the magnetotail it is not clear where the current closes—i.e., does it simply continue to be an azimuthal current disc confined inside a cylindrical volume, or does it actually close on the magnetopause similar to the terrestrial magnetotail. Jackman and Arridge (2011) studied the lobe field in Saturn's magnetotail and presented a radial profile for the lobe magnetic field strength. Using this profile one can derive a zeroth order estimate for the strength of the tail current sheet; falling from $\sim$0.6 MA/R_S at 20 R_S to 0.2 MA/R_S at 50 R_S. The geometry of the current sheet has been described by Arridge et al. (2008b, 2011a) who have shown that not only is the current sheet warped out of the equatorial plane away from equinox, but also that it flaps, with a period of 10 hours, in phase with other periodic signals in Saturn's magnetosphere. Small-scale flapping is discussed in more detail in Sect. 4.4 below.

Since the arrival of the MESSENGER spacecraft at Mercury, it has been possible to investigate the properties of the current sheet there, although at the time of writing a detailed analysis of the in-orbit data is still a work in progress. Slavin et al. (2012a) characterised Mercury's plasma sheet based on intervals when the spacecraft was in the plasma sheet by the field intensity, direction, and level of fluctuations. For cases with IMF $B_z > 0$, the current sheet appeared thick based upon the large positive B_z at its centre and an average plasma beta is $\sim$5, comparable to what was determined for this region from H$^+$ plasma ion measurements (Raines et al. 2011). During IMF $B_z < 0$, plasmoid formation and ejection in much thinner current sheets with plasma beta values up to $\sim$200 were observed (Slavin et al. 2009; 2010, 2012a).

2.2.3 Higher Latitudes

In the case of the Earth, the highest latitude regions of closed magnetic flux exhibit different plasma characteristics from those at lower latitudes, to the extent that they have been termed the plasma sheet boundary layer (PSBL) (Eastman et al. 1984; Parks et al. 1984). The PSBL is characterised by stronger magnetic field and lower plasma beta than the central plasma sheet and it is also home to strong current systems associated in part with the gradient in plasma pressure between the central plasma sheet and the magnetotail lobes (Elphic et al. 1985; Shi et al. 2010; see also Fig. 8). Particle characteristics in the PSBL are also different from the central plasma sheet: ions in the PSBL have been observed to evolve from unidirectional beams at the outer edge of the PSBL, on the most recently closed magnetic field lines, into bidirectional beams further into the PSBL whereas electrons in

the PSBL are generally bidirectional throughout (Forbes et al. 1981; Parks et al. 1984; Walsh and Forsyth 2011). While ion beams have been observed at the outer edge of the plasma sheet in both geomagnetically active and geomagnetically quiet times (Grigorenko et al. 2009) they are not ubiquitous. In some cases spacecraft crossing from the lobes to the plasma sheet have not observed any field-aligned ions (Angelopoulos et al. 1993). This tends to occur more often under steady northward IMF (Walsh et al. 2013a).

PSBL ion beams are thought to be accelerated Earthward through interactions with the magnetotail current sheet near the distant X-line (Speiser 1965; Cowley 1984). The existence of bidirectional ions on magnetic field lines that map to lower latitudes can thus be understood as a combination of the equatorward convection of those field lines as part of the Dungey cycle and the time it takes for ions accelerated along those field lines to travel from the vicinity of the distant X-line to the ionosphere and back to the point of observation. It is also the case that acceleration can occur elsewhere in the current sheet where there is a finite, slowly varying component of the magnetic field normal to the plane of the current sheet (Lyons and Speiser 1982; Büchner and Zelenyi 1986). This acceleration occurs when the radius of curvature of the magnetic field line threading the current sheet becomes much smaller than the particle gyroradius and therefore the particles can behave non-adiabatically. This can happen in small localised regions leading to fine structure in the PSBL (Ashour-Abdalla et al. 1993) rather than uniform layers of plasma all accelerated near a distant, or indeed near Earth neutral line. In practice, there is evidence of both of these processes operating in the terrestrial magnetotail (Grigorenko et al. 2009). Another explanation is that the ions are accelerated as they are reflected from Earthward moving dipolarization fronts (see Sect. 4.4), suggesting the ion beams are the PSBL manifestation of impulsive flux transport occurring at lower latitudes, in the central plasma sheet (Zhou et al. 2012).

Studies of PSBL-type structures at Saturn and Jupiter have been somewhat limited to date. However, Kasahara et al. (2011) presented a multi-instrument study of Galileo data in the Jovian tail, during intervals where the spacecraft was sweeping vertically through the plasma sheet. They reported observations of localized increases in magnetic field and dropouts in electron density at the northern/southern edges of the plasma sheet which they attributed to the presence of a significant PSBL at Jupiter. In turn, they found a significant velocity layer structure in the energetic particle data associated with tail reconnection. These observations were similar to those reported by Sarafopoulos et al. (1997) for the terrestrial distant tail. Furthermore, Kronberg et al. (2012) presented two examples of counter-streaming electron beams in the PSBL at Jupiter, again linking such behaviour with reconfiguration of the Jovian tail following reconnection.

At Saturn, many studies of the current sheet and lobes have been undertaken (e.g. Simon et al. 2010; Jackman and Arridge 2011). These authors commented that there is no sharp boundary between current sheet and lobe-type fields, opening up the possibility for the existence of a PSBL there. However, there have to date been no dedicated studies looking for such a layer.

To date, there have been no observations of the field-aligned particle distributions characteristic of a plasma sheet boundary layer in Mercury's magnetosphere. However, the accommodation of the plasma instrument on MESSENGER behind a sun-shade precludes the measurement of ions coming from the sunward and anti-sunward directions as would be expected for PSBL particles. Although a "nightside boundary layer" was discussed by Raines et al. (2011), this is more analogous to the region of transition between stretched, tail-like and dipolar field lines that exists in the terrestrial magnetotail between 8 and 12 R_E from the Earth and is not comparable to the PSBL at Earth. More recently, Ho et al. (2012) observed energetic electron events at 30–300 keV over the nightside of Mercury at latitudes that might be consistent with an X-line along a PSBL. Further work on this topic is ongoing.
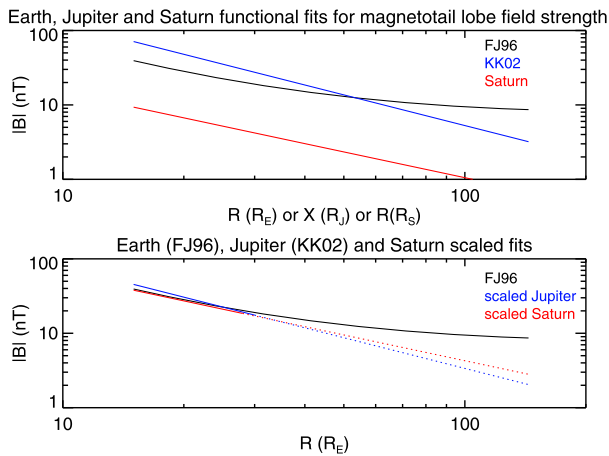
Fig. 9 Plots of the falloff of the lobe magnetic field strength at Earth, Jupiter, and Saturn: (*top*) unscaled relationships and (*bottom*) all values scaled to Earth. FJ96 refers to the Fairfield and Jones (1996) fit for Earth's tail. KK02 refers to the Kivelson and Khurana (2002) fit for Jupiter's tail. The *solid lines in the bottom panel* are valid for comparison as they represent areas sampled by spacecraft, while the behaviour represented by the *dashed lines* may not be physically representative of the deeper magnetotails of Jupiter and Saturn (from Jackman and Arridge 2011)

Moving to higher latitudes still, we can explore the magnetotail lobes. The lobes are typically regions of very lowplasma density, low plasma beta, and quiet magnetic field. The terrestrial and Hermean lobe magnetic fields are open to the IMF allowing plasma to escape (Seki et al. 1998; Abel et al. 2001), thus explaining the low densities measured by conventional plasma instruments. In rapidly-rotating magnetospheres, however, low plasma density measured at higher latitudes can also be a result of centrifugal confinement of plasma close to the equatorial plane (e.g. Hill and Michel 1976; Ray et al. 2009).

There are several plasma populations that have been observed to exist in the Earth's magnetotail lobes. Ionospheric outflow of H^+ and O^+ ions, readily observed over the polar cap at lower altitudes (e.g. Moore et al. 1997), has recently been shown to also exist at higher geocentric distances by Engwall et al. (2009) who detected an outflow of cold ions at a velocity of $\sim$30 km/s through the ions' production of an enhanced wake behind the spacecraft (Eriksson et al. 2006). The magnetotail lobes, have also been observed to contain the so-called "polar rain" (Winningham and Heikkila 1974) a flux of bidirectional, field-aligned electrons with energies of $\sim$0.1 keV. These electrons have their source in the field-aligned, suprathermal, "strahl" component of the solar wind electron distribution (Fairfield and Scudder 1985) thus the polar rain is a result of a direct magnetic connection between the Earth and the solar corona and is evidence of an open magnetic field topology in a planetary magnetosphere. The relative density of the strahl component of the solar wind has been measured to decrease with heliocentric distance (e.g. Štverák et al. 2009), so it remains an open question whether or not there are sufficient fluxes of strahl electrons to form a significant polar rain at the outer planets (Walsh et al. 2013b).

The total field strength in the tail lobes decreases with radial distance as the flaring of the magnetopause decreases. Jackman and Arridge (2011) compared several functional fits for Earth, Jupiter and Saturn, to understand how the field changes in corresponding magnetospheric regions, and the result is shown in Fig. 9. The terrestrial fit is from Fairfield and Jones (1996) who found a relationship of B (nT) $= 1659.2 \, (r \, (R_E))^{-1.46}$. The original Jovian

fit using cylindrical radial distance from Jupiter's spin axis, ρ, is from Kivelson and Khurana (2002), which took the form B (nT) $= 2900 \, (\rho(R_J))^{-1.37}$. The fit to the Saturn data is B (nT) $= 251 \, (r(R_S))^{-1.20}$ where r is radial distance from the planet. These fits were scaled in the lower panel to the Earth taking into account varying dipole field strengths and subsolar magnetopause distances. It was concluded that the near magnetotails of Earth, Jupiter and Saturn display similar characteristics in terms of the rate of falloff of the lobe field strength. However, beyond the common scaled distance of $\sim$30–40 R_E, the Kronian and Jovian traces fall off much more rapidly. In the absence of continuous magnetometer data down the length of these tails, our current understanding of the potential asymptotic behaviour of Jupiter and Saturn's lobe field strength is based on extrapolation and theory (e.g., Macek et al. 1992).

Analysis of the lobe field strength changes in Mercury's magnetotail was presented by Slavin et al. (2012a). Based on the one Mariner 10 flyby that sampled the tail and the three MESSENGER flybys prior to orbit insertion it was found that the field follows a power law decrease with exponent ranging from −5.4 for the case of northward IMF to −1.6 for southward IMF. The derivation of a more statistically significant falloff based on the subsequent MESSENGER orbits will be the subject of future work.

As well as a radial component of magnetic field, planetary magnetotails have azimuthal components, which can be governed through internal processes, such as mass loading, or through interaction with the interplanetary magnetic field and solar wind. In the case of planetary magnetospheres whose dynamics are dominated by the solar wind interaction (such as Earth and Mercury), the east-west component of the IMF (B_Y in RTN) is generally responsible for the azimuthal component (B_Y) of the magnetotail magnetic field (see Appendix for definitions of co-ordinate systems used in this paper).

The highest latitudes, just inside the magnetopause, are characterised by a population of tailward-flowing plasma that has been termed the plasma mantle (Rosenbauer et al. 1975). The terrestrial plasma mantle protons have energies of $\sim$0.1 keV (Sckopke and Paschmann 1978) and the mantle is in fact the nightside manifestation of the polar cusp. The tailward flowing mantle plasma is cusp plasma that has been mirrored at low altitudes and is hence travelling antisunward along magnetic field lines that are convecting tailward. The observed decreases in mantle density and temperature with decreasing latitude are consistent with this mechanism (Rosenbauer et al. 1975), as are the commonly measured velocity dispersions in the terrestrial cusp (Reiff et al. 1977). Cusp-like plasma structures exhibiting similar velocity dispersions to those measured at Earth have been observed in Saturn's magnetosphere (Arridge, personal communication), implying the existence of a plasma mantle; although to date there are no direct measurements of a plasma mantle at Saturn. The existence or lack of a plasma mantle is one possible diagnostic of whether or not there is solar wind-driven convection, and hence whether or not the planet's magnetic field is connected to the IMF. However, the search for a plasma mantle at a rapid rotator such as Jupiter or Saturn may be complicated due to shifts in the spatial location of the mantle due to rotational effects.

2.3 Longitudinal (Local Time) Structure

Planetary magnetotails are not two-dimensional structures; they also have longitudinal structure. The plasma and current sheet can be warped and twisted, in response to the IMF and dipole orientations (Russell and Brody 1967; Zhang et al. 2002), and the normal magnetic field component B_Z (and the corresponding current sheet thickness) tends to increase from the centre of the tail towards the flanks by a factor of about two for the Earth's case. The B_Y field also increases in magnitude toward the flanks, consistent with an increase in field line flaring (Fairfield 1979). In addition, there can be a net cross-tail component B_Y in response

to the azimuthal (i.e. B_Y) component of the IMF, which is discussed in Sect. 4.6 below. Additional longitudinal structure has been observed in the terrestrial magnetotail, such as the low latitude boundary layer (LLBL) (Fairfield 1979), the tailward extension of the dayside LLBL (Mitchell et al. 1987), that contains a mixture of magnetosheath and magnetospheric plasma (e.g. Lockwood and Hapgood 1997) and exists on both flanks of the magnetotail, just inside the magnetopause. Indeed, ISEE-3 observed the closed LLBL field lines at the flanks of the tail to the maximum downstream distances reached by this mission, $X \sim -240\ R_E$ (Slavin et al. 1985b). Asymmetric transport of plasma across the flank magnetopause, either through reconnection in rolled up Kelvin-Helmholtz vortices (Nykyri and Otto 2001; Hasegawa et al. 2004), via kinetic Alfvén waves (Johnson and Cheng 1997) or as a result of dual lobe reconnection (e.g. Imber et al. 2006; Oieroset et al. 2008), is also thought to have an effect on the plasma sheet itself. The cold component of plasma observed during steady northward IMF is observed primarily towards the flanks of the magnetotail (Nishino et al. 2011) and has higher fluxes in the premidnight sector than the postmidnight sector (Wing et al. 2005). Processes operating internally in the magnetosphere can also introduce longitudinal structure to the magnetotail. PSBL ion beams have been observed to be more energetic in the premidnight sector than the postmidnight sector (Grigorenko et al. 2009), whereas there are higher energetic electron fluxes postmidnight than premidnight (Åsnes et al. 2008; Imada et al. 2008). These observations have been explained in terms of the particles' acceleration by the cross-tail electric field. Furthermore, the occurrence of most reconnection signatures, including Bursty Bulk Flows (BBFs), earthward and tail ward moving plasmoids, and travelling compression regions are more common on the dusk than on the dawn-side of the plasma sheet for reasons that are still not understood (e.g. Slavin et al. 2005).

Recent studies at the outer planets have revealed the presence of some distinct cross-tail structure. At Saturn, evidence has been presented for a LLBL (Masters et al. 2011a). The estimated thickness of the layer is $\sim 1\ R_S$ with no clear dawn-dusk asymmetry. There appears to be no strong influence of the IMF orientation on the thickness of the layer, which is in contrast to the picture at Earth.

The magnetotail of Mercury exhibits some of the same longitudinal structure as that of the Earth, including a LLBL at the flanks of the magnetotail that has varying thickness depending on upstream conditions (Slavin et al. 2012a) and where the Kelvin-Helmholtz instability has been shown to be active (Sundberg et al. 2012a). The Hermean LLBL has been observed to be thicker when the upstream IMF was thought to be northward than when it was thought to be southward (Slavin et al. 2012a), similarly to the terrestrial case (Mitchell et al. 1987), although the thickness of Mercury's nightside LLBL relative to the width of the magnetotail as a whole is higher than that at Earth (Slavin et al. 1985b, 2012a).

3 Quasi-steady Mass and Energy Transport

3.1 Magnetospheric Flows

The plasma within a magnetospheric cavity is not static but moves subject to both internal and external influences. This plasma motion is important as it leads to large-scale structuring of the plasma environment within the magnetosphere. In the atmosphere, collisional friction between ions and neutrals produces a stress that is transmitted along magnetic field lines to the equatorial magnetospheric plasma. The plasma flow in the magnetosphere is determined by stress balance between this collisional friction and stresses in the magnetosphere and along its boundaries. In a dynamical state these stresses may be unbalanced and the system may take several planetary rotations to reach a steady state (e.g., Yates et al. 2014).

If the ionospheric conductivity is sufficiently high (related to the ion-neutral collision frequency), then the ionospheric plasma can be driven into rotation with the neutral atmosphere. In general, this neutral atmosphere rotates at some (significant) fraction of the deep interior or surface of the planet and an upward viscous transport of momentum is required to keep the neutral atmosphere from being decelerated by collisional friction in the ionosphere. This rotation with the neutral atmosphere is usually termed "corotation" (e.g., Vasyliunas 1983) although rigid (circular) corotation about the rotation axis of the planet typically only applies in the immediate vicinity of the planet. In the magnetosphere (in the absence of solar wind perturbations, for example) this doesn't imply purely azimuthal plasma flow because the magnetic field is distorted between the planet and magnetosphere—particularly in local time as the field geometry changes between the nightside and dayside. Note that the presence of plasma production and outflow implies a continual increase in the total angular momentum of the magnetospheric plasma, which requires a torque to be applied on the magnetospheric plasma (to transport angular momentum from the ionosphere to the magnetosphere). This requires that the plasma lag corotation with the planet and thus represents an inertial limit to corotation (Hill 1979).

The external influence stems from the solar wind, which acts through reconnection and viscous interaction at the magnetopause, transferring momentum to the magnetosphere and driving convection associated with the Dungey and/or viscous cycles (Sect. 1.1). The occurrence and strength of magnetopause reconnection depend strongly on the orientation of the IMF, such that the convection patterns also depend strongly on the IMF. Reconnection at the magnetopause between the internal planetary field and the IMF results in a magnetic field component, B_N, normal to the magnetopause. This B_N component, which connects the IMF and the planetary magnetic field, is associated with a local electric field, $-\mathbf{V}_{MSH} \times \mathbf{B}_N$, which can be integrated along one half of the circumference of the magnetosphere (i.e. the intersection of the magnetopause with the terminator plane) to obtain the cross-magnetospheric potential drop. This voltage is reduced, compared to the voltage difference of the unperturbed solar wind over the same distance, due to the diversion of most of the solar wind around the planet, to about 10 % of the unperturbed value. This reduced electric field is sometimes called the geoeffective component of the interplanetary electric field.

If the surface in which the planetary field is rooted is a non-conductor, such as is believed to be the case at Mercury which has no ionosphere, then the full (geoeffective) solar wind potential drop is felt by the magnetosphere. However, for the other planets which all have conducting ionospheres the magnetospheric electric field is reduced somewhat, leading to a saturation of the polar cap potential for large IMF (Reiff et al. 1981; Wygant et al. 1983). This reduction can be thought of as either a partial "shorting" of the applied electric potential by current flow across the ionosphere (e.g. Siscoe et al. 2002, 2004), or an impedance mis-match between the height-integrated conductance of the ionosphere and the Alfvén conductance of the solar wind (Kivelson and Ridley 2008).

Mapping the electric field from the boundary down to the planet assumes a quasi-steady state, in which field lines are equipotentials. While this assumption seems reasonable for Earth's dayside magnetosphere, where the cross-polar potential drop is obtained from such mapping, interpreting the Dungey cycle as a steady convection model faces severe problems in the tail. On the theoretical side, adiabatic transport of plasma from a distant reconnection site to the near tail would imply a pressure increase far above what is observed (e.g. Erickson and Wolf 1980). Observationally, plasma transport, even during quiet times, is predominantly tailward beyond distances of $\sim$40 R_E (Nishida et al. 1998). A more realistic model of convection in the geomagnetic tail therefore consists of relatively quiet periods,

during which the tail may change slowly, interrupted by sudden release events, which include not only substorms but also smaller-scale transient activations (Sergeev et al. 1996a), discussed in Sect. 4.

If the planet does not rotate or rotates very slowly relative to the characteristic plasma motions (e.g. Mercury), then the large-scale convection is dominated by the Dungey cycle when the IMF has a component antiparallel to the planetary magnetic field. This is associated with a two-cell circulation pattern in the ionosphere, illustrated by Fig. 4 for the case of the Earth. The inner parts of the ionospheric two-cell circulation pattern, which lie within the closed field line region (hatched areas in Fig. 4), are attributed to the viscous cycle. The outer parts, representing the Dungey cycle, involve anti-sunward transport on open (lobe) field lines, connected with sunward and azimuthal transport within the closed field line region. The magnitude of the potentials associated with the viscous cycle are estimated at ∼5–30 kV (e.g., Cowley 1982), minor but not insignificant compared to typical transpolar voltages of 40–100 kV.

The situation is quite different for Jupiter and Saturn. The large magnetic fields generated by the internal dynamos of these planets, combined with their rapid rotation, and significant ionospheres, indicate that (at least partial) corotation of the plasma with the planet will be the dominant flow within their magnetospheric cavities (Brice and Ioannidis 1970). Hill (1979) noted that corotation cannot extend to arbitrarily large distances from the planet, but must break down at some point, beyond which the field is too weak to transmit the azimuthal stress necessary to keep the plasma in corotation. The field lines thus become swept back and lag behind corotation in the middle and outer magnetosphere. For the case of Jupiter's magnetosphere, Hill calculated that the rotation frequency may decrease by a factor of two between the planet and the magnetopause and such corotation lags are observed. The dominance of corotation at Jupiter and Saturn does not preclude significant interactions taking place between the magnetosphere and the solar wind, through compressions/expansions of the magnetosphere due to changes in solar wind dynamic pressure (e.g. Hanlon et al. 2004), and through the excitation of magnetospheric convection by momentum coupling at the magnetopause boundary, with a possible dominance of solar wind-driven effects in the outer magnetosphere (e.g. Badman and Cowley 2007).

In the Earth's case, a good qualitative picture of the structure and size of the corotating region for southward IMF can be obtained by simply superposing a corotation electric field, given by $\mathbf{E} = -\mathbf{V}_n \times \mathbf{B}$ (based on Earth's dipole field), where $\mathbf{V}_n = \mathbf{\Omega} \times \mathbf{r}$ is the rotation speed, and a uniform dawn-to-dusk ("convection") electric field. For a nominal cross-tail field of 0.2 mV/m, this yields a stagnation streamline (Alfvén boundary), enclosing the corotating region, that extends to 8.3 R_E on the duskside and to ± 4 R_E at the noon-midnight meridian, compared with a subsolar magnetopause distance R_{mp} of ∼10 R_E. The size of this region increases (decreases) with decreasing (increasing) convection electric field. A similar estimate for Mercury indicates that the corotation region is negligibly small, while for Jupiter and Saturn the estimated sizes exceed the typical magnetopause distance. This supports the view that the effects of planetary rotation should dominate the magnetospheres on the dayside. However, a reliable estimate of the extent on the nightside cannot be made without taking the actual magnetospheric magnetic field as well as the convection electric field into better account. Figure 10 illustrates schematically the expected flows and consequent stagnation streamlines for the case of Mercury, Earth, Jupiter and Saturn.

3.2 Mass Sources

The nature of the plasma dynamics in a planetary magnetosphere depends largely on the nature of the plasma sources and sinks, and the nature of the transport processes which convey
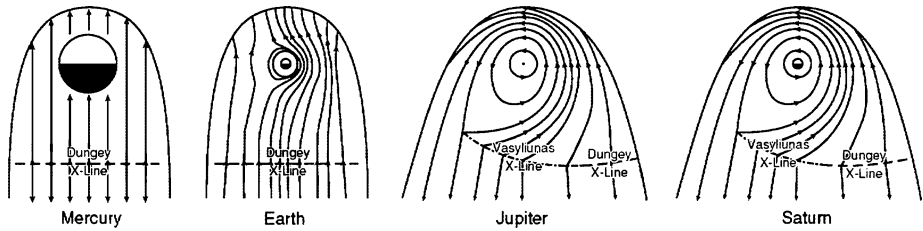
Fig. 10 Schematic of magnetospheric flow patterns for Mercury, Earth, Jupiter and Saturn illustrating the regions where corotation and convection dominate. We note that the sense of the X-line position may be altered such that the reconnection X-line(s) is further from the planet at dusk compared to dawn. The precise location of Dungey and Vasyliunas-type reconnection is also a topic of ongoing research. Thus the X-lines shown in this figure should be taken as illustrative only

the plasma from the former to the latter. The plasma found in a planetary magnetosphere can have a variety of sources: at the outer boundary plasma may leak across the magnetopause from the solar wind, at the inner boundary plasma may escape the planet's gravity and flow outward from the ionosphere, or magnetospheric plasma may originate from ionization of neutral material coming from satellites or rings embedded in the magnetosphere. Some examples of these mass loading processes are illustrated in Fig. 11.

The clearest indicator of which source is responsible for a particular planet's magnetospheric plasma is chemical composition and ionization state. For example, the O^+ ions in the Earth's magnetosphere must surely have come from the ionosphere (O ions from the solar wind would be multiply ionized). Meanwhile it is well known that at Jupiter the volcanic moon Io emits $\sim$1000 kg of sulphur and oxygen ions per second (reviewed by Thomas et al. 2004; Bagenal and Delamere 2011). At Saturn, a key finding of the Cassini mission has been to show that water group ions (H_2O^+, OH^+, O^+, H_3O^+, distinct from nitrogen) are the primary heavy ions in the magnetospheric plasma, and Enceladus has been identified as the main source (e.g. Dougherty et al. 2006). However, the source of protons in planetary magnetospheres is not so clear—protons could be either ionospheric (particularly for the hydrogen-dominated gas giants), or formed through dissociation of water ejected from icy satellites, or from the solar wind. One might consider that a useful source diagnostic would be the abundance of helium ions. Emanating from the hot ($\sim 5 \times 10^6$ K) solar corona, helium in the solar wind is fully ionized as He^{++} ions and comprises $\sim$3–5 % of the number density. Ionospheric plasma is much cooler (less than 1000 s of K), so that ionospheric helium ions are mostly singly ionized. Thus, a measurement of the abundance ratios He^{++}/H^+ and He^+/H^+ would clearly distinguish the relative importance of these sources. Unfortunately, measuring the composition to such a level of detail is difficult for the bulk of the plasma, with energies in the range 1×10^{-3} keV to 1 keV (e.g. Young 1997a, 1997b). Measurement of composition is more feasible at higher energies. However, one needs to consider whether the process that initially accelerated the ions at their source region is mass or charge dependent.

The temperature of a plasma can also be an indicator of its origin. Plasma in the ionosphere has characteristic temperatures of $< 1 \times 10^{-4}$ keV; the ionization of neutral gases produces ions with energies associated with the local plasma flow speed while material that has leaked in from the solar wind tends to have energies of a few keV. But, again, we need to consider carefully how a parcel of plasma may have been heated or cooled as it moved through the magnetosphere to the location at which it is measured. Figure 11a illustrates various ways in which ionospheric plasma enters the Earth's magnetosphere and evolves by
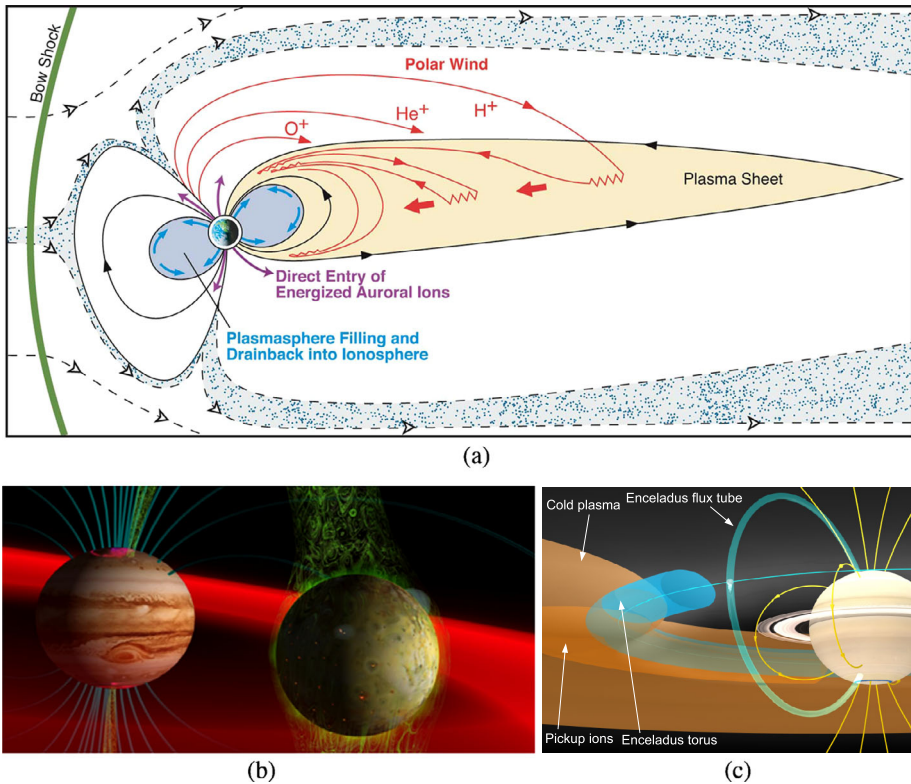
Fig. 11 Key mass loading process for planetary magnetospheres. (**a**) Sources of plasma for the Earth's magnetosphere (credit Fran Bagenal and Steve Bartlett, After Chappell 1988), (**b**) Volcanic outgassing from Io near Jupiter (credit John Spencer (SWRI)), (**c**) Creation of the Enceladus torus near Saturn (Arridge et al. 2011b)

different processes. As we explore other magnetospheres we should expect similar (or even higher) levels of complexity.

Table 2 summarizes the main plasma characteristics of Mercury, Earth, Jupiter and Saturn. To a first approximation one can say that escape of material from the satellites dominates the magnetospheres of Jupiter and Saturn, with ionospheric sources being secondary. With only the most tenuous of exospheres, Mercury's magnetosphere contains mostly solar wind material, but energetic particle and photon bombardment of the surface may be a significant source of O^+, Na^+, K^+, Mg^+, etc. (Zurbuchen et al. 2008, 2011; Raines et al. 2011).

3.3 Mass and Flux Transport

Mass that is added to a planetary magnetosphere via any of the mechanisms described above may subsequently be transported around the magnetosphere and ultimately lost across the magnetopause or down the magnetotail. The three key cycles of magnetic circulation were introduced above, the first involving "open" field lines (the Dungey cycle (Dungey 1961, 1963)), and the other two involving mainly closed field lines, the Vasyliunas cycle (Vasyliunas 1983) and the viscous cycle (Axford and Hines 1961). Here we consider the relative roles of the different cycles in the various planetary magnetospheres.

Table 2 Plasma characteristics of planetary magnetospheres

	Mercury	Earth	Jupiter	Saturn
Max. plasma density (cm^{-3})	~1	4000	~3000	~100
Neutral density (cm^{-3})	–	–	~50	~1000
Major ion species	H$^+$	O$^+$, H$^+$	O^{n+}, S^{n+}	O$^+$, [c]W$^+$, H$^+$
Minor ion species	[a]O$^+$, Na$^+$		[b]H$^+$, H3$^+$	[c]H$^+$, H2$^+$
Dominant source	Solar wind	Ionosphere[d]	Io	Enceladus
Neutral source[e] (kg/s)			600–2600	70–750
Primary plasma source[f] (kg/s)	~5	5 (from the solar wind)	260–1400 (from Io)	12–250 (from Enceladus)
Plasma source (ions/s)	10^{26}	2 × 10^{26}	>10^{28}	3–5 × 10^{26}
Lifetime	Minutes	hours–days[g]	20–80 days	30–50 days

[a]Mercury's tenuous atmosphere is a likely source of heavy ions

[b]There probably are ionospheric and solar wind sources but how they compare to satellite sources is not known

[c]Also water-group ions from ionization, dissociation and recombination of water (OH$^+$, H$_2$O$^+$, O$^+$, H$_3$O$^+$)

[d]Ionospheric plasma dominates the inner magnetosphere with solar wind sources being significant in the outer regions

[e]Net loss of neutrals from satellite/ring sources (Bagenal and Delamere 2011)

[f]Net production of plasma (Bagenal 1992; Bagenal and Delamere 2011)

[g]Typical residence time in the magnetosphere. Plasma stays inside the plasmasphere for days but is convected through the outer magnetosphere in hours

The differing upstream solar wind parameters, planetary rotation rates and ionospheric conditions mean that the relative importance of the above cycles can be very different at Mercury, Earth, Jupiter and Saturn. It is generally well agreed that solar wind effects dominate at Mercury and Earth. However, at both Saturn and Jupiter, the importance of the Dungey cycle compared to other flow regimes is an intensely debated topic (e.g. McComas and Bagenal 2007; Cowley et al. 2008).

Figure 12 (Cowley and Bunce 2003), illustrates the regions where Dungey and Vasyliunas cycles are expected to operate for the case of Jupiter. In this and subsequent papers (e.g. Badman and Cowley 2007), it is argued that the Dungey cycle can play a significant role at Jupiter, particularly in the outer magnetosphere under specific solar wind conditions. Contrary to this, McComas and Bagenal (2007) argued that perhaps Jupiter does not have a complete Dungey cycle but that their large calculated time scale for any reconnection flow suggests that magnetic flux that is opened near the sub-solar magnetopause re-closes on the magnetopause before it has travelled down the tail (illustrated schematically in Fig. 13). They suggested that the magnetotail comprises a pipe of internally generated plasma that disconnects from the planetary field and flows away from Jupiter in intermittent surges or bubbles, with no planetward Dungey return flow. They make this argument on the basis of tailward fluxes on internally generated plasma observed by the New Horizons spacecraft on its traversal of the deep Jovian tail. However, Cowley et al. (2008) dispute the claims made in this paper, questioning the estimates of distance to the tail reconnection site, and the rate
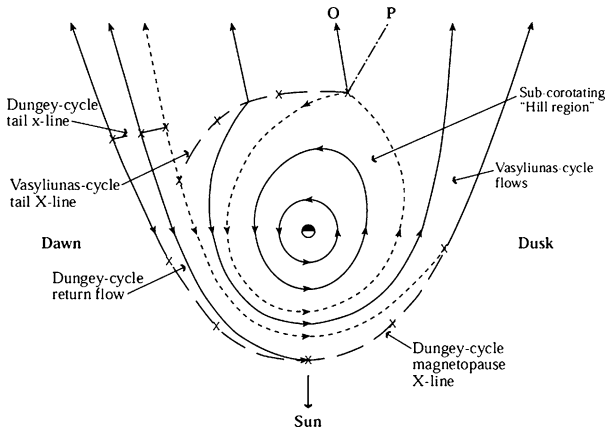
Fig. 12 Sketch of the flows in the Jovian equatorial plane, with the direction toward the Sun at the *bottom of the figure*. *Solid lines with arrows* show plasma streamlines, while *dashed lines with arrows* show streamlines which separate flow regions with differing origins and characteristics as indicated. *Dashed lines* with "X"s indicate X-type reconnection lines, while the *solid line* marked "O" indicates the O-type line of the Vasyliunas-cycle plasmoid which is ejected down-tail (which is a streamline). The *dot-dashed line* marked "P" is the outer boundary of the plasmoid, which reaches its asymptotic value at the dusk tail magnetopause (from Cowley and Bunce 2003)
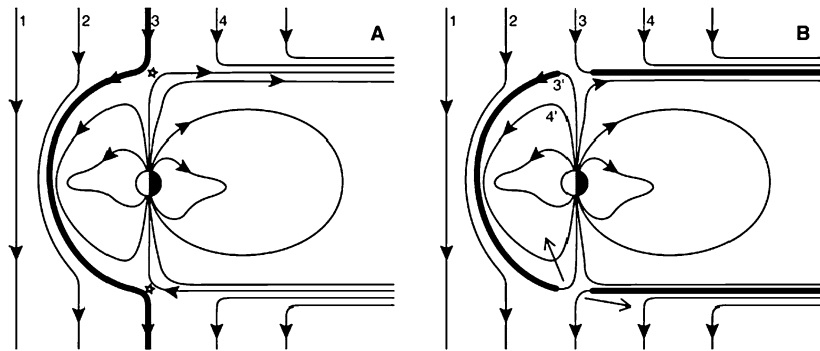
Fig. 13 Schematic diagram of magnetic flux closing at the magnetopause. (**A**) A significantly southward IMF (*1*) drapes around the dayside magnetopause (*2, 3*) until it reconnected with an oppositely-directed planetary field (*stars*). (**B**) Flux tube *3* reconnects near the magnetopause near both north and south cusps, creating newly closed (*3′*) and disconnected (*3*) flux tubes. After reconnection, the short, newly closed flux tube is free to work its way back toward a more normal closed shape (*4′*), while the long, newly disconnected flux tube (*4*) is lost down the flanks of the tail. After McComas and Bagenal (2007)

of contraction of closed field lines. It is certainly not the purpose of this review paper to decide between the alternative proposed scenarios. We merely note that this is a topic of intense interest, and one which we hope will be resolved in some way by the forthcoming Juno and JUICE spacecraft.

4 Magnetotail Dynamics

In addition to quasi-steady flows and transport, magnetospheres may also undergo rapid deformations and energy release events. Dynamic events in the Earth's magnetotail are characterized by rapid changes in the magnetic field, such as "dipolarizations," that is, rapid changes from stretched tail-like to more dipole-like field, and the generation of fast flows. The most significant such events are magnetospheric substorms, discussed in more detail in the following sections. However, substorm-like features, particularly fast flows and dipolarizations, may occur in the tail also in the absence of significant substorm signatures on the ground.

4.1 Substorms

Substorms constitute intermittent energy release events in the Earth's magnetotail and nightside auroral region with durations of roughly 1 hour and an occurrence of several per day under suitable conditions. They were initially defined on the basis of ground perturbations of the north-south magnetic field component ("negative magnetic bays"), which were found to be associated with rapid changes in auroral forms ("auroral breakup," Heppner 1954). They were called "polar elementary storms" (Chapman and Bartels 1962; Akasofu 1968, and references therein), "magnetic substorms" (Akasofu and Chapman 1961), and "auroral substorms" (Akasofu 1964). The discovery that auroral features were closely related to dynamic changes in Earth's magnetosphere led to the term "magnetospheric substorms" (Coroniti et al. 1968, and references therein), which is now the most commonly used.

   Through many thousands of studies of individual substorms, many other correlated phenomena have been identified. However, no unique, universally accepted, substorm definition exists. The most widely accepted phenomenological model (e.g., McPherron et al. 1973; Baker et al. 1996; Sergeev et al. 2012b) consists of three phases illustrated in Fig. 14 (after Hones 1979): During the "growth phase," energy and magnetic flux from the solar wind is accumulated primarily in the magnetotail lobes, expanding and stretching the tail, and expanding the polar cap size as a consequence of dayside reconnection. At the onset of the "expansion phase," the magnetotail undergoes a transition (substorm onset), widely interpreted as the result of reaching a point of instability or loss of equilibrium, at which accumulated energy becomes suddenly released. This release is closely related to reconnection in the near tail, leading to plasmoid ejection and a collapse of the near tail, as well as brightening and expansion of the aurora and an increase in auroral current (the auroral electrojet). In the "recovery phase," this energy is dissipated throughout the magnetosphere, auroral activity subsides and the mid-tail plasma sheet expands again.

   Many of the physical processes associated with terrestrial substorms have been observed at other planets. For example, at Mercury, observations of rapid variations in the tail magnetic fields accompanied by plasmoid ejection and charged particle acceleration have been collectively termed "substorms" as well (Siscoe et al. 1975; Slavin et al. 2010). This is despite the fact that, at Mercury, the strict terrestrial-style substorms involving auroras and the close coupling between an electrically conducting ionosphere and a magnetosphere cannot take place. For the case of Jupiter and Saturn, the absence of multi-point measurements or upstream solar wind measurements make it difficult to determine whether observed tail dynamics represent a system-wide magnetospheric reconfiguration, and the extent to which they are driven by interaction with the solar wind versus rotational stresses internal to the magnetosphere. Therefore, the use of the word "substorm" in the context of the giant planets can be ambiguous, and authors have instead tended to restrict their descriptions to using

PLASMA SHEET CONFIGURATION CHANGES DURING A SUBSTORM
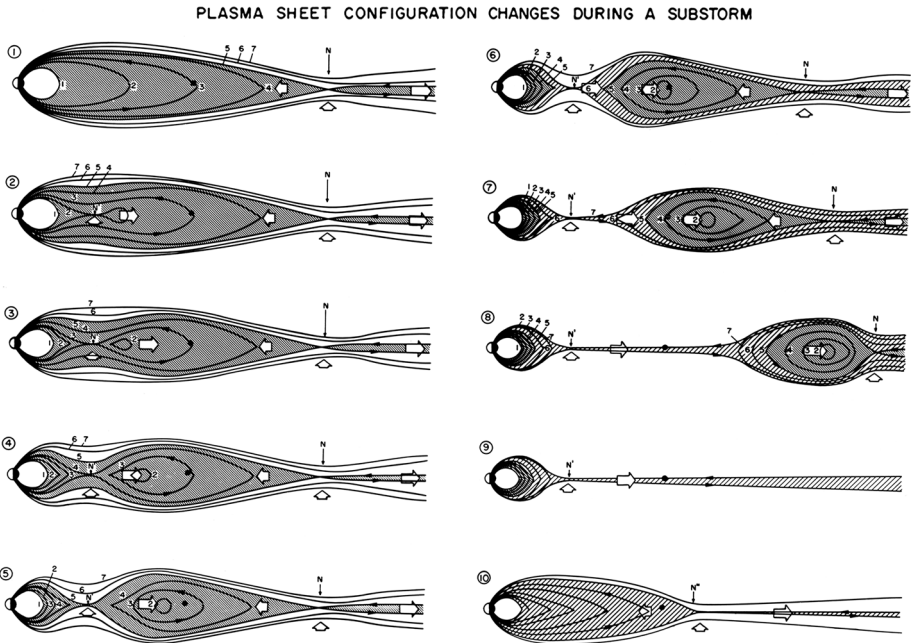
Fig. 14 Substorm sequence in the noon-midnight meridian plane; after Hones (1979). During the substorm growth phase the tail stretches and thins (*1*), until reconnection in the near tail (*2*) leads to the formation of a near-Earth neutral line and growth and ejection of a plasmoid (*3–8*). The departing plasmoid leaves behind a thin "post plasmoid plasma sheet" (*7–9*). During recovery the near-tail plasma sheet refills and the neutral line retreats tailward (*9–10*)

event-specific terminology, such as "flow bursts" (e.g. Kronberg et al. 2008 at Jupiter) and "plasmoid ejections" (e.g. Jackman et al. 2007 at Saturn).

Regardless of whether the term "substorm" is deemed appropriate for a particular environment, we know that magnetotail dynamics can encompass some or all of the following features: a stretching or compression of the magnetic field (from solar wind driving and/or rotational stresses) followed by a dipolarization, fast plasma flows that are predominantly planetward in the near tail, and the ejection of plasmoids into the more distant tail. These physical processes, as well as other aspects of magnetotail dynamics, are addressed in more detail in Sects. 4.3–4.8, following the description of a minimal substorm model, which permits inferring basic statistical properties of substorm occurrence without detailed knowledge of the onset and release physics.

4.2 Minimal Substorm Models

Identifying a substorm as some form of loading-unloading or integrate-and-fire process (e.g., Baker et al. 1996), Freeman and Morley (2004) postulated a minimal substorm model (MSM) with just three rules:

1. The substorm is driven by power from the solar wind P, which causes energy in the magnetotail E to accumulate at a rate:

$$dE/dt \propto P. \tag{6}$$

2. At any given time, there exists an energy state F that the magnetotail would like to exist in. That state is determined by the solar wind boundary condition such that F is some function of P. For simplicity, let us assume a linear relationship:

$$F = C - DP \tag{7}$$

where constant C is a critical energy threshold and constant D is related to a substorm periodicity.

3. The magnetotail is constrained by its magnetic topology from adopting the energy state F until it becomes sufficiently stressed with an energy C. At this point, the magnetotail moves to the lower energy state, F:

$$E \to F \quad \text{when } E \geq C. \tag{8}$$

This transition is identified with the substorm onset and expansion phase, the details of which are argued to be relatively unimportant to the set of substorm onset times $\{t_i\}$.

Integrating Eq. (6) from immediately after the substorm onset at t_i when $E = C - DP(t_i)$ to the next onset at t_{i+1} when $E = C$, we find the set of substorm onset times $\{t_i\}$ to be given by the recursive integral equation

$$\int_{ti}^{t_{i+1}} P(t)dt = DP(t_i) \tag{9}$$

This expresses the fact that the energy dissipated by the ith substorm at time t_i is proportional to the solar wind power input at this time (rule 2) and that this energy must be re-accumulated before the next $(i + 1)$th substorm occurs (rules 1 and 3), as was first explored by Freeman and Farrugia (1995, 1999). For constant $P(t)$ one finds that $t_{i+1} - t_i = D =$ constant and hence substorms occur periodically with period D for constant solar wind power input P, independent of the level of P. This result is supported by observations of cyclic substorms with period of 2–3 h during continuously southward IMF intervals (Huang et al. 2003, and references therein) and may be associated with the modal peak of the general substorm distribution between 2.5 and 3.0 h (Borovsky et al. 1993).

The variability of substorm waiting times is then essentially attributable to the variability of the solar wind power input P. Indeed, solving Eqs. (6)–(8) for the set of simulated substorm onset times $\{t_i\}$ using solar wind measurements made by the NASA Wind and ACE spacecraft over several years each, Freeman and Morley (2004) found that the waiting time distribution was not significantly different from that observed by Borovsky et al. (1993) and, importantly, additional external impulsive triggers are not required (Morley and Freeman 2007; Freeman and Morley 2009).

Thus the substorm cycle may be intrinsically simple, but the nonlinearities in even the minimal substorm model may allow only statistical rather than deterministic prediction of individual substorms (Morley et al. 2009). The application of the MSM idea to Jupiter and Saturn is the subject on ongoing work (Freeman, personal communication).

4.3 Magnetic Reconnection and Substorm Onset

Although the exact cause of substorm onset is still debated (Angelopoulos et al. 2008, 2009; Lui 2009; Sergeev et al. 2012a, 2012b), and there may be more than one, magnetic reconnection seems essential at some stage to release the magnetic energy accumulated in the

Fig. 15 Structure of a thin embedded current sheet (*colour*), generated by adiabatic deformation of a two-dimensional magnetotail equilibrium; after Birn et al. (2009)
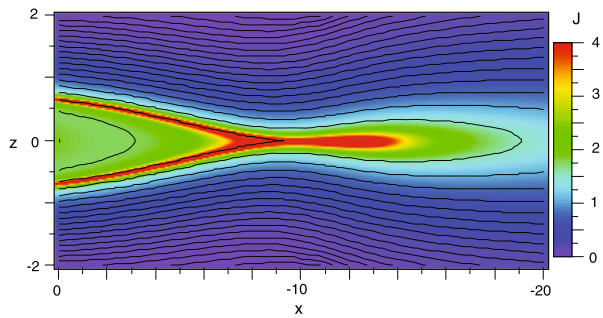
Fig. 16 Electric current density J_y (*color*) and magnetic field lines in a 2-D PIC simulation of thin current sheet formation and reconnection, initiated by a boundary deformation, shortly after the onset of reconnection and plasmoid formation (after Birn et al. 2012a, 2012b)
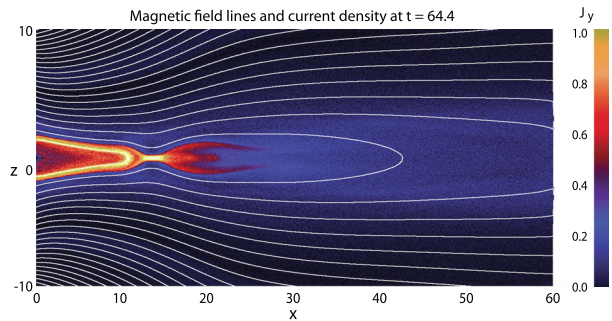
magnetotail during the growth phase through a change in magnetic topology, as evidenced by the change in polar cap area and plasmoid ejection.

An essential element in the onset of reconnection as well as of other activity is current sheet thinning, or the formation of a thin embedded current sheet within the thicker plasma/current sheet. It is now clear from observations at Earth (e.g., Sergeev et al. 1993; Baumjohann et al. 2007; Snekvik et al. 2012) and simulations of current sheet tearing (e.g., Birn et al. 2001), that a thickness of about an ion inertial length or smaller has to be reached to enable significant reconnection. Multi-satellite studies confirmed the predicted kinetic Hall structure of the reconnection site (Runov et al. 2003b). Thin current sheets may become unstable to tearing modes (e.g. Schindler 1974). However in very thin current sheets other smaller-scale kinetic instabilities may also be triggered (Baumjohann et al. 2007), so that it is still unclear whether a collisionless tearing instability is triggered directly or via other instabilities.

In addition to the reduction of the current sheet thickness, the normal, B_Z, component of the magnetic field also needs to be reduced to a very low value to enable collisionless tearing. Studying sequences of magnetotail equilibria deformed adiabatically (meaning both slow and isentropic) through modest, but nonuniform boundary perturbations, Birn and Schindler (2002) demonstrated that the magnetotail may reach a critical state at which neighbouring equilibria that satisfy the constraints cease to exist. The critical state is characterised by the formation of a thin embedded current sheet, which extends from a cusp type structure earthward into two bifurcated sheets, as shown in Fig. 15 (after Birn et al. 2009), with strongly intensified current density and reduced B_Z, which vanishes at the cusp. The increase of the current density within the thin sheet makes it likely, however, that a current-driven instability, such as tearing, may be initiated before the critical state is reached.

Through fully electrodynamic particle simulations, Hesse and Schindler (2001) confirmed that this onset mechanism works as well in a collisionless plasma, although the ideal MHD approximation may not be valid. Figure 16 illustrates a newer, more highly resolved

result from Hesse's particle-in-cell simulations, modified after Birn et al. (2012a), showing magnetic field lines and current density (colour) shortly after the onset of reconnection in a magnetotail configuration. The current intensification and ultimately the onset of reconnection were driven by a finite deformation applied at the top and bottom boundary, compressing the tail more strongly in the near tail.

The onset of reconnection need not immediately be fast. Using 3D resistive MHD simulations of magnetotail reconnection, Birn et al. (2011) showed that a transition from slow to fast reconnection occurred when reconnection proceeded from plasma sheet to lobe field lines. The main effect causing the increase in reconnection rate was apparently not the parametric influence of an increase of the characteristic Alfvén speed but rather the reduction of the entropy content of closed flux tubes, measured by $\int P^{1/\gamma} ds/B$, caused by plasmoid ejection and the drastic reduction of the plasma pressure on lobe field lines. This enables ballooning/interchange modes accelerating the collapse of entropy depleted flux tubes.

The problem of what drives magnetotails to instability has far-reaching implications beyond magnetospheric physics. However, while the local conditions for the onset of tearing/reconnection or other instabilities are now much better understood, the global conditions that trigger tail instabilities and the local and global conditions that might affect the differences in activity modes are still not understood. The factors determining the length of time that magnetic fields may be stored in the tail and the cause or "trigger" for the onset of unloading remain elusive (Henderson et al. 1996; Lyons et al. 1997; Hsu and McPherron 2004; Liou 2007).

A major reason for the remaining uncertainty is the fact that the connections between ground signatures and tail signatures and specifically between the initial arc brightening, generally taken as the earliest ground signature of substorm onset (Akasofu 1964, 1968), and the associated tail feature(s), are not well understood. Since this may have important consequences for the application of substorm onset models to other planets, it is discussed further in Sect. 5. Recent studies (Kepko et al. 2009; Nishimura et al. 2010; Zesta et al. 2011) showed that auroral forms, attributed to earthward flow channels in the tail, might propagate from the poleward boundary equatorward towards the onset location prior to onset and presumably trigger the arc brightening and subsequent auroral expansion. Other ground signatures accompanying the initial brightening are azimuthal structures ("beading"), taken as an indication of ballooning modes. It is not clear, however, whether such pre-onset signatures have a causal effect on the main onset or are just accompanying signatures.

Another open question concerns the role of external, i.e. solar wind, conditions in triggering substorm onset. A number of studies concluded that roughly half of all substorms may be triggered by a sudden change in solar wind properties, most notably a northward turning of the IMF (e.g., Lyons 1996; Milan et al. 2007). However, more recent analyses (Freeman and Morley 2009; Newell and Liou 2011) suggest that IMF triggering may not be as significant as previously envisioned. Section 4.2 illustrated that major statistical occurrence properties can be modelled without invoking external triggering.

Substorm onset in the geomagnetic tail is typically accompanied by energetic particle flux increases, documented extensively by geosynchronous observations (e.g., Lezniak et al. 1968; Parks and Winckler 1968; Arnoldy and Chan 1969; Baker et al. 1978). These can be attributed primarily to the acceleration by the impulsive electric field associated with the field collapse and dipolarization (for a recent review, see Birn et al. 2012b), causing not only flux increases but also significant changes in composition (Nosé et al. 2000a, 2000b). This is discussed further in Sect. 4.4.

Studies on the energetic ion composition at Jupiter also reveal pronounced changes during magnetotail reconnection (Radioti et al. 2007). Particularly, the observations at Jupiter

show that the relative abundance ratios of S/O, O/He and S/He are more enhanced at the pre-dawn sector along the orbits where Galileo observed several signatures of tail reconnection. Radioti et al. (2007) demonstrated that heavy ions are more efficiently energized by the electric field, which is induced by the time-varying magnetic field during magnetotail reconnection, in analogy to the terrestrial case (Delcourt et al. 1997; Nosé et al. 2000a, 2000b). Similar studies at Saturn and Mercury are the subject of future work.

4.4 Plasma Flows and Dipolarizations

One of the key dynamic phenomena in the terrestrial magnetotail is the occurrence of Bursty Bulk Flows (BBFs), sporadic bursts of high speed flow in the plasma sheet which transport magnetic flux, mass and energy. Angelopoulos et al. (1992a) defined a BBF as ∼10 minutes of enhanced plasma velocity (arbitrarily chosen as $v > 400$ km/s in their survey), containing within it individual peaks in velocity of duration ∼1 minute which they termed flow bursts. Bulk flows observed within ∼17 R_E of Earth are almost always directed planetward and they are more often observed during geomagnetically disturbed times (Angelopoulos et al. 1994) but occur also in the absence of substorm signatures on the ground. The cross-tail extent of bulk flows has been estimated using multi-spacecraft datasets to be ∼3–4 R_E (Nakamura et al. 2004; Walsh et al. 2009). BBFs have been shown to contribute in excess of 75 % of the earthward transport of mass, energy and magnetic flux in the central plasma sheet (Angelopoulos et al. 1992b).

Earthward propagating flow bursts typically drive "dipolarization fronts" (e.g. Nakamura et al. 2002; Runov et al. 2009), sharp increases in (northward) B_Z, which are often preceded by a brief reduction or even southward turning of B_Z (e.g., Ohtani et al. 2004; Schmid et al. 2011), and are observed ∼1 minute after the commencement of the plasma flow itself (Ohtani et al. 2004). They have an average thickness of the order of the ion inertial length (Sergeev et al. 2009; Schmid et al. 2011; Runov et al. 2011) and can propagate in excess of 10 R_E through the magnetotail (Runov et al. 2009).

Closer to Earth, more persistent dipolarizations are observed (e.g. Nakamura et al. 2004; Walsh et al. 2009), commonly in association with substorms. These dipolarizations, which may expand tailward and azimuthally (e.g., Jacquey et al. 1991; Baumjohann et al. 1999), may be the consequence of stopping of single or multiple flow bursts and associated flux pile-up (Hesse and Birn 1991). An alternative interpretation holds that these events are caused by "current disruption" in the near tail, not related to plasma flows (Lui 1991, 2009).

A widely accepted explanation of earthward propagating fast bulk flows in the terrestrial tail is that they are entropy-depleted flux tubes, or plasma bubbles (Pontius and Wolf 1990; Chen and Wolf 1993). These result from reconnection, and their plasma content is reduced by plasmoid severance and ejection and propagation of reconnection to the low-pressure lobes (Birn et al. 2004a, 2006; Sitnov et al. 2005, 2009), leading to pressure and density depletion (e.g. Sergeev et al. 1996b; Raj et al. 2002; Forsyth et al. 2008; Walsh et al. 2009). They propagate to Earth subject to a magnetic buoyancy force associated with interchange instability (Chen and Wolf 1993; Wolf et al. 2009, 2012a, 2012b) and are shown to stop at a location in the tail at which the entropy of the depleted flux tube matches that of its surroundings (Dubyagin et al. 2011), so that flows with a larger entropy depletion will stop closer to the Earth than those with a smaller entropy reduction, consistent with MHD simulations of depleted flux tubes (Birn et al. 2009).

Earthward flow bursts and dipolarization fronts are typically associated with tailward flows at the flanks of depleted flux tubes (Walsh et al. 2009; Keiling et al. 2009). Additionally, Sergeev et al. (1996b) noted a shear in the magnetic field at the leading edge of a fast

Fig. 17 Sketch of the terrestrial substorm current wedge. From McPherron et al. (1973)
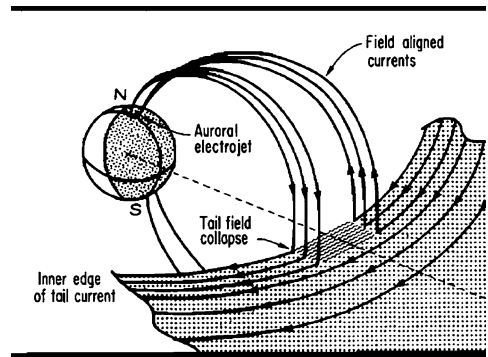
flow, indicating the presence of field-aligned currents, which have indeed been detected by Cluster (Snekvik et al. 2007). Dynamically, the magnetic field distortion can be attributed to flow diversion or vortex flow patterns at the edges of the flow burst, which shear or twist magnetic flux tubes and thereby generate field-aligned currents (Birn and Hesse 1996; Birn et al. 2004a; Keiling et al. 2009), similar to the field-aligned currents in the substorm current wedge picture (McPherron et al. 1973) shown in Fig. 17. The outward field-aligned current at the duskward edge of a flow burst is associated with precipitating electrons, which have been identified as the cause of auroral streamers (e.g., Fairfield et al. 1999; Lyons et al. 1999; Sergeev et al. 1999; Nakamura et al. 2001).

Reflections at an earthward propagating sharp front may be the cause of enhanced ion fluxes preceding a front (Zhou et al. 2010, 2011). In addition, kinetic waves may play a role: Lower-hybrid waves generated at the front of the bulk flows could lead to field-aligned electron acceleration preceding a front (Zhou et al. 2009; Khotyaintsev et al. 2011) while whistler waves behind a front may be the cause of pitch angle scattering, reducing the perpendicular anisotropy expected from betatron acceleration (Khotyaintsev et al. 2011).

At Jupiter, data from the Galileo energetic particle detector have revealed evidence for both tailward and planetward plasma flows associated with magnetic reconnection (e.g. Kronberg et al. 2008). It has been proposed that the reconnection signatures observed in the Galileo magnetometer data are analogous to terrestrial BBFs, rather than terrestrial substorms, which involve a system-wide field reconfiguration, due to their limited azimuthal extent, ∼1–2 % of the tail width (Vogt et al. 2010).

At Saturn, the vast majority of bipolar magnetic field signatures observed thus far correspond to tailward-moving structures (e.g. Jackman et al., 2007, 2008b, 2011). Three dipolarizations of the field have been reported thus far: the first by Bunce et al. (2005) which they suggested to be linked to solar wind compression-induced tail reconnection, and a second by Russell et al. (2008). A third example of a field dipolarization as measured by Cassini was reported by Jackman et al. (2013), and postulated to be related via a substorm current wedge-like paradigm to discrete auroral signatures. In situ evidence of tailward plasma flow following reconnection (McAndrews et al. 2009), planetward return flow via the Vasyliunas cycle (Masters et al. 2011b), and inward flow in the dusk sector (Thomsen et al. 2013) has been presented at Saturn. Chen and Hill (2008) found evidence of interchanging hot and cold plasma populations, with channels occupying a small fraction (∼5–10 %) of the available longitude space. In addition, Mitchell et al. (2005, 2009) presented observations of large-scale injections from the outer magnetosphere, believed to be associated with tail reconnection. However, a unified picture of the links between interchange, injections and reconnection remains a topic for future work.

At Mercury, high speed flow cannot be observed by MESSENGER because of obstructions to the field of view of the Fast Imaging Plasma Spectrometer and thermal constraints on spacecraft pointing. However, multiple examples of dipolarization of the field have been found in the magnetic field observations (Sundberg et al. 2012b). The Mercury dipolarizations have fast rise times for the B_Z component of the field, like at Earth, but they usually decay after ∼5–10 s.

4.4.1 Energetic Particles

Propagating dipolarization fronts, as well as more permanent dipolarizations in the terrestrial magnetotail, are typically accompanied by energetic particle flux increases (e.g., Sergeev et al. 2009). Energetic electrons are also found in association with tailward flows from near-tail reconnection sites. A likely acceleration mechanism is the electric field pulse propagating with the spatially localized flows or associated with the local dipolarization. This may lead to betatron and Fermi acceleration of electrons (Birn et al. 1997a, 2004a, 2004b; Li et al. 1998; Ashour-Abdalla et al. 2011) as well as nonadiabatic acceleration of protons and heavier ions (Birn et al. 1997b, 2004b).

Particularly, energetic particle fluxes of ions of ionospheric origin, such as O^+, are observed to be more enhanced than those of H^+ ions in the near-Earth tail during dipolarization events associated with substorms (Nosé et al. 2000a, 2000b). Based on a model of dipolarization by Delcourt et al. (1997), Nosé et al. explained the strong enhancements of O^+ by nonadiabatic acceleration from the impulsive electric field. Additionally, Mitchell et al. (2003) reported an increase in the oxygen energetic neutral atom (ENA) intensity accompanied with weaker hydrogen enhancements at each substorm onset during geomagnetic storm periods. Again, nonadiabatic heating was suggested as a possible mechanism for the observed enhancements, according to which oxygen ions whose gyroperiod is comparable to the timescales of dipolarization are more efficiently accelerated (Delcourt 2002).

4.5 Current Sheet Flapping

At Earth, magnetotail flapping, the up-and-down wavy motion of the current sheet is now a well-established phenomenon (Sergeev et al. 1998; Zhang et al. 2002; Sergeev et al. 2003; Runov et al. 2005b). It has been shown that the waves, with periods of several minutes travel from the centre of the magnetotail to the flanks. The flapping motion of the magnetotail is specific in that it makes the spacecraft cross the centre of the current sheet multiple times; showing reversals of the X_{GSM} coordinate of the magnetic field. Sergeev et al. (1998) found that there was a correlation to the plasma velocity perpendicular to the plane of the current sheet (V_Z, GSM) and the dB_X, GSM/dt. The magnetotail moves up-and-down at velocities of some hundreds km/s. From the AMPTE/IRM data it was found that flapping was more intense during periods of fast flows in the magnetotail, indicating that this possibly is a substorm related process.

Magnetotail flapping, similar to that observed in the Earth's tail, is also observed at the giant planets, and we refer the reader to Volwerk et al. (2013) for a detailed review of comparative magnetotail flapping at Earth, Jupiter and Saturn. At the time of writing, the MESSENGER data from Mercury are currently being analysed to search for evidence of current sheet flapping.

Fig. 18 Schematic illustration showing the magnetic field signatures that would arise following a spacecraft track through and near an idealised plasmoid. After Slavin et al. (1989)
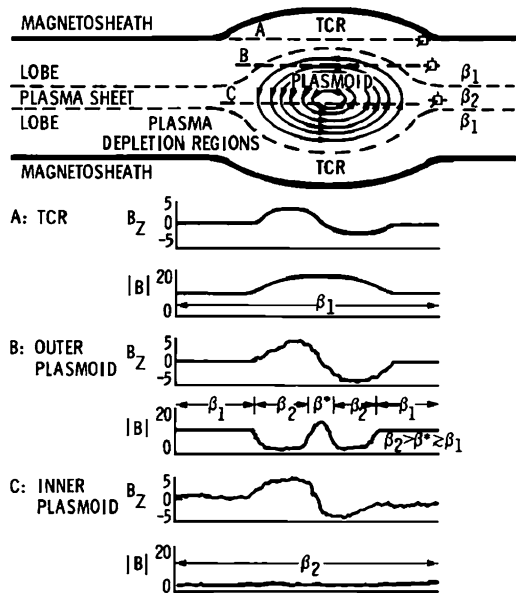
4.6 Plasmoids and Travelling Compression Regions

Following reconnection in a planetary magnetotail, part of the plasma sheet may break off and form what is known as a "plasmoid". In a two-dimensional view (Hones 1976, 1977), plasmoids are magnetic islands which, once disconnected from the planet, are free to move downtail, releasing mass from the magnetosphere. As they do so, magnetic forces within the structure can act to reduce the dimensions in the radial direction while the structure can thicken in the north-south-direction (e.g. Slavin et al. 1989, 1993). Thus plasmoids may produce "bulges" in the tail. Lobe field lines in the vicinity of plasmoids then drape around the bulges as they move down tail, resulting in the formation of signatures known as "travelling compression regions" (TCRs) (Slavin et al. 1984b). Figure 18 shows the magnetic field signatures that would arise following a spacecraft trajectory through and near an idealised plasmoid. This figure is for the case of the Earth, but the field directions merely reverse for the oppositely-directed planetary fields of Jupiter and Saturn. Plasmoids and TCRs are identified from magnetic field data by a deflection in the north-south component of the field. The sense of the field deflection tells us which side of the reconnection site the spacecraft is on. We note that a single reconnection episode can result in the release of multiple plasmoids. The presence of planetward and tailward moving structures can also be indicative of multiple X-lines, as illustrated schematically in Fig. 19.

Where are plasmoids released from? By looking at the sense of field deflection in large catalogues of plasmoids and TCRs, it is possible to estimate the statistical position of the X-line. This technique was employed by Imber et al. (2011) at Earth, who found a statistical X-line position of (X GSM, Y^* GSM) = $(-30\ R_E, 5\ R_E)$, where Y^* includes a correction for the solar aberration angle. At Jupiter, Vogt et al. (2010) used statistics from 249 magnetic field reconnection signatures to place the separatrix at $\sim$60–90 R_J at dawn, extending to $\sim$90–120 R_J pre-midnight. To date there are insufficient numbers of plasmoids and TCRs observed at Saturn and Mercury to enable us to place constraints on the likely reconnection site from magnetic field measurements alone. For the case of Saturn, Energetic Neutral Atom
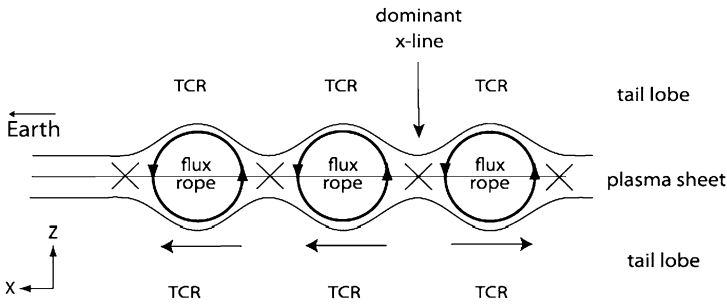
Fig. 19 Schematic illustrating the formation of multiple X-lines, leading to planetward and tailward-moving TCRs. From Imber et al. (2011)

(ENA) measurements (discussed in Sect. 5.4 below) can shed more light on this topic. At Mercury, results from the flybys of the MESSENGER spacecraft indicate an X-line position very close to the planet, $X = -2.8\ R_M$ for the southward IMF during the second flyby and a closer $-1.8\ R_M$ for the variable polarity IMF B_z and tail loading-unloading events during the third flyby (Slavin et al. 2010). Further exploration of this location awaits a statistical analysis of the orbital data. In Fig. 20 we show the locations of reconnection signatures measured *in situ* at Mercury, Earth, Jupiter and Saturn. We note that the figure at Jupiter represents a "complete" list of all examples reported to date from magnetometer data, while the Saturn figure shows the results of the most recent survey of tail data at Saturn which unveiled 99 reconnection events (Jackman et al. 2014). The Mercury plot shows only examples from the first three flybys of the MESSENGER spacecraft, and at the time of writing work is ongoing to compile a list of the many tens and hundreds more examples that have been uncovered during the MESSENGER orbits (DiBraccio, personal communication). The terrestrial example is just a brief snapshot of typical locations of near-planet events. There are many more! For Jupiter and Saturn at least, Fig. 20 illustrates the spacecraft coverage in the magnetotail and the region where reconnection can be active. The coverage by spacecraft in the Earth's tail means that in the terrestrial case it is possible to have in situ knowledge of not only the near-planet X-line, but also distant reconnection site(s). For the other planets, coverage has been restricted to a radial range that just encompasses a near-planet reconnection site.

What is the internal structure of plasmoids? Direct encounters with plasmoids involve the spacecraft penetrating the interior of the structures, and through this, information can be gleaned about the nature of the interior magnetic field topology. Plasmoids can be classified into two main groups: loops and flux ropes, and Fig. 21 illustrates schematically the expected topology and associated field signatures from such structures. Loops have a simpler field structure and can be identified by a localized dip in |B| as the spacecraft passes close to the centre. Flux ropes, on the other hand, are composed of helical, twisted field lines. These have what is known as a "core field", whereby the total field strength at the centre can be almost twice that in the external lobes (Sibeck et al. 1984; Slavin et al. 1995). Moldwin and Hughes (1992) found a strong link between the polarity of the B_Y component inside flux ropes and the polarity of the IMF B_Y (which in turn has been found to correlated with the dawn-dusk magnetic field component in the tail (Hughes and Sibeck 1987). However, later studies which analyzed much larger ensembles of plasmoid-type flux ropes have found that this correlation between the direction and intensity of the core field and the IMF By field component is generally weak (Slavin et al. 2003). Most
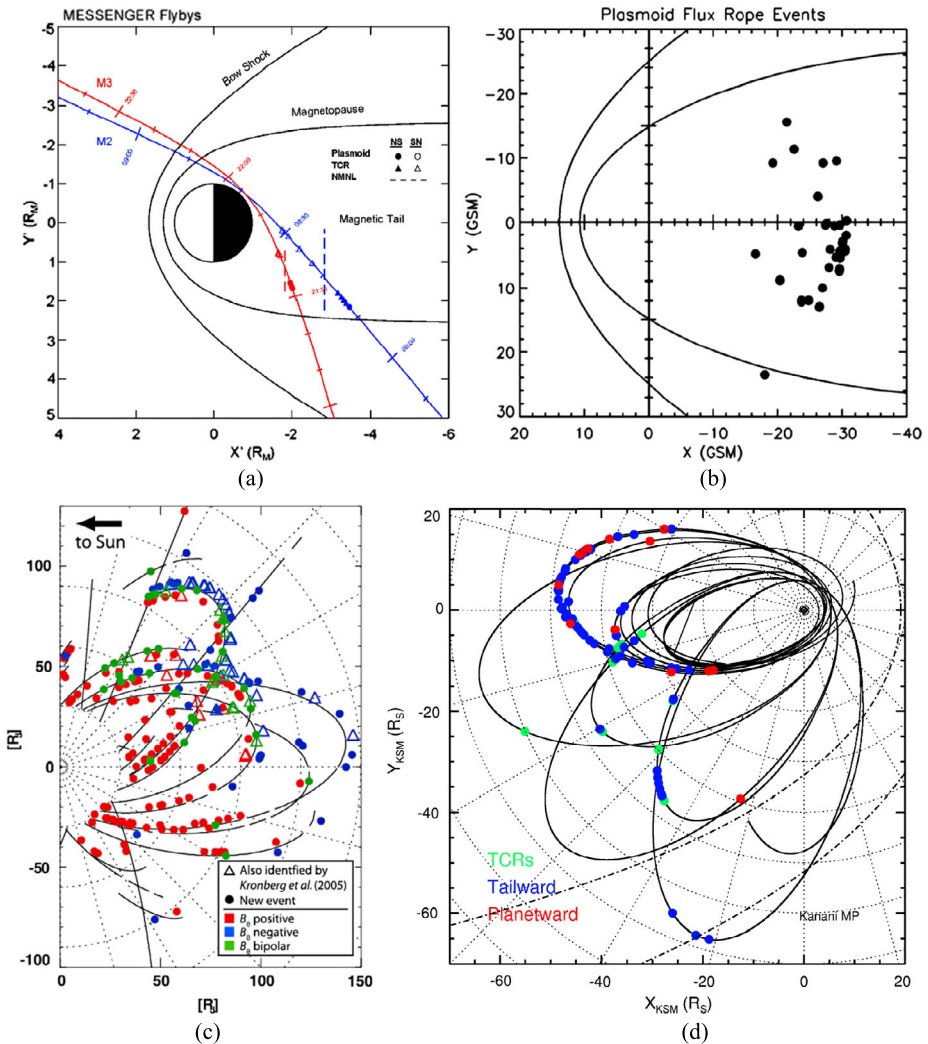
Fig. 20 Distribution of in situ observations at different planets: (**a**) Plasmoids and TCRs observed during the MESSENGER flybys at Mercury (Slavin et al. 2012a, 2012b), (**b**) 38 plasmoids seen by Geotail during just one season of 1998–1999 (Slavin et al. 2003), (**c**) 249 magnetic reconnection events from Galileo (Vogt et al. 2010), (**d**) 99 reconnection events (69 plasmoids, 17 TCRs and 13 planetward-moving events) identified using Cassini data at Saturn (Jackman et al. 2014)

recently, Teh et al. (2014) examined the core field of 13 flux ropes using the Cluster spacecraft and found that the correlation between the core field and the IMF B_Y depends on the guide field, with no external IMF B_Y influence on tail flux rope geometry when the guide field is weak (<10 % of the reconnecting field). At Mercury, the initial MESSEN-GER flybys indicated the presence of loop-like plasmoids (Slavin et al. 2012a), however subsequent in-orbit observations have revealed many flux ropes (Slavin et al. 2012b). Analysis of the interior morphology of plasmoids at Saturn and Jupiter is ongoing but preliminary results indicate that loop-like plasmoids are most common. This has been preliminar-
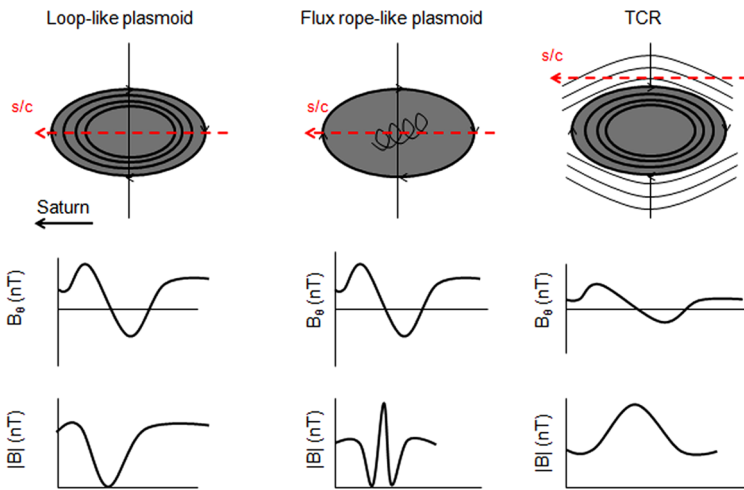
Fig. 21 Schematic illustrating the topology and field signatures associated with loop-like and flux rope-like plasmoids for Saturn. B_θ is the positive southward, and the field directions shown reverse for Earth and Mercury due to the oppositely directed planetary dipoles. From Jackman et al. (2014)

ily interpreted as related to the weakness of the upstream IMF and the associated inability of the solar wind to shear the tail lobes to create significant B_Y (Jackman et al. 2014; Vogt et al. 2014).

One can estimate the size of plasmoids and TCRs to gain an understanding of the size of the regions affected by reconnection. A simple estimate of the length of plasmoids can be obtained by multiplying the duration of the events by the speed at which the structures are travelling. However, we note plasmoids may be strongly tilted in the X–Y plane, and thus this simple length estimation must be treated with caution (e.g. Slavin et al. 2003; Kiehas et al. 2012). At Earth, typical lengths range from 5–35 R_E with the smaller plasmoids being observed in the near-tail, $\sim$15 to 30 R_E, and the larger ones in the distant tail beyond $X \sim -100$ R_E (Slavin et al. 1993, 1995, 2003; Ieda et al. 1998; Imber et al. 2011). At Jupiter, Kronberg et al. (2008) presented statistics on the length of Jovian plasmoids, based on measurements taken using the Galileo energetic particles detector. They found a typical length of $\sim$9 R_J. More recently, Vogt et al. (2014) examined the length of 43 Jovian plasmoids identified with the Galileo magnetometer and found a mean length of $\sim$3 R_J. At Saturn, the average plasmoid duration based on 69 examples is $\sim$17.71 min (Jackman et al. 2014). Plasma data were available for a subset (29) of these plasmoids, with speeds ranging from 144–1240 km/s, which yield plasmoid lengths of 0.44–23.9 R_S, with an average of 4.28 R_S. At Mercury, plasmoids and TCRs have been observed with typical durations of $\sim$1–3 s, suggesting diameters of $\sim$500–1500 km (Slavin et al. 2012a).

4.7 Diffusive Processes

Estimates of the typical plasmoid sizes at the outer planets show that these plasmoids cannot account for the expected mass loss rates and therefore play a relatively minor role in the overall magnetospheric mass transport. For example, Bagenal (2007) assumed a typical plasmoid is a disk with a 25 R_J diameter and 10 R_J height, with density 0.01 cm^{-3}, and calculated that releasing one plasmoid per day (higher than the observed 2–3 day recurrence period) is equivalent to a mass loss rate of $\sim$30 kg/s. More recently, a survey of

plasmoids identified with the Galileo magnetometer found a mass loss rate ranging from 0.7–120 kg/s (Vogt et al. 2014). Both studies indicate that the estimated rate of mass release supported by the observed plasmoids at Jupiter is far lower than the rate of mass input from Io (500–1000 kg/s). Several studies at Saturn have also explored the issue of how to balance the average of ∼100 kg/s estimated to be loaded into Saturn's magnetosphere by Enceladus (Bagenal and Delamere 2011). Thomsen et al. (2013) estimate a mass loss rate of 34 kg/s based on plasma data from Cassini, while Jackman et al. (2014) estimate an average rate of 2.59 kg/s. Overall the numbers indicate a strong mass imbalance at both Jupiter and Saturn.

What other mechanisms can account for the required mass loss rate? Bagenal (2007) discusses three possible explanations. The first is a diffusive "drizzle," similar to an interchange motion (Southwood and Kivelson 1987, 1989) across the highly stretched field lines in the dusk-to-midnight local time sector, where the plasma sheet is likely to be highly unstable (Kivelson and Southwood 2005). Other potential mechanisms for mass loss include a quasi-steady small-scale reconnection of small plasmoids occurring simultaneously across the magnetotail, or a planetary wind. Further study and observational evidence, including multi-point measurements from across the magnetotail, is needed to distinguish between these proposed loss mechanisms.

Although plasmoid ejection seems to play a relatively minor role in mass transport at Jupiter and Saturn (hence opening up the possibility of important diffusive processes), it appears that tail reconnection is an important method of magnetic flux transport. For example, analysis of the observed plasmoids at Jupiter suggests an average flux closure rate of ∼7–70 GWb/day (Vogt et al. 2014), which closely matches the estimated rate of average flux opening through dayside reconnection, 18 GWb/day (Nichols et al. 2006). Meanwhile, estimates suggest the average reconnection event at Saturn closes ∼0.26–2.2 GWb of previously open flux (Jackman et al. 2014). When compared to the typical ∼15–50 GWb of open flux estimated from auroral images (Badman et al. 2005), this indicates that tail reconnection can close a significant fraction of the total flux at Saturn.

4.8 Global Models

As discussed above, reconnection in the magnetotail is an important process that not only results in topological changes in the magnetospheric configuration, but also generates products, such as BBFs, dipolarization fronts, and plasmoids. In a solar wind-dominated magnetosphere such as Mercury, magnetotail dynamics are strongly influenced by the strength and orientation of the upstream IMF. By contrast, in a rotationally driven magnetosphere, such as those of Jupiter and Saturn, the interplay between internal processes (e.g., planetary rotation and internal plasma sources) and external processes associated with the solar wind complicates the way in which magnetotail reconnection occurs. In the absence of continuous monitoring of tail conditions by spacecraft, global simulation models play an important role in providing global context for interpreting localized sparse spacecraft observations and in enabling the visualisation of the response of the magnetosphere to changing conditions. Such models have been of particular benefit when looking at planets such as Mercury, Jupiter and Saturn, where data is scarcer than in the relatively well-sampled terrestrial environment. In the following sections we explore three types of simulation; magnetohydrodynamic (MHD), multi-fluid and kinetic. MHD models compute the average temperature, density, and velocity of all ion species by solving a single energy, continuity and momentum equation. Multi-fluid models, an extension of classical MHD, solve these equations for each ion species in the simulation and track the dynamics of individual plasma fluids and include mass-dependent asymmetric behaviour and forces arising from pressure gradients. Kinetic simulations treat ions/electrons kinetically, with the gyromotion of individual particles solved for.
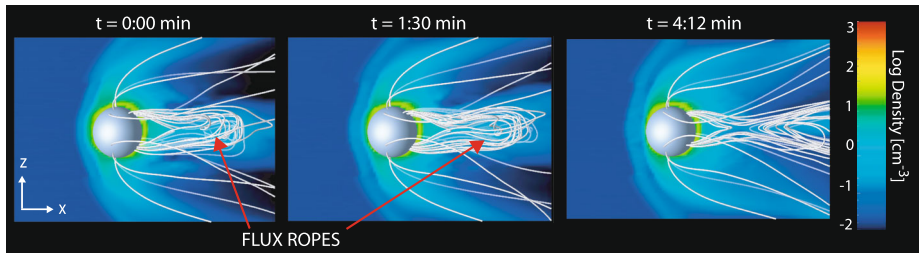
Fig. 22 Time evolution of the formation of a flux rope-like plasmoid in Mercury's tail from a multi-fluid simulation. The view is of the noon-midnight meridian in all panels and field lines are overlaid on the density of the He$^+$ species. From Kidder et al. (2008)

The solar-wind-dominated magnetosphere of Mercury provides a fascinating environment for simulation. The large-scale structure of Mercury's magnetosphere and its response to solar wind driving have been modelled by a number of authors (Kabin et al. 2000; Ip and Kopp 2002; Kallio and Janhunen 2003; Kabin et al. 2008; Kidder et al. 2008; Benna et al. 2010; Travnicek et al. 2010; Wang et al. 2010). Kabin et al. (2000) demonstrated that a solar wind velocity of 1100 km s^{-1} was required to obtain direct impact of solar wind protons onto the regolith, and as such, this was a rare occurrence. The multi-fluid simulation of Benna et al. (2010) employed solar wind inputs present at the time of the first MESSENGER flyby on January 14, 2008. They found the ion impact rate is about four times higher at the northern versus southern cusp, providing a possible explanation for the observed north-south asymmetry in exospheric neutral sodium.

Several of the simulations produce plasmoids in the hermean tail. For example, running under conditions of southward IMF, conducive to reconnection at Mercury's dayside magnetopause, Travnicek et al. (2010) found a plasmoid which yielded a bipolar signature in B_Z and a local minimum in the total field strength, suggesting a loop-like plasmoid. Kidder et al. (2008) also used a 3-D multifluid simulation to predict Mercury's magnetospheric response to forcing from the solar wind (Fig. 22). In this case they observed the formation of a magnetotail flux rope-type plasmoid with a core field of ~20–25 nT.

By contrast with Mercury, Jupiter's huge rotation-dominated magnetosphere provides another unique modelling challenge. At Jupiter, global MHD simulations have focused on the dynamics in the magnetotail. For example, Fukazawa et al. (2005, 2010) have shown plasmoid release with ~30–100 hour recurrence periods that varied with solar wind conditions. An example of one such plasmoid from their simulation is shown in Fig. 23. A 2–3 day periodicity has been observed in flow bursts, auroral spots, and reconnection events at Jupiter (Krupp et al. 1998; Woch et al. 2002; Kronberg et al. 2007; Radioti et al. 2008; Vogt et al. 2010) and this period was proposed to be related to the time scale for internally-driven mass loading and release process (Kronberg et al. 2007). However, the 2–3 day periodicity is seen only for specific intervals or orbits, and does not appear to be statistically significant (Vogt et al. 2010). The simulation results suggest that it is possible that the solar wind modulates this characteristic period, which could explain why the strong periodicity is only observed during specific intervals. There are as yet few published results from multi-fluid models at Jupiter. However, Winglee et al. (2009) have used a multi-fluid/multi-scale model to couple Io's plasma to the Jovian magnetosphere. They demonstrate that the injection of plasma at 1000 kg/s from an extended source is able to sustain a plasma torus with overall densities comparable to inferred density profiles out to several Jovian radii. The
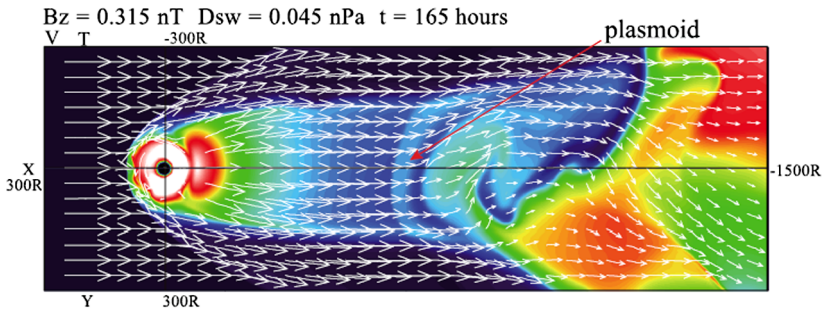
Fig. 23 Output of a Jovian simulation showing the plasma temperature and flow vectors in the equatorial plane. The location of a plasmoid is indicated by the *red arrow*. From Fukazawa et al. (2010)

application of similar multi-fluid models to the Jovian system remains the subject of future work.

At Saturn, several global MHD models have been used to investigate the global configuration of the magnetosphere, its interaction with the solar wind and reconnection dynamics in the tail (Hansen et al. 2000, 2005; Fukazawa et al. 2007; Zieger et al. 2010; Jia et al. 2012a, 2012b). Although differing in the assumptions about the internal plasma sources and the imposed solar wind conditions and in the way in which the large-scale magnetosphere-ionosphere coupling is handled, those global simulations all feature plasmoid formation in the tail. Two types of tail reconnection leading to plasmoid formation have been identified in the global models. The first is the so-called "Vasyliunas-cycle" reconnection (Vasyliunas 1983) in which the centrifugal acceleration of mass-loaded flux tubes imposed by the planet's rapid rotation leads to reconnection on closed field lines forming plasmoids (e.g., Jia et al. 2012b). Plasmoids formed through this process are found to exhibit a loop-like structure with enhanced plasma density and very weak core fields inside. The release of plasmoids provides a means of removing plasma from the magnetosphere.

In addition to the "Vasyliunas-cycle", another type of reconnection found in global simulations of Saturn's magnetosphere involves "open" field lines (referred to as the Dungey-cycle). When the magnetosphere is open, i.e., the polar cap and the tail lobes are populated with open fluxes that are produced by dayside magnetopause reconnection, plasmoid formation in the tail involves reconnection between open field lines from the lobes. Figure 24 shows the dynamical consequences of plasmoid formation seen in a global simulation (Jia et al. 2012b) where the IMF is in a Parker spiral direction, an IMF orientation typically seen at Saturn (Jackman et al. 2008a). Different from the plasmoid formed purely through the Vasyliunas-cycle, the plasmoid formed in this case usually displays a flux rope-like structure with strong core fields (Fig. 24a). Due to the properties of the lobe plasma (low plasma density and high Alfvén speed), the lobe-lobe reconnection associated with plasmoid release not only produces tailward fast flows that accelerate the plasmoid downtail but also generates hot flux tubes returning to the dayside magnetosphere (Fig. 24b), thereby generating stronger global impacts on the magnetosphere and ionosphere compared to that imposed by the Vasyliunas-cycle directly. The subsequent motion of those rapidly moving return flux tubes through the magnetosphere can generate strong disturbances, such as intensification of field-aligned currents (FACs), in the ionosphere, especially on the dawn side. Such intensification of FACs associated with tail reconnection may produce auroral brightenings in the dawnside ionosphere such as those seen in the aurora observed at Saturn (Clarke et al. 2005; Mitchell et al. 2009).
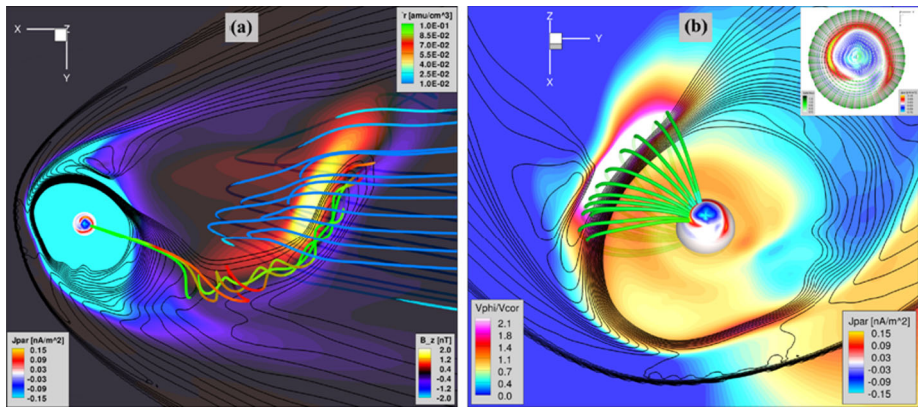
Fig. 24 Plasmoid formation and its associated global dynamics seen in a global simulation (Jia et al. 2012b) during an interval when the IMF is roughly aligned with the Parker spiral. (**a**) 3D structure of the reconnection products seen in the tail. Shown in the background are color contours of B_z (according to the *bottom-right color bar*) and line contours of plasma density in the equatorial plane. Selected field lines showing the magnetic structure of the plasmoid are color-coded with plasma density (according to the *top-right color bar*). The pattern of field-aligned currents in the ionosphere is also shown (mapped to a sphere of radius $4R_S$ for clarity). (**b**) 3D perspective from a viewpoint above the equator in the noon meridian plane of the flux tubes returning from tail reconnection site to the magnetosphere for the same reconnection event shown in (**a**). Plotted in the equatorial plane are color contours of V_{phi}/V_{cor} (ratio of the azimuthal speed to the rigid corotation speed) overlaid with line contours of plasma density. Distribution of field-aligned currents along with unit flow vectors color coded with V_{phi}/V_{cor} in the northern ionosphere are shown in the *top-right insert* as well as in the magnetospheric plot (mapped to a sphere of radius 4 R_S for clarity). *Green traces* show sampled field lines traced through the region of rapidly moving flows in the equatorial magnetosphere

It is clear from the global simulation results that the interplay between the Vasyliunas-cycle and the Dungey-cycle results in a complex way in which tail reconnection occurs in Saturn's magnetotail. Properties of tail reconnection and associated plasmoid release, such as the repetition time and the location of tail X-line, therefore, may depend on both external and internal conditions. Zieger et al. (2010) and Jia et al. (2012b) studied the dependence of plasmoid release on the external solar wind conditions and found that the solar wind dynamic pressure affects the recurrence rate of plasmoid release in the tail, i.e., the release rate becomes higher as the dynamic pressure increases. On the other hand, the mass-loading rate of the internal plasma sources (e.g., Enceladus and its extended neutral cloud) may also influence how tail reconnection occurs and how frequently plasmoids are released in the tail. In the simulation study of Fukazawa et al. (2007) that used a total mass-loading rate >300 kg/s, they found plasmoids are ejected downtail every one hour or so, much more frequently than seen in other global simulations (e.g., Zieger et al. 2010; Jia et al. 2012a and 2012b) that used lower mass-loading rates. Although the differences between different global models remain to be fully understood, the difference in plasmoid ejection rate seen in different models suggests that the mass addition rate of the inner magnetosphere plasma source is also an important factor that may affect the characteristics of plasmoid formation in Saturn's magnetosphere. Further investigations on what controls the plasmoid recurrence rate through both global modeling and analysis of in-situ data are needed to better understand the role of tail reconnection in driving global dynamics in Saturn's magnetosphere.

Multi-fluid simulations have also been used at Saturn to explore the size, composition, speed and location of plasmoids after release (e.g. Kidder et al. 2012). The model shows that plasmoids in Saturn's magnetotail can be externally triggered by both flips in the ori-

entation of the IMF as well as a pulse in the solar wind dynamic pressure. They reproduce the observed hinging of the current sheet in response to the solar wind flow direction, and illustrate thickening and thinning of the current sheet before and during reconnection. They find that plasmoids at Saturn develop in multiple sectors, form at different distances from the planet with varying widths and lengths, and are composed primarily of water group ions.

5 Observing Magnetotail Dynamics Remotely

In addition to studying magnetotail dynamics through *in situ* observations, one can also remotely observe changes in the magnetotail and their effects across the entire magnetosphere. Here we will look at three remote diagnostics of magnetospheric dynamics: auroral changes, radio emissions, and energetic particle effects on neutral atom dynamics.

5.1 Auroral Signatures

Planetary aurorae can act as a giant 'television screen', providing information as to events occurring throughout the magnetosphere, from the innermost regions to the deep magnetotail. Auroral images are particularly useful for study of the outer planets, where multi-point spacecraft observations are unavailable. Here we give a brief overview of the key auroral features associated with magnetotail dynamics. We refer throughout to Fig. 25, which shows examples of "typical" auroral images at Earth, Jupiter and Saturn.

5.1.1 Earth

As detailed above, Earth's magnetospheric dynamics are largely controlled by the solar wind, and this is reflected in the auroral dynamics also. The Dungey cycle as first proposed for Earth was viewed as steady-state, with uniform opening of magnetic flux on the dayside and an equal rate of flux closure in the magnetotail, such that the proportion of open magnetic flux was steady with time. The amount of open flux housed in the magnetotail has direct implications for the main auroral oval emission at Earth, as illustrated schematically in Fig. 26. This figure shows that the magnetic field lines which participate in the Dungey cycle of opening and closing are rooted in the polar ionospheres, with the open-closed field line boundary marking the size of the main oval emission.

Since the original Dungey model, it has subsequently become clear that the system is not in steady state, but rather that the dayside reconnection rate varies as the interplanetary parameters such as solar wind speed and IMF strength and orientation vary (e.g., Milan et al. 2012). As the rates of opening of flux on the dayside and closure of flux on the nightside are unlikely to be instantaneously equal, the proportion of the flux associated with the terrestrial dipole that is open must vary with time, that is

$$\frac{dF_{PC}}{dt} = \Phi_D - \Phi_N \tag{10}$$

where F_{PC} is the open magnetic flux of the polar cap, and Φ_D and Φ_N are the dayside and nightside reconnection rates (Siscoe and Huang 1985). As the amount of open flux waxes and wanes under the operation of day- and nightside reconnection, the area of the polar ionospheres occupied by the open flux increases and decreases, and the auroral ovals move to lower and higher latitudes respectively, giving the name the "expanding/contracting polar cap" (ECPC) paradigm to this conceptual model of solar wind-magnetosphere coupling.

16/12/2000, 14:00

(a)   (b)

2008 day 129, 08:08

(c)
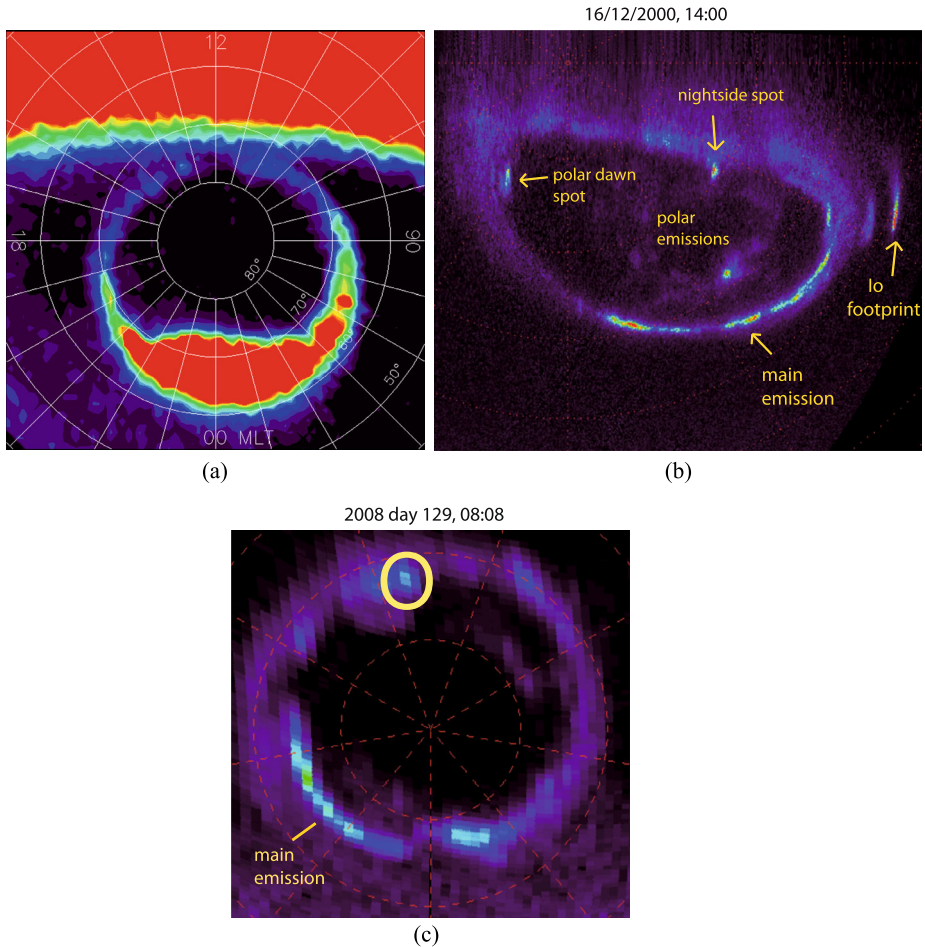
Fig. 25 Polar projections of the aurora at Earth, Jupiter and Saturn illustrating the particular morphologies. (**a**) An image of the northern hemisphere auroras taken by the Wideband Imaging Camera of the Far Ultraviolet instrument (FUV/WIC) at 00 UT on 6th February 2001. The image is projected onto a geomagnetic latitude and local time frame, with noon at the top of the panel, and *concentric circles* showing lines of geomagnetic latitude. The image is shown in false-colour, with *red* indicating bright auroras, except for the band across the top of the image which is a result of dayglow. The image is taken during the expansion phase of a substorm, with the substorm auroral bulge developing on the nightside of the oval. (**b**) Polar projection of the auroral image taken on 16/12/2000 at 14:00 UT at the north pole of Jupiter. The main emission, Io footprint and the polar emissions are indicated. A polar dawn spot and a nightside spot both associated with magnetotail reconnection are indicated. The image is aligned with noon to the bottom, dawn to the left and dusk to the right (adapted from Grodent et al. 2003b). (**c**) UVIS pseudo-image of Saturn's northern polar region for 2008 day 129. The image is aligned with noon to the bottom, dawn to the left and dusk to the right. The main emission is indicated and the *circle* shows a small spot suggested to be associated with dipolarization in the tail (adapted from Jackman et al. 2013)

The variability of the interplanetary medium is such that the dayside rate tends to be low for periods of 1 to 2 h and then high for periods of 1 to 2 h. The nightside reconnection rate does not immediately increase to remove the accumulating open flux during the latter periods, so these correspond to times of rapid expansion of the polar cap. Eventu-
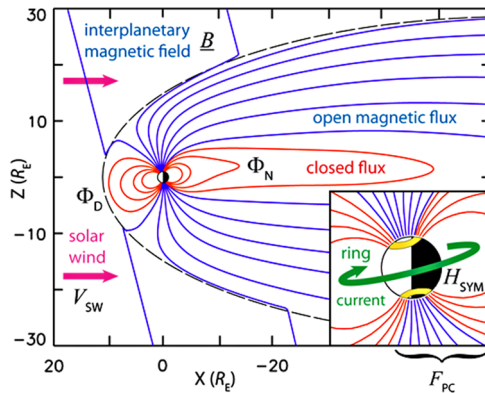
Fig. 26 A schematic diagram of the magnetosphere illustrating the relationship between the magnetotail and the auroral zone. Closed and open magnetic field lines are indicated by *red* and *blue lines*, respectively. Φ_D quantifies the rate at which flux is opened at the dayside, while Φ_N is the rate at which it is reclosed on the nightside. The *inset panel* shows the relationship between the footprints of the open flux FPC and the size of the polar cap, the dim ionospheric regions encircled by the auroral ovals. After Milan (2009)

ally, reconnection in the magnetotail is initiated and occurs rapidly to remove excess open flux, with attendant contractions of the polar cap. These expansions and contractions have now come to be recognized as the substorm growth and expansion phases (Lockwood and Cowley 1992; Milan et al. 2007, 2008). The trigger for the onset of nightside reconnection is not presently understood, but is thought to be in part associated with increased solar wind pressure on the magnetotail as the lobes flare to accommodate the increasing open flux (e.g. Slavin et al. 1983, 1985b); this can be seen as enhancements of the lobe field strength during periods of increased F_{PC} (Milan et al. 2008). The overall size of the polar cap also appears to depend on the intensity of the ring current, suggesting that the nightside reconnection rate is modulated by the associated magnetic perturbation (Milan et al. 2008; Milan 2009). Thus the size of the main auroral oval at Earth directly reflects the amount of flux present, expanding and contracting in concert with the addition of open flux via dayside reconnection and the closure of open flux via nightside reconnection. This ECPC paradigm is a key feature of the auroral physics at Earth.

The source of additional, more localized, bright auroral features is less well established. The enhanced electron precipitation associated with such features can be attributed to electron heating, an increase in (outward) field-aligned currents, and/or field-aligned electric fields, the latter particularly for auroral arcs. As discussed in Sect. 4.3 the association of outward field-aligned currents, generated at the duskward edge of earthward flow bursts, with auroral streamers appears to be the best understood. The source mechanism(s) for auroral arcs remains less clear and more controversial. In situ measurements of electron precipitation associated with arcs indicate two classes of events (e.g., Newell 2000). One is characterised by broadband spectra, presumably associated with dispersive Alfvén waves (e.g., Chaston et al. 2003), while monoenergetic "inverted V" events show acceleration only in a narrow band, ascribed to quasi-static electric potentials of "U" or "S"-shape (Carlqvist and Boström 1970; Mozer et al. 1980; Mizera et al. 1982; Marklund et al. 1997; Johansson et al. 2006). At larger scales, the perpendicular electric field associated with such potentials corresponds to plasma velocity shear (e.g., Echim et al. 2007), while at smaller scales ions are demagnetized and only electrons show the corresponding $\mathbf{E} \times \mathbf{B}$ drift velocity, representing Hall current (Birn et al. 2012a).

5.1.2 Jupiter

At Jupiter, the main auroral emission is associated with the breakdown of plasma corotation in the middle magnetosphere (e.g. Cowley and Bunce 2001; Hill 2001) rather than the open/closed field line boundary. The high-latitude aurora inside the main emission are extremely variable and are suggested to be magnetically connected to the middle and outer magnetosphere and possibly related to a sector of the Dungey and/or Vasyliunas cycle flows (Cowley et al. 2003; Grodent et al. 2003a; Stallard et al. 2003). This makes it difficult to identify a clear signature of a polar cap, and though mapping models can predict the time-averaged location of the open/closed field line boundary (e.g. Vogt et al. 2011), the case for a corresponding ECPC paradigm at Jupiter is certainly not clear. However, there are other auroral emissions (apart from the main emission) at Jupiter that clearly respond to magnetotail dynamics.

Auroral observations have shown the occasional appearance of "multiple dawn arcs" taking the form of parallel arc structures located poleward of the main emission in the dawn sector (Grodent et al. 2003b) and "nightside polar spots", isolated spots appearing in the dusk-midnight sector, poleward of the main emission (Grodent et al. 2004). These polar spots have been observed in both the UV and IR auroral emissions (Radioti et al. 2011). Given their observed location and properties the multiple dawn arcs and the nightside spots were proposed to be triggered by reconnection processes in the Jovian magnetotail. A more recent analysis based on daily UV auroral observations (Radioti et al. 2008) revealed the presence of "polar dawn spots" consisting of transient auroral emissions in the polar dawn region (Fig. 25b), with a characteristic recurrence period of 2–3 days. Because of their periodic recurrence and observed location, the polar dawn spots were interpreted as auroral signatures of inward moving flow bursts released during internally driven magnetic reconnection in the Jovian magnetotail (Radioti et al. 2010). The association of the polar dawn auroral spots with tail reconnection was also studied by Ge et al. (2010). The authors magnetically mapped tail reconnection events into Jupiter's ionosphere, by tracing field lines using a Jovian magnetosphere model (Khurana 1997). More recently, Radioti et al. (2011) reported observations of a dusk side spot occurring at nearly the same time as a reconnection signature was observed in the Galileo magnetometer data (Vogt et al. 2010). This spot was mapped using an updated mapping model (Vogt et al. 2011) to an equatorial position close to the Galileo spacecraft, and inside of a statistical X-line, further confirming the association of the auroral spots with inward flow from tail reconnection. Additionally, Kasahara et al. (2013) reported on prominent reconnection jet fronts mainly on the dawnside of the nightside magnetosphere and suggested that they are consistent with significant field-aligned currents which would generate localised aurora.

Finally, auroral observations can provide a hint for the extent of the tail X-line. The ionospheric signatures of inward moving flows released during tail reconnection are sometimes instantaneously detected over a wide local time range, suggesting that reconnection may occur simultaneously, in narrow channels, across the width of the tail (Radioti et al. 2011). Whether reconnection at Jupiter's tail can result in simultaneous release of flow bursts over a large local time sector is a question still to be resolved by future missions to Jupiter and/or remote observations.

5.1.3 Saturn

The main auroral ring at Saturn is suggested to be produced by magnetosphere-solar wind interaction, through the shear in rotational flow across the open closed field line

boundary (e.g. Cowley and Bunce 2003; Bunce et al. 2008). Magnetotail reconnection leaves its signature at Saturn's main auroral emission since its morphology is controlled by the balance between the magnetic field reconnection rate at the dayside magnetopause and the reconnection rate in the nightside tail (Badman et al. 2005, 2014). This is similar to the ECPC paradigm applied to the Earth above. Reconnection of open field lines (via the Dungey cycle) in the tail is expected to result in bright and fast rotating aurorae, which expand poleward in the dawn sector, reducing significantly the size of the polar cap and thus resulting in closure of flux (Cowley et al. 2005; Badman et al. 2005; Jia et al. 2012b). Finally, tail reconnection on closed field lines (Vasyliunas-type) is not expected to modify the polar cap size as it does not change the total amount of flux. Changes in open flux obtained from the auroral images and comparison with open flux estimated from the upstream interplanetary data allowed the estimation of the average tail reconnection rates at Saturn (Badman et al. 2005, 2014).

Enhancements in energetic neutral atom (ENA) emission and Saturn kilometric radiation (SKR) data, together with auroral emission from HST and UVIS reported the initiation of several acceleration events in the midnight to dawn quadrant at radial distance of 15 to 20 R_S, related to tail reconnection (Mitchell et al. 2009). Additionally, small spots of auroral emission lying near the main emission observed by the UVIS instrument onboard Cassini, are suggested to be associated with dipolarizations in the tail (Fig. 25c) (Jackman et al. 2013). These auroral features are suggested to be the precursor to a more intense activity associated with recurrent energisation via particle injections from the tail following reconnection (Mitchell et al. 2009). Most recently, auroral dawn enhancements observed with HST have been shown by Nichols et al. (2014) who suggested that intensifications in the dawn sector of Saturn's aurora are indicative of ongoing, bursty reconnection of lobe flux in the magnetotail, with flux closure rates of 280 kV.

Another study discusses the possible mechanisms that injected plasma population from tail reconnection can create aurora emissions (Radioti et al. 2013). Based on simultaneous UV and ENA observations and comparison with simulations the authors describe the evolution of an injected population, possibly related to tail reconnection as well as its auroral counterpart. They discuss whether pitch angle diffusion and electron scattering or/and field aligned currents driven by pressure gradients along the boundaries of the injected hot plasma are responsible for the auroral emissions related to injections.

5.2 Mercury

At Mercury, the discussion of auroral features is not currently applicable as the planet lacks an ionosphere and hence lacks a site in which large-scale field-aligned currents can close. Nonetheless, Joule heating due to magnetospheric field-aligned currents closing at very shallow depths beneath Mercury's surface may create a "warm" auroral oval that might be visible at infrared wavelengths (Baker et al. 1987). Intensive work is currently underway to understand the morphology of the system in the absence of traditional ionospheric current closure.

5.3 Magnetospheric Radio Emissions

Auroral radio emissions have been discovered at five magnetised planets: Earth, Jupiter, Saturn, Uranus and Neptune (see e.g. review by Zarka 1998). No radio emission has been detected at Mercury. In this review paper we are concerned primarily with radio emissions that are produced via the cyclotron maser instability (Wu and Lee 1979). The terrestrial emission is known as Auroral Kilometric Radiation (AKR), and the Jovian emission includes
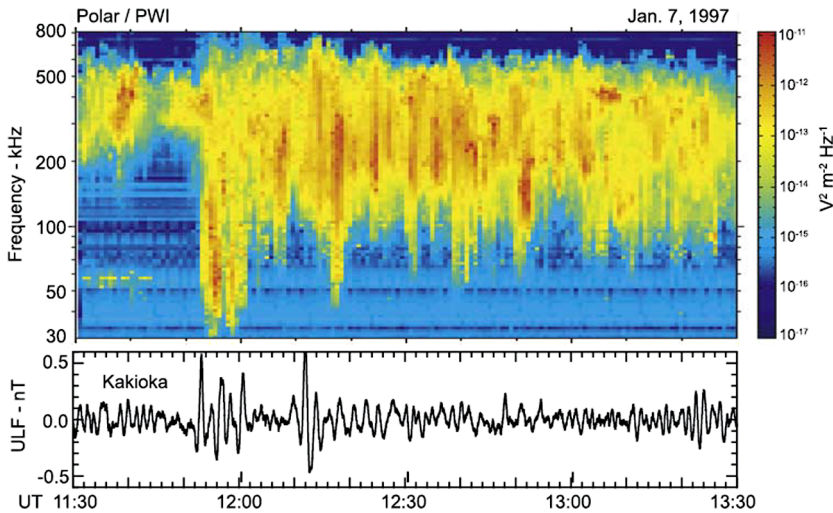
Fig. 27 Radio and geomagnetic data observed on January 7th 1997 over two hours. The *top panel* shows a dynamic spectrogram of AKR, taken by the Polar spacecraft orbiting in the region 4.8–7.0 R_E. The *bottom panel* shows Pi2 pulsations observed at the low-latitude Kakioka ground station. From Morioka et al. (2007)

Decametric radio emission (DAM), some of which is linked to the moon Io. At Saturn, the main component of radio emission is called Saturn Kilometric Radiation (SKR). Radio emissions have been used as a means to determine planetary rotation rates (although the debate at Saturn still rages!), but also to remotely sense magnetospheric dynamics. Here we focus specifically on the relationship between the terrestrial and Kronian radio emissions and magnetotail dynamics. Studies of the link between Jovian radio emission and global dynamics have been much rarer, with the exception of some work by Louarn et al. (2000, 2007) who associated sporadic energy release events with enhancements in the flux of radio emissions.

At Earth, many authors have explored the correlation between magnetotail reconnection and sudden intensification in the AKR (Benediktov et al. 1968; Gurnett 1974; Voots et al. 1977; Kurth et al. 1998). While the average power of AKR is found to increase with substorm activity, there are additional effects. It has been shown that the AKR can exhibit sudden expansion to lower frequencies coincident with substorm onset (e.g. Kaiser and Alexander 1977; Anderson et al. 1997). More recently, Morioka et al. (2007, 2010) have studied this frequency response in detail. The top panel of Fig. 27 shows what is termed a "dual-component AKR spectrum", as measured by the Polar spacecraft's Plasma Wave Instrumentation (PWI). The lower panel shows Pi2 pulsations, as measured by a ground-based magnetometer at Kakioka. Such pulsations are a good indicator of substorm onset, and in this case we observe the beginning of a large substorm at ∼11:55. This is accompanied by a strong intensification of the AKR and an expansion of the emission down to ∼30 kHz. Two distinct types of AKR emission are visible on this plot. The first is a low altitude, middle-frequency source (MF-AKR) which is active before and after substorm onset. The second is a high-altitude, low-frequency source (LF-AKR). This source appears abruptly with intense power (increasing by a factor of up to 1000 times) at substorm onset.

Figure 28 shows the physical interpretation of this change in emission frequency. For radio emission such as AKR and SKR, where the emission is generated at or close to the local electron cyclotron frequency, f_{CE}, the frequency of the emission is inversely proportional to
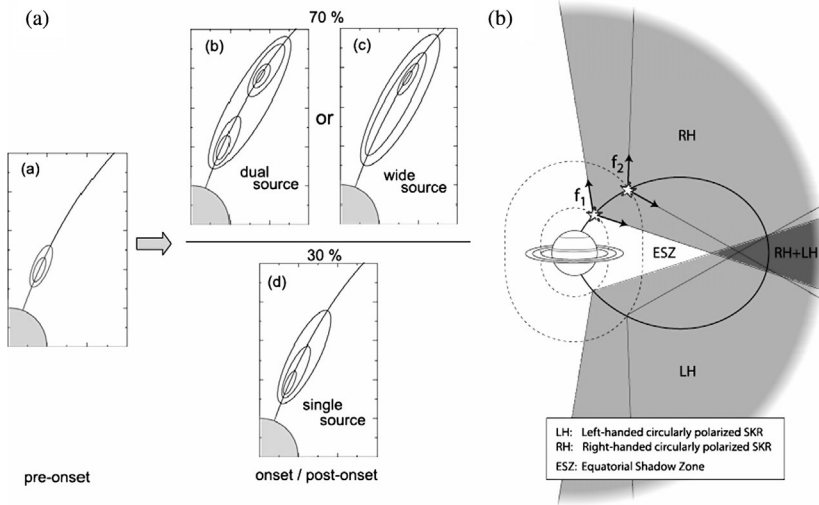
Fig. 28 (**a**) Schematic illustration of AKR source development along a magnetic field line during a substorm. Changes in the source altitude through movement/merging/growth can result in a change in the frequency of the emission. From Morioka et al. (2007). (**b**) Schematic diagram showing the relationship between radio source altitude and emission frequency. From Lamy et al. (2008)

the altitude of the radio source along the field line (f_{CE} is inversely proportional to B, e.g. Lamy et al. 2008). Morioka et al. (2007, 2010) suggested for Earth that precipitation into the auroral zones following energetic magnetotail reconnection can cause the radio sources to move/merge/grow to higher altitudes along the field lines. Does such a frequency response exist at other planets?

It has long been known that Saturn's auroral radio emissions respond to solar wind conditions (e.g. Kaiser et al. 1980; Desch 1982; Desch and Rucker 1983), with a strong correlation between solar wind compressions and intensified SKR emission (e.g. Badman et al. 2008). The period of the SKR emission is also sensitive to upstream solar wind conditions (Zarka et al. 2007), varying systematically by ∼1 % with a characteristic timescale of ∼20–30 days. However it is the response of the SKR to dynamics in Saturn's magnetotail that make it an intriguing terrestrial analogue and also a potentially useful remote proxy of tail dynamics.

During the Saturn Orbit Insertion (SOI) manoeuvre by Cassini in 2004, Bunce et al. (2005) noted a strong intensification of the SKR emission on the outbound pass of the spacecraft. This was correlated with a hot plasma injection, and the entire interval was interpreted as evidence of compression-induced tail reconnection. Jackman et al. (2009) collated a list of nine plasmoids and TCRs from Saturn's magnetotail and examined their correlation with SKR. This comparison revealed a very similar frequency response to that observed with the AKR at terrestrial substorm onset. In situ reconnection signatures were found to be associated with intensification and continuous extension to low frequencies of the SKR.

Overall, there is a good correlation between the timing of reconnection events at the Earth and Saturn and the intensification and frequency expansion of planetary radio emissions. More study is required to establish the exact nature of the correlation, but there is potential for such radio emissions to be used as a remote proxy for magnetotail conditions in the absence of *in situ* orbiting spacecraft.
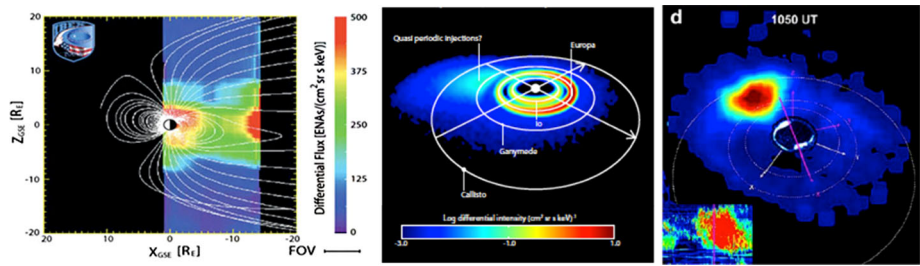
Fig. 29 *Left*: IBEX's composite image of the plasma sheet in the Earth's magnetotail. *Middle*: Simulated ENA image of Jupiter's middle magnetosphere (from JUICE Yellow book, 2012). *Right*: Cassini INCA observations of an ENA brightening observed in the midnight-to-dawn quadrant of Saturn's magnetosphere, superposed with Cassini UVIS and RPWS auroral observations (from Mitchell et al. 2009)

5.4 Energetic Neutral Atom Imaging

Energetic neutral atoms (ENAs) emitted from planetary neutral environments are energetic ions that neutralize by charge exchange with the cold (few eV) neutral atoms in the space environment of a planet. In the process, a high-energy ion picks up an electron from a neutral atom, producing a cold ion and an energetic neutral atom. The energetic neutral atom so formed is reflective of the source ion in composition and energy, and its motion is no longer governed by the magnetic and electric fields. It therefore propagates in a straight trajectory like a photon. The realization that these charge-exchange processes occur frequently in space environments gave birth to the ENA imaging technique that permits the remote detection and investigation of global scale magnetospheric dynamics.

At Earth, the first global image of the terrestrial ring current during a storm was obtained using ENA data from the NASA/ESA ISEE 1 (e.g., Roelof et al. 1997). Since then, ENA imaging has contributed substantially to storm and substorm research. As reviewed by Pollock et al. (2003), ENA imaging has indeed enabled experimental confirmation of global particle drift as a function of energy, elucidation of dynamics in the tail related to the effects of the imposed (growth phase) and induced (expansion phase) electric fields on the plasma, evidence of the prompt extraction or energization of oxygen from the ionosphere during substorms, clarification of the storm/substorm relation and rudimentary measurements of the inward propagation of substorm injection fronts. Recent IBEX ENA observations displayed in Fig. 29 (left) show the plasma sheet and magnetotail of the Earth in profile. This image shows a significant intensification of ENA emissions in the nightside magnetosphere. A plausible interpretation among others of these ENA observations is that the Earth's plasma sheet was magnetically disconnected at about 10 Earth radii and ejected down the tail as a plasmoid (McComas et al. 2011). The combination of such ENA observations with contemporary multi-point spacecraft observations should lead to even more sophisticated understanding of magnetotail dynamics at Earth.

No dedicated ENA imager has been yet flown on an orbiting mission to Mercury and Jupiter, but the first images of Jupiter's magnetosphere in ENAs have been obtained by the Cassini/INCA sensor during its Jupiter flyby in December 2000. These remote observations revealed two distinct regions of emissions in ENA: the upper atmosphere of Jupiter itself, and a torus of emission residing just outside the orbit of Jupiter's satellite Europa (Mauk et al. 2003). There will be however dedicated ENA sensors on the ESA/JAXA BepiColombo mission to Mercury to be launched in 2015, and on the ESA-led Jupiter ICy moon Explorer mission currently due to arrive in 2031.
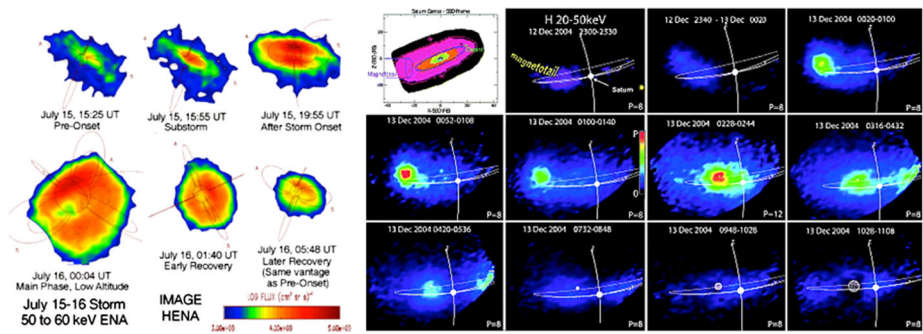
Fig. 30 *Left*: ENA fluxes observed by IMAGE/HENA at Earth during a major geomagnetic storm on July 15–16, 2000. *Red* indicates the highest flux, and *blue* the lowest. *Right*: successive Cassini INCA images at Saturn obtained on 13 December 2004 showing the initiation, growth, and decay of a burst of neutral hydrogen atoms apparently originating from the magnetotail of Saturn (from Mitchell et al. 2005)

The first dedicated ENA sensor in history has however been included in the Cassini spacecraft payload. The INCA sensor of the Magnetospheric Imaging Instrument (MIMI) aboard the Cassini spacecraft has observed ENAs and charged particles at Earth in 1997, Jupiter in 2000, and Saturn/Titan from mid-2004 to present, from high latitudes or large radial distances. At Saturn, ENA imaging has revealed a highly dynamic magnetosphere. INCA observations of bursts of ENAs from Saturn's magnetosphere seem to be consistent with an ion acceleration region between 15 and 20 R_S (Mitchell et al. 2009) and subsequent inward motion of ion populations (to about 7 R_S). Mitchell et al. suggested that ion populations are injected near or just after midnight and brighten through dawn. As these particles are carried around the magnetosphere, losses dominate and soon the source ions are attenuated. In Mitchell's description, the corotating ion blob or its remnants are again replenished in the post-midnight sector (Fig. 29, right). This means that there will be a periodic brightening of a corotating ion population near dawn. This periodic brightening has been associated with auroral features and SKR, in the same way that particle bursts are correlated with auroral activity in terrestrial substorms. Figure 30 enables one to compare and contrast the underlying magnetospheric dynamics at Earth and Saturn. Simultaneous in-situ and remote observations obtained when Cassini is in the solar wind outside Saturn's magnetosphere indicated a possible link between the magnetospheric response at Saturn and the dynamic solar wind (Mitchell et al. 2005). Second, in situ magnetic field and plasma observations between 40 and 50 R_S down the magnetotail were interpreted as a tailward moving plasmoid originating in the inner magnetosphere between Cassini and Saturn (Hill et al. 2008). Careful analysis of INCA remote observations of ENAs during that period of time allowed a precise determination of their common source, location and time, which turned out to be midway between Saturn and Cassini (20–30 R_S) and about half an hour before the in situ detection (Hill et al. 2008). New synergistic observations from Cassini in situ and remote instruments will undoubtedly bring additional constraints during the mission extensions to these unique observations.

6 Summary

In this review we have compared and contrasted the magnetotails of Mercury, Earth, Jupiter and Saturn. Earth's magnetotail and its structure and dynamics are by far the most thoroughly explored in situ and remotely and thus provide guides for the understanding of other

planetary tails. The varying planetary field strengths, rotation rates, ionospheric conductivities and external solar wind conditions result in dramatic differences in the dynamics of the individual magnetospheres. However, despite many years of in situ and remote observations, combined with increasingly sophisticated models, much is still unknown about the dynamics of planetary magnetotails. For the future, we look to the continuation of the MESSENGER, Cluster, THEMIS, and Cassini missions, as well as planned planetary missions such as Juno and JUICE. In the longer term future, it may perhaps become possible to explore the more remote magnetotails of Neptune and Uranus in situ. Certainly magnetotail science is a flourishing field which will continue to excite and challenge the scientific community for many years to come.

Appendix: Co-ordinate Systems

Here we define three co-ordinate systems used throughout this paper:

RTN: The most commonly used co-ordinate system for the IMF is RTN, a right-handed system referenced to the Sun's spin axis, in which B_R is directed radially outward from the Sun, B_T is the azimuthal component positive in the direction of planetary motion, and B_N is the 'minus theta' component positive northward in the solar equatorial plane

Geocentric Solar Magnetospheric (GSM): The X axis points from Earth to the Sun, the X–Z plane contains the planetary magnetic dipole axis, and the Y component completes the right-handed set and is positive towards dusk.

Jovicentric Solar Orbital (JSO): This system was employed by Khurana and Schwarzl (2005) to study structures at Jupiter that are influenced by the solar wind. The X axis points from Jupiter to the Sun and the Z axis is perpendicular to the orbital plane of Jupiter. The Y axis completes the right-handed set and is positive towards dusk. The coordinate system is analogous to Geocentric Solar Ecliptic (GSE) coordinates but generalised for a body that does not orbit the Sun in the ecliptic plane.

References

G.A. Abel, A.J. Coates, A.M. Rymer, D.R. Linder, M.F. Thomsen, D.T. Young, M.K. Dougherty, Cassini plasma spectrometer observations of bidirectional lobe electrons during the Earth flyby, August 18, 1999. J. Geophys. Res. **106**, 30199–30208 (2001). doi:10.1029/2001JA900076

N. Achilleos, C.S. Arridge, C. Bertucci, C.M. Jackman, M.K. Dougherty, K.K. Khurana, C.T. Russell, Large-scale dynamics of Saturn's magnetopause: observations by Cassini. J. Geophys. Res. **113**, A11209 (2008). doi:10.1029/2008JA013265

S.-I. Akasofu, The development of the auroral substorm. Planet. Space Sci. **12**, 273 (1964)

S.-I. Akasofu, *Polar and Magnetospheric Substorm* (Reidel, Dordrecht, 1968)

S. Akasofu, S. Chapman, The ring current, geomagnetic disturbance, and the Van Allen radiation belts. J. Geophys. Res. **66**(5), 1321–1350 (1961). doi:10.1029/JZ066i005p01321

R.R. Anderson, D.A. Gurnett, H. Matsumoto, K. Hashimoto, H. Kojima, Y. Kasaba, M.L. Kaiser, G. Rostoker, J.-L. Bougeret, J.-L. Steinberg, I. Nagano, H. Singer, Observations of low frequency terrestrial type III bursts by GEOTAIL and WIND and their association with isolated geomagnetic disturbances detected by ground and space-borne instruments, in *Planetary Radio Emissions IV*, ed. by H.O. Rucker, S.J. Bauer, A. Lecacheux (Austrian Academy of Sciences Press, Vienna, 1997), pp. 241–250

B.J. Anderson, M.H. Acuna, H. Korth, M.E. Purucker, C.L. Johnson, J.A. Slavin, S.C. Solomon, R.L. McNutt Jr., The structure of Mercury's magnetic field from MESSENGER's first flyby. Science **321**, 82–85 (2008)

B.J. Anderson, C.L. Johnson, H. Korth, R.M. Winslow, J.E. Borovsky, M.E. Purucker, J.A. Slavin, S.C. Solomon, M.T. Zuber, R.L. McNutt Jr., Low-degree structure in Mercury's planetary magnetic field. J. Geophys. Res. **117**, E00L12 (2012). doi:10.1029/2012JE004159

V. Angelopoulos, W. Baumjohann, C.F. Kennel, F.V. Coronti, M.G. Kivelson, R. Pellat, R.J. Walker, H. Luehr, G. Paschmann, Bursty bulk flows in the inner central plasma sheet. J. Geophys. Res. **97**, 4027–4039 (1992a)

V. Angelopoulos, C.F. Kennel, F.V. Coroniti, R. Pellat, M.G. Kivelson, R.J. Walker, W. Baumjohann, G. Paschmann, H. Luhr, Bursty bulk flows in the inner plasma sheet: an effective means of earthward transport in the magnetotail, in *Proceedings of the First International Conf. on Substorms*, ESA Special Publication, vol. 335 (1992b), pp. 303–308

V. Angelopoulos, C.F. Kennel, F.V. Coroniti, W.C. Feldman, J.T. Gosling, M.G. Kivelson, R.J. Walker, C.T. Russell, Observations of a quasi-static plasma sheet boundary. Geophys. Res. Lett. **20**, 2813–2816 (1993). doi:10.1029/93GL01979

V. Angelopoulos, C.F. Kennel, F.V. Coroniti, R. Pellat, M.G. Kivelson, R.J. Walker, C.T. Russell, W. Baumjohann, W.C. Feldman, J.T. Gosling, Statistical characteristics of bursty bulk flow events. J. Geophys. Res. **99**, 21257–21280 (1994). doi:10.1029/94JA01263

V.C. Angelopoulos, J.P. McFadden, D. Larson et al., Tail reconnection triggering substorm onset. Science **321**(5891), 931–935 (2008). doi:10.1126/science.1160495

V.C. Angelopoulos, J.P. McFadden, D. Larson et al., Response to Comment on "Tail reconnection triggering substorm onset". Science **324**(5933) (2009). doi:10.1126/science.1168045

R.L. Arnoldy, K.W. Chan, Particle substorms observed at the geostationary orbit. J. Geophys. Res. **74**, 5019 (1969)

C.S. Arridge, Magnetotails of Uranus and Neptune, in *Magnetotails in the Solar System*. Geophys. Monogr. Ser. (2014, in press)

C.S. Arridge, N. Achilleos, M.K. Dougherty, K.K. Khurana, C.T. Russell, Modeling the size and shape of Saturn's magnetopause with variable dynamic pressure. J. Geophys. Res. **111**, A11227 (2006). doi:10.1029/2005JA011574

C.S. Arridge, C.T. Russell, K.K. Khurana, N. Achilleos, S.W.H. Cowley, M.K. Dougherty, D.J. Southwood, E.J. Bunce, Saturn's magnetodisc current sheet. J. Geophys. Res. **113**, A04214 (2008a). doi:10.1029/2007JA012540

C.S. Arridge, K.K. Khurana, C.T. Russell, D.J. Southwood, N. Achilleos, M.K. Dougherty, A.J. Coates, H.K. Leinweber, Warping of Saturn's magnetospheric and magnetotail current sheets. J. Geophys. Res. **113**, A08217 (2008b). doi:10.1029/2007JA012963

C.S. Arridge, H.J. McAndrews, C.M. Jackman, C. Forsyth, A.P. Walsh, E.C. Sittler, L.K. Gilbert, G.R. Lewis, C.T. Russell, A.J. Coates, M.K. Dougherty, G.A. Collinson, A. Wellbrock, D.T. Young, Plasma electrons in Saturn's magnetotail: structure, distribution and energization. Planet. Space Sci. **57**(14–15), 2032–2047 (2009)

C.S. Arridge et al., Periodic motion of Saturn's nightside plasma sheet. J. Geophys. Res. **116**, A11205 (2011a). doi:10.1029/2011JA016827

C.S. Arridge et al., Mapping magnetospheric equatorial regions at Saturn from Cassini Prime mission observations. Space Sci. Rev. **164**, 1–83 (2011b). doi:10.1007/s11214-011-9850-4

A. Artemyev, L. Zelenyi, Mechanisms of spontaneous reconnection: from magnetospheric to fusion plasma. Space Sci. Rev. (2013). doi:10.1007/s11214-013-9959-8

A.V. Artemyev, W. Baumjohann, A.A. Petrukovich, R. Nakamura, I. Dandouras, A. Fazakerley, Proton/electron temperature ratio in the magnetotail. Ann. Geophys. **29**(12), 2253–2257 (2011). doi:10.5194/angeo-29-2253-2011

Y. Asano, T. Mukai, M. Hoshino, Y. Saito, H. Haysakawa, T. Nagai, Statistical study of thin current sheet evolution around substorm onset. J. Geophys. Res. **109**, A05213 (2004). doi:10.1029/2004JA010413

Y. Asano, R. Nakamura, W. Baumjohann, A. Runov, Z. Vörös, M. Volwerk, T.L. Zhang, A. Balogh, B. Klecker, H. Rème, How typical are atypical current sheets? Geophys. Res. Lett. **32**, L03108 (2005). doi:10.1029/2004GL021834

M. Ashour-Abdalla, J.P. Berchem, J. Buechner, L.M. Zelenyi, Shaping of the magnetotail from the mantle—global and local structuring. J. Geophys. Res. **98**, 5651–5676 (1993). doi:10.1029/92JA01662

M. Ashour-Abdalla, M. El-Alaoui, M.L. Goldstein, M. Zhou, D. Schriver, R. Richard, R. Walker, M.G. Kivelson, K.-J. Hwang, Observations and simulations of non-local acceleration of electrons in magnetotail magnetic reconnection events. Nat. Phys. **7**, 360–365 (2011). doi:10.1038/nphys1903

A. Åsnes, R.W.H. Friedel, B. Lavraud, G.D. Reeves, M.G.G.T. Taylor, P. Daly, Statistical properties of tail plasma sheet electrons above 40 keV. J. Geophys. Res. **113**(A12), A03202 (2008). doi:10.1029/2007JA012502

M.P. Aubry, C.T. Russell, M.G. Kivelson, Inward motion of the magnetopause before a substorm. J. Geophys. Res. **75**, 7018 (1970)

W.I. Axford, C.O. Hines, A unifying theory of high-latitude geophysical phenomena and geomagnetic storms. Can. J. Phys. **39**, 1433–1464 (1961)

W.I. Axford, Viscous interaction between the solar wind and the Earth's magnetosphere. Planet. Space Sci. **12**, 45–53 (1964)

W.I. Axford, H.E. Petschek, G.L. Siscoe, Tail of the magnetosphere. J. Geophys. Res. **70**(5), 1231–1236 (1965). doi:10.1029/JZ070i005p01231

S.V. Badman, E.J. Bunce, J.T. Clarke, S.W.H. Cowley, J.-C. Gérard, D. Grodent, S.E. Milan, Open flux estimates in Saturn's magnetosphere during the January 2004 Cassini-HST campaign, and implications for reconnection rates. J. Geophys. Res. **110**, A11216 (2005). doi:10.1029/2005JA011240

S.V. Badman, S.W.H. Cowley, Significance of Dungey-cycle flows in Jupiter's and Saturn's magnetospheres, and their identification on closed equatorial field lines. Ann. Geophys. **25**, 941–951 (2007)

S.V. Badman, S.W.H. Cowley, L. Lamy, B. Cecconi, P. Zarka, Relationship between solar wind corotating interaction regions and the phasing and intensity of Saturn kilometric radiation bursts. Ann. Geophys. **26**, 3641–3651 (2008)

S.V. Badman, C.M. Jackman, J.D. Nichols, J.T. Clarke, J.-C. Gérard, Open flux in Saturn's magnetosphere. Icarus **231**, 137–145 (2014). doi:10.1016/j.icarus.2013.12.004

F. Bagenal, Giant planet magnetospheres. Annu. Rev. Earth Planet. Sci. **20**, 289–328 (1992). doi:10.1146/annurev.ea.20.050192.001445

F. Bagenal, T. Dowling, W. McKinnon (eds.), *Jupiter: Planet, Satellites, Magnetosphere* (Cambridge University Press, Cambridge, 2004)

F. Bagenal, The magnetosphere of Jupiter: coupling the equator to the poles. J. Atmos. Sol.-Terr. Phys. **69** (2007)

F. Bagenal, Comparative planetary environments, in *Heliophysics: Plasma Physics of the Local Cosmos*, ed. by C.J. Schrijver, G.L. Siscoe (Cambridge University Press, Cambridge, 2009), pp. 360–398

F. Bagenal, P.A. Delamere, Flow of mass and energy in the magnetospheres of Jupiter and Saturn. J. Geophys. Res. **116**, A05209 (2011). doi:10.1029/2010JA016294

D.N. Baker, P.R. Higbie, E.W. Hones Jr., R.D. Belian, High-resolution energetic particle measurements at 6.6 R_E: 3. Low-energy electron anisotropies and short-term substorm predictions. J. Geophys. Res. **83**, 4863 (1978)

D.N. Baker, J.E. Borovsky, J.O. Burns, G.R. Gisler, M. Zeilik, Possible calorimetric effects at Mercury due to solar wind-magnetosphere interactions. J. Geophys. Res. **92**(A5), 4707–4712 (1987). doi:10.1029/JA092iA05p04707

D.N. Baker, T.I. Pulkkinen, V. Angelopoulos, W. Baumjohann, R.L. McPherron, Neutral line model of substorms: past results and present view. J. Geophys. Res. **101**, 12975–13010 (1996). doi:10.1029/95JA03753

W. Baumjohann, G. Paschmann, C.A. Cattell, Average plasma properties in the central plasma sheet. J. Geophys. Res. **94**, 6597–6606 (1989). doi:10.1029/JA094iA06p06597

W. Baumjohann, M. Hesse, S. Kokubun, T. Mukai, T. Nagai, A.A. Petrukovich, Substorm dipolarization and recovery. J. Geophys. Res. **104**(A11), 24995–25000 (1999). doi:10.1029/1999JA900282

W. Baumjohann, A. Roux, O. Le Contel, R. Nakamura, J. Birn et al., Dynamics of thin current sheets: Cluster observations. Ann. Geophys. **25**, 1365–1389 (2007)

K.W. Behannon, Mapping of the Earth's bow shock and magnetic tail by Explorer 33. J. Geophys. Res. **73** (1968). doi:10.1029/JA073i003p00907

K.W. Behannon, Heliocentric distance dependence of the interplanetary magnetic field. Rev. Geophys. Space Phys. **16**, 126 (1978)

K.W. Behannon, L.F. Burlaga, N.F. Ness, The Jovian magnetotail and its current sheet. J. Geophys. Res. **86**, 8385–8401 (1981)

E.A. Benediktov, G.G. Getmansev, N.A. Mityakov, V.O. Papoport, A.F. Tarozov, Relation between geomagnetic activity and the sporadic radio emission recorded by the Electron-2 satellite. Kosm. Issled. **6**, 7 (1968) (in Russian)

J. Benkhoff et al., Bepi-Colombo-Comprehensive exploration of Mercury: mission overview and science goals. Planet. Space Sci. **58**(1–2) (2010)

M. Benna et al., Modeling of the magnetosphere of Mercury at the time of the first MESSENGER flyby. Icarus **209**(1), 3–10 (2010). doi:10.1016/j.icarus.2009.11.036

J. Birn, The boundary value problem of magnetotail equilibrium. J. Geophys. Res. **96**, 19441 (1991)

J. Birn, Three-dimensional magnetotail equilibria with prescribed boundary shapes. J. Geophys. Res. **110**, A07203 (2005). doi:10.1029/2004JA010869

J. Birn, M. Hesse, Details of current disruption and diversion in simulations of magnetotail dynamics. J. Geophys. Res. **101**(A7), 15345–15358 (1996). doi:10.1029/96JA00887

J. Birn, K. Schindler, Thin current sheets in the magnetotail and the loss of equilibrium. J. Geophys. Res. **107**(A7), SMP18 (2002). doi:10.1029/2001JA0291

J. Birn, R. Sommer, K. Schindler, Open and closed magnetospheric tail configurations and their stability. Astrophys. Space Sci. **35**, 389–402 (1975)

J. Birn, M.F. Thomsen, J.E. Borovsky, G.D. Reeves, D.J. McComas, R.D. Belian, M. Hesse, Substorm ion injections: geosynchronous observations and test particle orbits in three-dimensional dynamic MHD fields. J. Geophys. Res. **102**(A2), 2325–2341 (1997a). doi:10.1029/96JA03032

J. Birn, M.F. Thomsen, J.E. Borovsky, G.D. Reeves, D.J. McComas, R.D. Belian, Characteristic plasma properties during dispersionless substorm injections at geosynchronous orbit. J. Geophys. Res. **102**, 2309–2324 (1997b)

J. Birn, J.F. Drake, M.A. Shay, B.N. Rogers, R.E. Denton, M. Hesse, M.M. Kuznetsova, Z.W. Ma, A. Bhattacharjee, A. Otto, P.L. Pritchett, Geospace Environment Modeling (GEM) magnetic reconnection challenge. J. Geophys. Res. **106**, 3715–3720 (2001)

J. Birn, J. Raeder, Y.L. Wang, R.A. Wolf, M. Hesse, On the propagation of bubbles in the geomagnetic tail. Ann. Geophys. **22**, 1773 (2004a)

J. Birn, M.F. Thomsen, M. Hesse, Acceleration of oxygen ions in the dynamic magnetotail. Ann. Geophys. **22**, 1305–1315 (2004b)

J. Birn, M. Hesse, K. Schindler, On the role of entropy conservation and entropy loss governing substorm phases, in *Proc. of the Eighth International Conference of Substorms*, Banff, Canada, ed. by M. Syrjasuo, E. Donovan (Univ. of Calgary, Calgary, 2006), pp. 19–24

J. Birn, M. Hesse, K. Schindler, S. Zaharia, Role of entropy in magnetotail dynamics. J. Geophys. Res. **114**, A00D03 (2009). doi:10.1029/2008JA014015

J. Birn, R. Nakamura, E. Panov, M. Hesse, Bursty bulk flows and dipolarization in MHD simulations of magnetotail reconnection. J. Geophys. Res. **116**, A01210 (2011). doi:10.1029/2010JA016083

J. Birn, K. Schindler, M. Hesse, Magnetotail aurora connection: the role of thin current sheets, in *Relationship Between Auroral Phenomenology and Magnetospheric Processes: Earth and Other Planets*, ed. by A. Keiling, E. Donovan, F. Bagenal, T. Karlsson. Geophysical Monograph, vol. 197 (Am. Geophysical Union, Washington, 2012a), p. 337

J. Birn, A.V. Artemyev, D.N. Baker, M. Echim, M. Hoshino, L.M. Zelenyi, Particle acceleration in the magnetotail and aurora. Space Sci. Rev. **173**, 49–102 (2012b). doi:10.1007/s11214-012-9874-4

S.J. Bolton, The Juno mission, in *Proceedings of the International Astronomical Union*, IAU Symposium, vol. 269 (2010), pp. 92–100

J.E. Borovsky, R.J. Nemzek, R.D. Belian, The occurrence rate of magnetospheric-substorm onsets: random and periodic substorms. J. Geophys. Res. **98**, 3807 (1993)

J.E. Borovsky, M.F. Thomsen, R.C. Elphic, The driving of the plasma sheet by the solar wind. J. Geophys. Res. **103**, 17617–17640 (1998). doi:10.1029/97JA02986

N.M. Brice, G.A. Ioannidis, The magnetospheres of Jupiter and Earth. Icarus **13**, 173 (1970)

J. Büchner, L.M. Zelenyi, Deterministic chaos in the dynamics of charged particles near a magnetic field reversal. Phys. Lett. A **118**, 395–399 (1986). doi:10.1016/0375-9601(86)90268-9

E.J. Bunce, S.W.H. Cowley, D.M. Wright, A.J. Coates, M.K. Dougherty, N. Krupp, W.S. Kurth, A.M. Rymer, In situ observations of a solar wind compression-induced hot plasma injection in Saturn's tail. Geophys. Res. Lett. **32**, L20S04 (2005)

E.J. Bunce, S.W.H. Cowley, I.I. Alexeev, C.S. Arridge, M.K. Dougherty, J.D. Nichols, C.T. Russell, Cassini observations of the variation of Saturn's ring current parameters with system size. J. Geophys. Res. **112**, A10202 (2007). doi:10.1029/2007JA012275

E.J. Bunce et al., Origin of Saturn's aurora: simultaneous observations by Cassini and the Hubble Space Telescope. J. Geophys. Res. **113**, A09209 (2008). doi:10.1029/2008JA013257

L.F. Burlaga, Magnetic fields and plasmas in the inner heliosphere: Helios results. Planet. Space Sci. **49**(14–15), 1619–1627 (2001)

P. Carlqvist, R. Boström, Space-charge regions above the aurora. J. Geophys. Res. **75**, 7140 (1970)

S. Chapman, J. Bartels, *Geomagnetism* (Clarendon Press, Oxford, 1962)

R. Chappell, The terrestrial plasma source: a new perspective in solar-terrestrial processes from Dynamics Explorer. Rev. Geophys. **26**(2), 229–248 (1988)

C.C. Chaston, J.W. Bonnell, C.W. Carlson, J.P. McFadden, R.E. Ergun, R.J. Strangeway, Properties of small-scale Alfvén waves and accelerated electrons from FAST. J. Geophys. Res. **108**, 8003 (2003). doi:10.1029/2002JA009420

Y. Chen, T.W. Hill, Statistical analysis of injection/dispersion events in Saturn's inner magnetosphere. J. Geophys. Res. **113**, A07215 (2008). doi:10.1029/2008JA013166

C.X. Chen, R.A. Wolf, Interpretation of high-speed flows in the plasma sheet. J. Geophys. Res. **98**, 21409–21419 (1993)

J.T. Clarke, J. Gerard, D. Grodent, S. Wannawichian, J. Gustin, J. Connerney, F. Crary, M. Dougherty, W. Kurth, S.W.H. Cowley, E.J. Bunce, T. Hill, J. Kim, Morphological differences between Saturn's ultraviolet aurorae and those of Earth and Jupiter. Nature **433**, 717–719 (2005). doi:10.1038/nature03331

J.E.P. Connerney, M.H. Acuña, N.F. Ness, Currents in Saturn's magnetosphere. J. Geophys. Res. **88**(A11), 8779–8789 (1983). doi:10.1029/JA088iA11p08779

F.V. Coroniti, C.F. Kennel, Changes in magnetospheric configuration during the substorm growth phase. J. Geophys. Res. **77**(19), 3361–3370 (1972). doi:10.1029/JA077i019p03361

F.V. Coroniti, R.L. McPherron, G.K. Parks, Studies of the magnetospheric substorm: 3. Concept of the magnetospheric substorm and its relation to electron precipitation and micropulsations. J. Geophys. Res. **73**(5), 1715–1722 (1968). doi:10.1029/JA073i005p01715

S.W.H. Cowley, The causes of convection in the Earth's magnetosphere: a review of developments during the IMS. Rev. Geophys. **20**(3), 531–565 (1982). doi:10.1029/RG020i003p00531

S.W.H. Cowley, The distant geomagnetic tail in theory and observation, in *Magnetic Reconnection in Space and Laboratory Plasmas*, ed. by E.W. Hones Jr. (1984), pp. 228–238

S.W.H. Cowley, The structure and length of tail-associated phenomena in the solar wind downstream from the Earth. Planet. Space Sci. **7**, 1039 (1991)

S.W.H. Cowley, E.J. Bunce, Origin of the main auroral oval in Jupiter's coupled magnetosphere-ionosphere system. Planet. Space Sci. **49**, 1067 (2001)

S.W.H. Cowley, E.J. Bunce, Corotation-driven magnetosphere-ionosphere coupling currents in Saturn's magnetosphere and their relation to the auroras. Ann. Geophys. **21**, 1691 (2003)

S.W.H. Cowley, E.J. Bunce, T.S. Stallard, S. Miller, Jupiter's polar ionospheric flows: theoretical interpretation. Geophys. Res. Lett. **30**(5), 1220 (2003). doi:10.1029/2002GL016030

S.W.H. Cowley, S.V. Badman, E.J. Bunce, J.T. Clarke, J.C. Gerard, D. Grodent, C.M. Jackman, S.E. Milan, T.K. Yeoman, Reconnection in a rotation-dominated magnetosphere and its relation to Saturn's auroral dynamics. J. Geophys. Res. **110**, A02201 (2005). doi:10.1029/2004JA010796

S.W.H. Cowley, S.V. Badman, S.M. Imber, S.E. Milan, Comment on "Jupiter: a fundamentally different magnetospheric interaction with the solar wind" by D.J. McComas and F. Bagenal. Geophys. Res. Lett. **35**, L10101 (2008). doi:10.1029/2007GL032645

D.C. Delcourt, Particle acceleration by inductive electric fields in the inner magnetosphere. J. Atmos. Sol.-Terr. Phys. **64**, 551–559 (2002)

D.C. Delcourt, J.-A. Sauvaud, T.E. Moore, Phase bunching during substorm dipolarization. J. Geophys. Res. **102**(A11), 24313–24324 (1997). doi:10.1029/97JA02039

M.D. Desch, Evidence for solar wind control of Saturn radio emission. J. Geophys. Res. **87**, 4549–4554 (1982)

M.D. Desch, H.O. Rucker, The relationship between Saturn kilometric radiation and the solar wind. J. Geophys. Res. **88**, 8999–9006 (1983)

A.J. Dessler, Length of magnetospheric tail. J. Geophys. Res. **69**(19), 3913–3918 (1964). doi:10.1029/JZ069i019p03913

G.A. DiBraccio, J.A. Slavin, S.A. Boardsen, B.J. Anderson, H. Korth, T.H. Zurbuchen, J.M. Raines, D.N. Baker, R.L. McNutt Jr., S.C. Solomon, MESSENGER observations of magnetopause structure and dynamics at Mercury. J. Geophys. Res. **118** (2013). doi:10.1002/jgra.50123

M.K. Dougherty et al., Identification of a dynamic atmosphere at Enceladus with the Cassini magnetometer. Science **311**, 1406–1409 (2006)

S. Dubyagin, V. Sergeev, S. Apatenkov, V. Angelopoulos, A. Runov, R. Nakamura, W. Baumjohann, J. McFadden, D. Larson, Can flow bursts penetrate into the inner magnetosphere? Geophys. Res. Lett. **38**, L08102 (2011). doi:10.1029/2011GL047016

J.W. Dungey, Interplanetary magnetic field and the auroral zones. Phys. Rev. Lett. **6**, 47–48 (1961). doi:10.1103/PhysRevLett.6.47

J.W. Dungey, The structure of the exosphere or adventures in velocity space, in *Geophysics, the Earth's Environment*, ed. by C. DeWitt, J. Hieblot, L. Le Beau (Gordon and Breach, New York, 1963), p. 503

J.W. Dungey, The length of the magnetospheric tail. J. Geophys. Res. **70**, 1753 (1965)

T.E. Eastman, L.A. Frank, W.K. Peterson, W. Lennartsson, The plasma sheet boundary layer. J. Geophys. Res. **89**, 1553–1572 (1984). doi:10.1029/JA089iA03p01553

M.M. Echim, M. Roth, J. De Keyser, Sheared magnetospheric plasma flows and discrete auroral arcs: a quasi-static coupling model. Ann. Geophys. **25**(1), 317–330 (2007). doi:10.5194/angeo-25-317-2007

R.C. Elphic, P.A. Mutch, C.T. Russell, Observations of field-aligned currents at the plasma sheet boundary—an ISEE-1 and 2 survey. Geophys. Res. Lett. **12**, 631–634 (1985). doi:10.1029/GL012i010p00631

E. Engwall, A.I. Eriksson, C.M. Cully, M. Andre, R. Torbert, H. Vaith, Earth's ionospheric outflow dominated by hidden cold plasma. Nat. Geosci. **2**(1), 24–27 (2009). doi:10.1038/ngeo387

G.M. Erickson, R.A. Wolf, Is steady convection possible in the Earth's magnetotail? Geophys. Res. Lett. **7**, 897 (1980)

A.I. Eriksson, M. André, B. Klecker, H. Laakso, P.-A. Lindqvist, F. Mozer, G. Paschmann, A. Pedersen, J. Quinn, R. Torbert, K. Torkar, H. Vaith, Electric field measurements on Cluster: comparing the double-probe and electron drift techniques. Ann. Geophys. **24**, 275–289 (2006). doi:10.5194/angeo-24-275-2006

D.H. Fairfield, On the average configuration of the geomagnetic tail. J. Geophys. Res. **84**, 1950–1958 (1979). doi:10.1029/JA084iA05p01950

D.H. Fairfield, J. Jones, Variability of the tail lobe field strength. J. Geophys. Res. **101**, 7785–7791 (1996). doi:10.1029/95JA03713

D.H. Fairfield, J.D. Scudder, Polar rain—solar coronal electrons in the Earth's magnetosphere. J. Geophys. Res. **90**, 4055–4068 (1985). doi:10.1029/JA090iA05p04055

D.H. Fairfield et al., Earthward flow bursts in the inner magnetotail and their relation to auroral brightenings, AKR intensifications, geosynchronous particle injections and magnetic activity. J. Geophys. Res. **104**, 355–370 (1999)

T.G. Forbes, E.W. Hones Jr., S.J. Bame, J.R. Asbridge, G. Paschmann, N. Sckopke, C.T. Russell, Evidence for the tailward retreat of a magnetic neutral line in the magnetotail during substorm recovery. Geophys. Res. Lett. **8**, 261 (1981)

C. Forsyth, M. Lester, S.W.H. Cowley, I. Dandouras, A.N. Fazakerley, R.C. Fear, H.U. Frey, A. Grocott, A. Kadokura, E. Lucek, H. Rème, S.E. Milan, J. Watermann, Observed tail current systems associated with bursty bulk flows and auroral streamers during a period of multiple substorms. Ann. Geophys. **26**, 167–184 (2008)

L.A. Frank, W.R. Paterson, K.K. Khurana, Observations of thermal plasmas in Jupiter's magnetotail. J. Geophys. Res. **107**(A1), 1003 (2002). doi:10.1029/2001JA000077

M.P. Freeman, C.J. Farrugia, A statistical study of the possible effects of solar wind variability on the recurrence rate of substorms. J. Geophys. Res. **100**, 23607 (1995)

M.P. Freeman, C.J. Farrugia, Solar wind input between substorm onsets during and after the October 18–20, 1995, magnetic cloud. J. Geophys. Res. **104**, 22729 (1999)

M.P. Freeman, S.K. Morley, A minimal substorm model that explains the observed statistical distribution of times between substorms. Geophys. Res. Lett. **31**, L12807 (2004). doi:10.1029/2004GL019989

M.P. Freeman, S.K. Morley, No evidence for externally triggered substorms based on superposed epoch analysis of IMF B_z. Geophys. Res. Lett. **36**, L21101 (2009). doi:10.1029/2009GL040621

K. Fukazawa, T. Ogino, R.J. Walker, Dynamics of the Jovian magnetosphere for northward interplanetary magnetic field (IMF). Geophys. Res. Lett. **32** (2005). doi:10.1029/2004GL021392

K. Fukazawa, T. Ogino, R.J. Walker, Vortex-associated reconnection for northward IMF in the Kronian magnetosphere. Geophys. Res. Lett. **34** (2007). doi:10.1029/2007GL031784

K. Fukazawa, T. Ogino, R.J. Walker, A simulation study of dynamics in the distant Jovian magnetotail. J. Geophys. Res. **115**, A09219 (2010). doi:10.1029/2009JA015228

Y.S. Ge, C.T. Russell, K.K. Khurana, Reconnection sites in Jupiter's magnetotail and relation to Jovian auroras. Planet. Space Sci. **58**(11), 1455–1469 (2010)

K.-H. Glassmeier, H.-U. Auster, U. Motschmann, A feedback dynamo generating Mercury's magnetic field. Geophys. Res. Lett. **34**, L22201 (2007). doi:10.1029/2007GL031662

T. Gold, Motions in the magnetosphere of the Earth. J. Geophys. Res. **644**(9), 1219–1224 (1959)

M.L. Goldstein, R.P. Lepping, E.C. Sittler Jr., Magnetic field properties of Jupiter's tail at distances from 80 to 7500 Jovian radii. J. Geophys. Res. **90**, 8223–8239 (1985)

O. Grasset et al., JUpiter ICy moons Explorer (JUICE): an ESA mission to orbit Ganymede and to characterise the Jupiter system. Planet. Space Sci. **78**, 1–21 (2013)

E.E. Grigorenko, M. Hoshino, M. Hirai, T. Mukai, L.M. Zelenyi, "Geography" of ion acceleration in the magnetotail: X-line versus current sheet effects. J. Geophys. Res. **114**(A13), A03203 (2009). doi:10.1029/2008JA013811

A. Grocott, S.V. Badman, S.W.H. Cowley, S.E. Milan, J.D. Nichols, T.K. Yeoman, Magnetosonic Mach number dependence of the efficiency of reconnection between planetary and interplanetary magnetic fields. J. Geophys. Res. **114**, A07219 (2009). doi:10.1029/2009JA014330

D. Grodent, J.T. Clarke, J.H. Waite Jr., S.W.H. Cowley, J.-C. Gérard, J. Kim, Jupiter's polar auroral emissions. J. Geophys. Res. **108**(A10), 1366 (2003a). doi:10.1029/2003JA010017

D. Grodent, J.T. Clarke, J. Kim, J.H. Waite Jr., S.W.H. Cowley, Jupiter's main auroral oval observed with HST-STIS. J. Geophys. Res. **108**(A11), 1389 (2003b). doi:10.1029/2003JA009921

D. Grodent, J.-C. Gérard, J.T. Clarke, G.R. Gladstone, J.H. Waite Jr., A possible auroral signature of magnetotail reconnection process on Jupiter. J. Geophys. Res. **109**, A05201 (2004). doi:10.1029/2003JA010341

D.A. Gurnett, The Earth as a radio source: terrestrial kilometric radiation. J. Geophys. Res. **79**, 4227 (1974)

P.G. Hanlon, M.K. Dougherty, N. Krupp, K.C. Hansen, F.J. Crary, D.T. Young, G. Tóth, Dual spacecraft observations of a compression event within the Jovian magnetosphere: signatures of externally triggered supercorotation? J. Geophys. Res. **109**, A09S09 (2004). doi:10.1029/2003JA010116

K.C. Hansen, T.I. Gombosi, D. Dezeeuw, C.P.T. Groth, K.G. Powell, A 3D global MHD simulation of Saturn's magnetosphere. Adv. Space Res. **26**, 1681–1690 (2000). doi:10.1016/S0273-1177(00)00078-8

K.C. Hansen, A.J. Ridley, G.B. Hospodarsky, N. Achilleos, M.K. Dougherty, T.I. Gombosi, G. Tóth, Global MHD simulations of Saturn's magnetosphere at the time of Cassini approach. Geophys. Res. Lett. **32**, L20S06 (2005). doi:10.1029/2005GL022835

E.G. Harris, On a plasma sheath separating regions of oppositely directed magnetic field. Nuovo Cimento **23**, 115–121 (1962)

H. Hasegawa, M. Fujimoto, T. Phan, H. Reme, A. Balogh, M. Dunlop, C. Hashimoto, R. TanDokoro, Transport of solar wind into Earth's magnetosphere through rolled-up Kelvin-Helmholtz vortices. Nature **430**(7001), 755–758 (2004). doi:10.1038/nature02799

M.G. Henderson, G.D. Reeves, R.D. Belian, J.S. Murphree, Observations of magnetospheric substorms occurring with no apparent solar wind/IMF trigger. J. Geophys. Res. **101**(A5), 10773–10791 (1996). doi:10.1029/96JA00186

J.P. Heppner, Time sequences and spatial relations in auroral activity during magnetic bays at College, Alaska. J. Geophys. Res. **59**(3), 329–338 (1954). doi:10.1029/JZ059i003p00329

M. Hesse, J. Birn, On dipolarization and its relation to the substorm current wedge. J. Geophys. Res. **96**(A11), 19417–19426 (1991). doi:10.1029/91JA01953

M. Hesse, K. Schindler, The onset of magnetic reconnection in the magnetotail. Earth Planets Space **53**, 645–653 (2001)

T.W. Hill, Inertial limit on corotation. J. Geophys. Res. **84**, A11 (1979)

T.W. Hill, The Jovian auroral oval. J. Geophys. Res. **106**(A5), 8101–8107 (2001). doi:10.1029/2000JA000302

T.W. Hill, F.C. Michel, Heavy ions from the Galilean satellites and the centrifugal distortion of the Jovian magnetosphere. J. Geophys. Res. **81**, 4561–4565 (1976)

T.W. Hill, A.J. Dessler, F.C. Michel, Configuration of the Jovian magnetosphere. Geophys. Res. Lett. **1**, 3–6 (1974). doi:10.1029/GL001i001p00003

T.W. Hill et al., Plasmoids in Saturn's magnetotail. J. Geophys. Res. **113**, A01214 (2008). doi:10.1029/2007JA012626

G.C. Ho, S.M. Krimigis, R.E. Gold, D.N. Baker, B.J. Anderson, H. Korth, J.A. Slavin, R.L. McNutt Jr., S.C. Solomon, Spatial distribution and spectral characteristics of energetic electrons in Mercury's magnetosphere. J. Geophys. Res. **117**, A00M04 (2012). doi:10.1029/2012JA017983

R.E. Holzer, J.A. Slavin, Magnetic flux transfer associated with expansions and contractions of the dayside magnetosphere. J. Geophys. Res. **83**(A8), 3831–3839 (1978). doi:10.1029/JA083iA08p03831

R.E. Holzer, J.A. Slavin, A correlative study of magnetic flux transfer in the magnetosphere. J. Geophys. Res. **84**(A6), 2573–2578 (1979). doi:10.1029/JA084iA06p02573

E.W. Hones Jr., The magnetotail: its generation and dissipation, in *Physics of Solar Planetary Environments*, ed. by D.J. Williams (AGU, Washington, 1976), pp. 559–571

E.W. Hones Jr., Substorm processes in the magnetotail: comments on "On hot tenuous plasma, fireballs, and boundary layers in the Earth's magnetotail" by L.A. Frank et al J. Geophys. Res. **82**, 5633 (1977)

E.W. Hones Jr., Plasma flow in the magnetotail and its implications for substorm theories, in *Dynamics of the Magnetosphere*, ed. by S.I. Akasofu (D. Reidel, Dordrecht, 1979), p. 545

M. Hoshino, A. Nishida, T. Mukai, Y. Saito, T. Yamamoto, Structure of plasma sheet in magnetotail: double-peaked electric current sheet. J. Geophys. Res. **101**, 24775 (1996)

T.-S. Hsu, R.L. McPherron, Average characteristics of triggered and nontriggered substorms. J. Geophys. Res. **109**, A07208 (2004). doi:10.1029/2003JA009933

C.-S. Huang, J.C. Foster, G.D. Reeves, G. Le, H.U. Frey, C.J. Pollock, J.-M. Jahn, Periodic magnetospheric substorms: multiple space-based and ground-based instrumental observations. J. Geophys. Res. **108**(A11), 1411 (2003). doi:10.1029/2003JA009992

D.E. Huddleston, C.T. Russell, M.G. Kivelson, K.K. Khurana, L. Bennett, Location and shape of the Jovian magnetopause and bow shock. J. Geophys. Res. **103**(E9), 20075–20082 (1998)

W.J. Hughes, D.G. Sibeck, On the 3-dimensional structure of plasmoids. Geophys. Res. Lett. **14**, 636–639 (1987). doi:10.1029/GL014i006p00636

A. Ieda, S. Machida, T. Mukai, Y. Saito, T. Yamamoto, A. Nishida, T. Terasawa, S. Kokubun, Statistical analysis of the plasmoid evolution with geotail observations. J. Geophys. Res. **103**(A3), 4453–4465 (1998). doi:10.1029/97JA03240

S. Imada, M. Hoshino, T. Mukai, The dawn-dusk asymmetry of energetic electron in the Earth's magnetotail: observation and transport models. J. Geophys. Res. **113**(A12), A11201 (2008). doi:10.1029/2008JA013610

S.M. Imber, S.E. Milan, B. Hubert, The auroral and ionospheric flow signatures of dual lobe reconnection. Ann. Geophys. **24**, 3115–3129 (2006). doi:10.5194/angeo-24-3115-2006

S.M. Imber, J.A. Slavin, H.U. Auster, V. Angelopoulos, A THEMIS survey of flux ropes and travelling compression regions: location of the near-Earth reconnection site during solar minimum. J. Geophys. Res. **116**, A02201 (2011). doi:10.1029/2010JA016026

D.S. Intriligator, H.R. Collard, J.D. Mihalov, O.L. Vaisberg, J.H. Wolf, Evidence for Earth magnetic tail associated phenomena at 3100 R_E. Geophys. Res. Lett. **6**, 585 (1979)

W.-H. Ip, A. Kopp, MHD simulations of the solar wind interaction with Mercury. J. Geophys. Res. **107**(A11), 1348 (2002). doi:10.1029/2001JA009171

J. Isbell, A.J. Dessler, J.H. Waite Jr., Magnetospheric energization by interaction between planetary spin and the solar wind. J. Geophys. Res. **89**, 10716–10722 (1984)

P.L. Israelevich, A.I. Ershkovich, Bifurcation of Jovian magnetotail current sheet. Ann. Geophys. **24**, 1479–1481 (2006)

P.L. Israelevich, A.I. Ershkovich, R. Oran, Bifurcation of the tail current sheet in Jovian magnetosphere. Planet. Space Sci. **55**, 2261–2266 (2007)

C.M. Jackman, C.S. Arridge, Statistical properties of the magnetic field in the Kronian magnetotail lobes and current sheet. J. Geophys. Res. **116**, A05224 (2011). doi:10.1029/2010JA015973

C.M. Jackman, N. Achilleos, E.J. Bunce, S.W.H. Cowley, M.K. Dougherty, G.H. Jones, S.E. Milan, E.J. Smith, Interplanetary magnetic field at ∼9 AU during the declining phase of the solar cycle and its implications for Saturn's magnetospheric dynamics. J. Geophys. Res. **109**, 11203 (2004). doi:10.1029/2004JA010614

C.M. Jackman, C.T. Russell, D.J. Southwood, C.S. Arridge, N. Achilleos, M.K. Dougherty, Strong rapid dipolarizations in Saturn's magnetotail: in situ evidence of reconnection. Geophys. Res. Lett. **34**, L11203 (2007). doi:10.1029/2007GL029764

C.M. Jackman, R.J. Forsyth, M.K. Dougherty, The overall configuration of the interplanetary magnetic field upstream of Saturn as revealed by Cassini observations. J. Geophys. Res. **113**, A08114 (2008a). doi:10.1029/2008JA013083

C.M. Jackman et al., A multi-instrument view of tail reconnection at Saturn. J. Geophys. Res. **113**, A11213 (2008b). doi:10.1029/2008JA013592

C.M. Jackman, L. Lamy, M.P. Freeman, P. Zarka, B. Cecconi, W.S. Kurth, S.W.H. Cowley, M.K. Dougherty, On the character and distribution of lower-frequency radio emissions at Saturn and their relationship to substorm-like events. J. Geophys. Res. **114**, A08211 (2009)

C.M. Jackman, J.A. Slavin, S.W.H. Cowley, Cassini observations of plasmoid structure and dynamics: implications for the role of magnetic reconnection in magnetospheric circulation at Saturn. J. Geophys. Res. **116**, A10212 (2011). doi:10.1029/2011JA016682

C.M. Jackman, N. Achilleos, S.W.H. Cowley, E.J. Bunce, A. Radioti, D. Grodent, S.V. Badman, M.K. Dougherty, W. Pryor, Auroral counterpart of magnetic field dipolarizations in Saturn's tail. Planet. Space Sci. **82–83**, 34–42 (2013). doi:10.1016/j.pss.2013.03.010

C.M. Jackman, J.A. Slavin, M.G. Kivelson, D.J. Southwood, N. Achilleos, M.F. Thomsen, G.A. Di-Braccio, J.P. Eastwood, M.P. Freeman, M.K. Dougherty, M.F. Vogt, Saturn's dynamic magnetotail: a comprehensive magnetic field and plasma survey of plasmoids and traveling compression regions and their role in global magnetospheric dynamics. J. Geophys. Res. Space Phys. **119** (2014). doi:10.1002/2013JA019388

C. Jacquey, J.A. Sauvaud, J. Dandouras, Location and propagation of the magnetotail current disruption during substorm expansion: analysis and simulation of an ISEE multi-onset event. Geophys. Res. Lett. **18**(3), 389–392 (1991). doi:10.1029/90GL02789

X. Jia, M.G. Kivelson, T.I. Gombosi, Driving Saturn's magnetospheric periodicities from the upper atmosphere/ionosphere. J. Geophys. Res. **117**, A04215 (2012a). doi:10.1029/2011JA017367

X. Jia, K.C. Hansen, T.I. Gombosi, M.G. Kivelson, G. Tóth, D.L. DeZeeuw, A.J. Ridley, Magnetospheric configuration and dynamics of Saturn's magnetosphere: a global MHD simulation. J. Geophys. Res. **117**, A05225 (2012b). doi:10.1029/2012JA017575

T. Johansson, G. Marklund, T. Karlsson, S. Liléo, P.-A. Lindqvist, A. Marchaudon, H. Nilsson, A. Fazakerley, On the profile of intense high-altitude auroral electric fields at magnetospheric boundaries. Ann. Geophys. **24**, 1713 (2006)

J.R. Johnson, C.Z. Cheng, Kinetic Alfvén waves and plasma transport at the magnetopause. Geophys. Res. Lett. **24**(11), 1423–1426 (1997). doi:10.1029/97GL01333

S.P. Joy, M.G. Kivelson, R.J. Walker, K.K. Khurana, C.T. Russell, T. Ogino, Probabilistic models of the Jovian magnetopause and bow shock locations. J. Geophys. Res. **107**(A10), 1309 (2002). doi:10.1029/2001JA009146

K. Kabin, T.I. Gombosi, D.L. DeZeeuw, K.G. Powell, Interaction of Mercury with the solar wind. Icarus **143**(2), 397–406 (2000)

K. Kabin et al., Global MHD modelling of Mercury's magnetosphere with applications to the MESSENGER mission and dynamo theory. Icarus **195**, 1–15 (2008)

M.L. Kaiser, J.K. Alexander, Terrestrial kilometric radiation 3. Average spectral properties. J. Geophys. Res. **82**, 3273–3280 (1977)

M.L. Kaiser, M.D. Desch, J.W. Warwick, J.B. Pearce, Voyager detection of nonthermal radio emission from Saturn. Science **209**, 1238–1240 (1980)

E. Kallio, P. Janhunen, Modelling the solar wind interaction with Mercury by a quasi-neutral hybrid model. Ann. Geophys. **21**(11), 2133–2145 (2003)

S.J. Kanani, C.S. Arridge, G.H. Jones, A.N. Fazakerley, H.J. McAndrews, N. Sergis, S.M. Krimigis, M.K. Dougherty, A.J. Coates, D.T. Young, K.C. Hansen, N. Krupp, A new form of Saturn's magnetopause using a dynamic pressure balance model, based on in-situ, multi-instrument Cassini measurements. J. Geophys. Res. **115**, A06207 (2010). doi:10.1029/2009JA014262

M. Kane, B.H. Mauk, E.P. Keath, S.M. Krimigis, Hot ions in Jupiter's magnetodisc: a model for Voyager 2 low-energy charged particle measurements. J. Geophys. Res. **100**(A10), 19473–19486 (1995). doi:10.1029/95JA00793

M. Kane, D.J. Williams, B.H. Mauk, R.W. McEntire, E.C. Roelof, Galileo energetic particles detector measurements of hot ions in the neutral sheet region of Jupiter's magnetodisk. Geophys. Res. Lett. **26**(1), 5–8 (1999). doi:10.1029/1998GL900267

S. Kasahara, E.A. Kronberg, N. Krupp, T. Kimura, C. Tao, S.V. Badman, A. Retinò, M. Fujimoto, Magnetic reconnection in the Jovian tail: *X*-line evolution and consequent plasma sheet structures. J. Geophys. Res. **116**, A11219 (2011). doi:10.1029/2011JA016892

S. Kasahara, E.A. Kronberg, T. Kimura, C. Tao, S.V. Badman, A. Masters, A. Retinò, N. Krupp, M. Fujimoto, Asymmetric distribution of reconnection jet fronts in the Jovian nightside magnetosphere. J. Geophys. Res. **118**, 375–384 (2013). doi:10.1029/2012JA018130

A. Keiling, V. Angelopoulos, A. Runov, J. Weygand, S.V. Apatenkov, S. Mende, J. McFadden, D. Larson, O. Amm, K.-H. Glassmeier, H.U. Auster, Substorm current wedge driven by plasma flow vortices: THEMIS observations. J. Geophys. Res. **114**(A13), A00C22 (2009). doi:10.1029/2009JA014114

C.F. Kennel, Magnetospheres of the planets. Space Sci. Rev. **14**, 511–533 (1973)

L. Kepko, E. Spanswick, V. Angelopoulos, E. Donovan, J. McFadden, K.-H. Glassmeier, J. Raeder, H.J. Singer, Equatorward moving auroral signatures of a flow burst observed prior to auroral onset. Geophys. Res. Lett. **36**, L24104 (2009). doi:10.1029/2009GL041476

Y.V. Khotyaintsev, C.M. Cully, A. Vaivads, M. André, C.J. Owen, Plasma jet braking: energy dissipation and nonadiabatic electrons. Phys. Rev. Lett. **106**, 165001 (2011). doi:10.1103/PhysRevLett.106.165001

K.K. Khurana, Euler potential models of Jupiter's magnetospheric field. J. Geophys. Res. **102**(A6), 11295–11306 (1997)

K.K. Khurana, Influence of solar wind on Jupiter's magnetosphere deduced from currents in the equatorial plane. J. Geophys. Res. **106**, 25999–26016 (2001)

K.K. Khurana, H.K. Schwarzl, Global structure of Jupiter's magnetospheric current sheet. J. Geophys. Res. **110**, A07227 (2005). doi:10.1029/2004JA010757

A. Kidder, R.M. Winglee, E.M. Harnett, Erosion of the dayside magnetosphere at Mercury in association with ion outflows and flux rope generation. J. Geophys. Res. **113**, A09223 (2008). doi:10.1029/2008JA013038

A. Kidder, C.S. Paty, R.M. Winglee, E.M. Harnett, External triggering of plasmoid development at Saturn. J. Geophys. Res. **117**, A07206 (2012). doi:10.1029/2012JA017625

S.A. Kiehas, V. Angelopoulos, A. Runov, M.B. Moldwin, C. Möstl, On the formation of tilted flux ropes in the Earth's magnetotail observed with ARTEMIS. J. Geophys. Res. **117**, A05231 (2012). doi:10.1029/2011JA017377

M.G. Kivelson, Planetary magnetospheres, in *Solar-Terrestrial Environment*, ed. by Y. Kamide, C.-L. Chian (Springer, New York, 2007), pp. 470–492. Chap. 19

M.G. Kivelson, K.K. Khurana, Properties of the magnetic field in the Jovian magnetotail. J. Geophys. Res. **107**(A8), 1196 (2002). doi:10.1029/2001JA000249

M.G. Kivelson, D.J. Southwood, First evidence of IMF control of Jovian magnetospheric boundary locations: Cassini and Galileo magnetic field measurements compared. Planet. Space Sci. **51**, 891–898 (2003)

M.G. Kivelson, D.J. Southwood, Dynamical consequences of two modes of centrifugal instability in Jupiter's outer magnetosphere. J. Geophys. Res. **110**, A12209 (2005). doi:10.1029/2005JA011176

M.G. Kivelson, A.J. Ridley, Saturation of the polar cap potential: inference from Alfvén wing arguments. J. Geophys. Res. **113**, A05214 (2008). doi:10.1029/2007JA012302

H. Korth, B.J. Anderson, J.M. Raines, J.A. Slavin, T.H. Zurbuchen, C.L. Johnson, M.E. Purucker, R.M. Winslow, S.C. Solomon, R.L. McNutt Jr., Plasma pressure in Mercury's equatorial magnetosphere derived from MESSENGER magnetometer observations. Geophys. Res. Lett. **38**, L22201 (2011). doi:10.1029/2011GL049451

E.A. Kronberg, K.-H. Glassmeier, J. Woch, N. Krupp, A. Lagg, M.K. Dougherty, A possible intrinsic mechanism for the quasi-periodic dynamics of the Jovian magnetosphere. J. Geophys. Res. **112**, A05203 (2007). doi:10.1029/2006JA011994

E.A. Kronberg, J. Woch, N. Krupp, A. Lagg, Mass release process in the Jovian magnetosphere: statistics on particle burst parameters. J. Geophys. Res. **113**, A10202 (2008). doi:10.1029/2008JA013332

E.A. Kronberg, S. Kasahara, N. Krupp, J. Woch, Field-aligned beams and reconnection in the Jovian magnetotail. Icarus **217**, 55–65 (2012)

N. Krupp, J. Woch, A. Lagg, B. Wilken, S. Livi, D.J. Williams, Energetic particle bursts in the predawn Jovian magnetotail. Geophys. Res. Lett. **25**(8), 1249–1252 (1998). doi:10.1029/98GL00863

W.S. Kurth, J.D. Sullivan, D.A. Gurnett, F.L. Scarf, H.S. Bridge, E.C. Sittler Jr., Observations of Jupiter's distant magnetotail and wake. J. Geophys. Res. **87**(A12), 10373–10383 (1982). doi:10.1029/JA087iA12p10373

W.S. Kurth, T. Murata, G. Lu, D.A. Gurnett, H. Matsumoto, Auroral kilometric radiation and the auroral electrojet index for the January 1997 magnetic cloud event. Geophys. Res. Lett. **25**, 3027–3030 (1998)

H.R. Lai, H.Y. Wei, C.T. Russell, C.S. Arridge, M.K. Dougherty, Reconnection at the magnetopause of Saturn: perspective from FTE occurrence and magnetosphere size. J. Geophys. Res. **117**, A05222 (2012). doi:10.1029/2011JA017263

L. Lamy, P. Zarka, B. Cecconi, R. Prangé, W.S. Kurth, D.A. Gurnett, Saturn kilometric radiation: average and statistical properties. J. Geophys. Res. **113**, A07201 (2008). doi:10.1029/2007JA012900

R.P. Lepping, M.D. Desch, L.W. Klein, E.C. Sittler Jr., J.D. Sullivan, W.S. Kurth, K.W. Behannon, Structure and other properties of Jupiter's distant magnetotail. J. Geophys. Res. **88**(A11), 8801–8815 (1983). doi:10.1029/JA088iA11p08801

T.W. Lezniak, R.L. Arnoldy, G.K. Parks, J.R. Winckler, Measurement and intensity of energetic electrons at the equator at 6.6 R_E. Radio Sci. **3**, 710 (1968)

X. Li, D.N. Baker, M. Temerin, G.D. Reeves, Simulation of dispersionless injections and subsequent drift echoes of energetic electrons associated with substorms. Geophys. Res. Lett. **25**, 3763 (1998)

K. Liou, Large, abrupt pressure decreases as a substorm onset trigger. Geophys. Res. Lett. **34**, L14107 (2007). doi:10.1029/2007GL029909

M. Lockwood, S.W.H. Cowley, Ionospheric convection and the substorm cycle, in *Proceedings of the International Conference on Substorms (ICS-1)*. ESA Spec. Publ., vol. SP-335 (1992), pp. 99–109

M. Lockwood, M.A. Hapgood, How the magnetopause transition parameter works. Geophys. Res. Lett. **24**, 373–376 (1997). doi:10.1029/97GL00120

P. Louarn, A. Roux, S. Perraut, W.S. Kurth, D.A. Gurnett, A study of the Jovian "energetic magnetospheric events" observed by Galileo: role in the radial plasma transport. J. Geophys. Res. **105**(A6), 13073–13088 (2000). doi:10.1029/1999JA900478

P. Louarn et al., Observation of similar radio signatures at Saturn and Jupiter: implications for the magnetospheric dynamics. Geophys. Res. Lett. **34**, L20113 (2007). doi:10.1029/2007GL030368

A.T.Y. Lui, A synthesis of magnetospheric substorm models. J. Geophys. Res. **96**, 1849 (1991)

A.T.Y. Lui, Comment on "Tail reconnection triggering substorm onset". Science **324**(5933) (2009). doi:10.1126/science.1167726

L.R. Lyons, Substorms: fundamental observational features, distinction from other disturbances, and external triggering. J. Geophys. Res. **101**(A6), 13011–13025 (1996). doi:10.1029/95JA01987

L.R. Lyons, T.W. Speiser, Evidence for current sheet acceleration in the geomagnetic tail. J. Geophys. Res. **87**, 2276–2286 (1982). doi:10.1029/JA087iA04p02276

L.R. Lyons, G.T. Blanchard, J.C. Samson, R.P. Lepping, T. Yamamoto, T. Moretto, Coordinated observations demonstrating external substorm triggering. J. Geophys. Res. **102**(A12), 27039–27051 (1997). doi:10.1029/97JA02639

L. Lyons, T. Nagai, G. Blanchard, J. Samson, T. Yamamoto, T. Mukai, A. Nishida, S. Kokubun, Association between geotail plasma flows and auroral poleward boundary intensifications observed by CANOPUS photometers. J. Geophys. Res. **104**(A3), 4485–4500 (1999)

W.M. Macek, W.S. Kurth, R.P. Lepping, D.G. Sibeck, Distant magnetotails of the outer magnetic planets. Adv. Space Res. **12**(8), 847–855 (1992)

G. Marklund, T. Karlsson, J. Clemmons, On low-altitude particle acceleration and intense electric fields and their relationship to black aurora. J. Geophys. Res. **102**, 17509–17522 (1997)

A. Masters, D.G. Mitchell, A.J. Coates, M.K. Dougherty, Saturn's low-latitude boundary layer: 1. Properties and variability. J. Geophys. Res. **116**, A06210 (2011a). doi:10.1029/2010JA016421

A. Masters, M.F. Thomsen, S.V. Badman, C.S. Arridge, D.T. Young, A.J. Coates, M.K. Dougherty, Supercorotating return flow from reconnection in Saturn's magnetotail. Geophys. Res. Lett. **38**, L03103 (2011b). doi:10.1029/2010GL046149

B.H. Mauk et al., Energetic neutral atoms from a trans-Europa gas torus at Jupiter. Nature **421**, 920–922 (2003)

H.J. McAndrews, M.F. Thomsen, C.S. Arridge, C.M. Jackman, R.J. Wilson, M.G. Henderson, R.L. Tokar, K.K. Khurana, E.C. Sittler, A.J. Coates, M.K. Dougherty, Plasma in Saturn's nightside magnetosphere and the implications for global circulation. Planet. Space Sci. **57**(14–15), 1714–1722 (2009). doi:10.1016/j.pss.2009.03.003

D.J. McComas, F. Bagenal, Jupiter: a fundamentally different magnetospheric interaction with the solar wind. Geophys. Res. Lett. **34**, L20106 (2007). doi:10.1029/2007GL031078

D.J. McComas, F. Allegrini, F. Bagenal, F. Crary, R.W. Ebert, H. Elliott, A. Stern, P. Valek, Diverse plasma populations and structures in Jupiter's magnetotail. Science **318** (2007). doi:10.1126/science.1147393

D.J. McComas et al., First IBEX observations of the terrestrial plasma sheet and a possible disconnection event. Geophys. Res. Lett. **116**, A02211 (2011)

R.L. McNutt Jr., Force balance in the magnetospheres of Jupiter and Saturn. Adv. Space Res. **3**, 55–58 (1983)

R.L. McNutt Jr. et al., Energetic particles in the Jovian magnetotail. Science **318**, 220 (2007)

R.L. McPherron, C.T. Russell, M.P. Aubry, Satellite studies of magnetospheric substorms on August 15, 1968. 9. Phenomenological model for substorms. J. Geophys. Res. **78**, 3131–3149 (1973). doi:10.1029/JA078i016p03131

F.C. Michel, P.A. Sturrock, Centrifugal instability of the Jovian magnetosphere and its interaction with the solar wind. Planet. Space Sci. **22**, 1501 (1974)

S.E. Milan, A simple model of the flux content of the distant magnetotail. J. Geophys. Res. **109**, A07210 (2004). doi:10.1029/2004JA010397

S.E. Milan, Both solar wind-magnetosphere coupling and ring current intensity control of the size of the auroral oval. Geophys. Res. Lett. **36**, L18101 (2009). doi:10.1029/2009GL039997

S.E. Milan, J.A. Slavin, An assessment of the length and variability of Mercury's magnetotail. Planet. Space Sci. **59**, 2058–2065 (2011)

S.E. Milan, E.J. Bunce, S.W.H. Cowley, C.M. Jackman, Implications of rapid planetary rotation for the Dungey magnetotail of Saturn. J. Geophys. Res. **110**, A03209 (2005). doi:10.1029/2004JA010716

S.E. Milan, G. Provan, B. Hubert, Magnetic flux transport in the Dungey cycle: a survey of dayside and nightside reconnection rates. J. Geophys. Res. **112**, A01209 (2007). doi:10.1029/2006JA011642

S.E. Milan, P.D. Boakes, B. Hubert, Response of the expanding/contracting polar cap to weak and strong solar wind driving: implications for substorm onset. J. Geophys. Res. **113**, A09215 (2008). doi:10.1029/2008JA013340

S.E. Milan, J.S. Gosling, B. Hubert, Relationship between interplanetary parameters and the magnetopause reconnection rate quantified from observations of the expanding polar cap. J. Geophys. Res. **117**, A03226 (2012). doi:10.1029/2011JA017082

A. Milillo et al., The BepiColombo mission: an outstanding tool for investigating the Hermean environment. Planet. Space Sci. **58**, 40–60 (2010)

D.G. Mitchell, F. Kutchko, D.J. Williams, T.E. Eastman, L.A. Frank, An extended study of the low-latitude boundary layer on the dawn and dusk flanks of the magnetosphere. J. Geophys. Res. **92**, 7394–7404 (1987). doi:10.1029/JA092iA07p07394

D.G. Mitchell, P.C. Brandt, E.C. Roelof, D.C. Hamilton, K.C. Retterer, S. Mende, Global imaging of O^+ from IMAGE/HENA. Space Sci. Rev. **109**, 63–75 (2003)

D.G. Mitchell et al., Energetic ion acceleration in Saturn's magnetotail: substorms at Saturn? Geophys. Res. Lett. **32**, L20S01 (2005). doi:10.1029/2005GL022647

D.G. Mitchell, S.M. Krimigis, C. Paranicas, P.C. Brandt, J.F. Carbary, E.C. Roelof, W.S. Kurth, D.A. Gurnett, J.T. Clarke, J.D. Nichols, J. Gerard, D.C. Grodent, M.K. Dougherty, W.R. Pryor, Recurrent energization of plasma in the midnight to-dawn quadrant of Saturn's magnetosphere, and its relationship to auroral UV and radio emissions. Planet. Space Sci. **57**, 1732–1742 (2009). doi:10.1016/j.pss.2009.04.002

P.F. Mizera, D.J. Gorney, J.F. Fennell, Experimental verification of an S-shaped potential structure. J. Geophys. Res. **87**, 1535 (1982)

M. Moldwin, W. Hughes, On the formation and evolution of plasmoids: a survey of ISEE 3 geotail data. J. Geophys. Res. **97**, 19259–19282 (1992). doi:10.1029/92JA01598

T. Moore, C. Chappell, M. Chandler, P. Craven, B. Giles, C. Pollock, J. Burch, D. Young, J. Waite, J. Nordholt, M. Thomsen, D. McComas, J. Berthelier, W. Williamson, R. Robson, F. Mozer, High-altitude observations of the polar wind. Science **277**(5324), 349–351 (1997). doi:10.1126/science.277.5324.349

A. Morioka, Y. Miyoshi, F. Tsuchiya, H. Misawa, T. Sakanoi, K. Yumoto, R.R. Anderson, J.D. Menietti, E.F. Donovan, Dual structure of auroral acceleration regions at substorm onsets as derived from AKR spectra. J. Geophys. Res. **112**, A06245 (2007). doi:10.1029/2006JA012186

A. Morioka, Y. Miyoshi, Y. Miyashita, Y. Kasaba, H. Misawa, F. Tsuchiya, R. Kataoka, A. Kadokura, T. Mukai, K. Yumoto, D.J. Menietti, G. Parks, K. Liou, F. Honary, E. Donovan, Two-step evolution of auroral acceleration at substorm onset. J. Geophys. Res. **115**, A11213 (2010). doi:10.1029/2010JA015361

S.K. Morley, M.P. Freeman, On the association between northward turnings of the interplanetary magnetic field and substorm onsets. Geophys. Res. Lett. **34**, L08104 (2007). doi:10.1029/2006GL028891

S.K. Morley, A.P. Rouillard, M.P. Freeman, Recurrent substorm activity during the passage of a corotating interaction region. J. Atmos. Sol.-Terr. Phys. **71**(10–11), 1073–1081 (2009). doi:10.1016/j.jastp.2008.11.009

F.S. Mozer, C.A. Cattell, M.K. Hudson, R.L. Lysak, M. Temerin, R.B. Torbert, Satellite measurements and theories of low-altitude auroral particle acceleration. Space Sci. Rev. **27**, 155 (1980)

R. Nakamura et al., Earthward flow bursts, auroral streamers, and small expansions. J. Geophys. Res. **106**, 10791 (2001)

R. Nakamura, W. Baumjohann, A. Runov, M. Volwerk, T.L. Zhang, B. Klecker, Y. Bogdanova, A. Roux, A. Balogh, H. Reme, J.A. Sauvaud, H.U. Frey, Fast flow during current sheet thinning. Geophys. Res. Lett. **29**, 2140 (2002)

R. Nakamura, W. Baumjohann, C. Mouikis, L.M. Kistler, A. Runov, M. Volwerk, Y. Asano, Z. Vörös, T.L. Zhang, B. Klecker, H. Rème, A. Balogh, Spatial scale of high-speed flows in the plasma sheet observed by Cluster. Geophys. Res. Lett. **31**, L09804 (2004). doi:10.1029/2004GL019558

N.F. Ness, The Earth's magnetic tail. J. Geophys. Res. **70**(13), 2989–3005 (1965). doi:10.1029/JZ070i013p02989

N. Ness, Magnetic fields of Mercury, Mars, and Moon. Annu. Rev. Earth Planet. Sci. **7**, 249–288 (1979)

N.F. Ness, K.W. Behannon, R.P. Lepping, Y.C. Whang, K.H. Schatten, Magnetic field observations near Mercury: preliminary results from Mariner 10. Science **185**, 151–160 (1974)

N.F. Ness, K.W. Behannon, L.F. Burlaga, Configuration of Jupiter's magnetic tail and equatorial current sheet. Adv. Space Res. **1**, 225 (1981)

P.T. Newell, Reconsidering the inverted-V particle signature: relative frequency of large-scale electron acceleration events. J. Geophys. Res. **105**, 15779–15794 (2000). doi:10.1029/1999JA000051

P.T. Newell, K. Liou, Solar wind driving and substorm triggering. J. Geophys. Res. **116**, A03229 (2011). doi:10.1029/2010JA016139

J.D. Nichols, S.W.H. Cowley, D.J. McComas, Magnetopause reconnection rate estimates for Jupiter's magnetosphere based on interplanetary measurements at ∼5 AU. Ann. Geophys. **24**, 393–406 (2006)

J.D. Nichols et al., Dynamic auroral storms on Saturn as observed by the Hubble Space Telescope. Geophys. Res. Lett. **41** (2014). doi:10.1002/2014GL060186

A. Nishida, T. Mukai, T. Yamamoto, S. Kokubun, K. Maezawa, A unified model of the magnetotail convection in geomagnetically quiet and active times. J. Geophys. Res. **103**, 4409–4418 (1998)

Y. Nishimura, L. Lyons, S. Zou, V. Angelopoulos, S. Mende, Substorm triggering by new plasma intrusion: THEMIS all-sky imager observations. J. Geophys. Res. **115**, A07222 (2010). doi:10.1029/2009JA015166

M.N. Nishino, H. Hasegawa, M. Fujimoto, Y. Saito, T. Mukai, I. Dandouras, H. Rème, A. Retinò, R. Nakamura, E. Lucek, S.J. Schwartz, A case study of Kelvin-Helmholtz vortices on both flanks of the Earth's magnetotail. Planet. Space Sci. **59**, 502–509 (2011). doi:10.1016/j.pss.2010.03.011

M. Nosé, A.T.Y. Lui, S. Ohtani, B.H. Mauk, R.W. McEntire, D.J. Williams, T. Mukai, K. Yumoto, Acceleration of oxygen ions of ionospheric origin in the near-Earth magnetotail during substorms. J. Geophys. Res. **105**(A4), 7669–7677 (2000a). doi:10.1029/1999JA000318

M. Nosé, S. Ohtani, A.T.Y. Lui, S.P. Christon, R.W. McEntire, D.J. Williams, T. Mukai, Y. Saito, K. Yumoto, Change of energetic ion composition in the plasma sheet during substorms. J. Geophys. Res. **105**(A10), 23277–23286 (2000b). doi:10.1029/2000JA000129

K. Nykyri, A. Otto, Plasma transport at the magnetospheric boundary due to reconnection in Kelvin-Helmholtz vortices. Geophys. Res. Lett. **28**(18), 3565–3568 (2001). doi:10.1029/2001GL013239

K. Nykyri, A. Otto, B. Lavraud, C. Mouikis, L.M. Kistler, A. Balogh, H. Rème, Cluster observations of reconnection due to the Kelvin-Helmholtz instability at the dawnside magnetospheric flank. Ann. Geophys. **24**, 2619–2643 (2006)

K.W. Ogilvie et al., Observations at Mercury encounter by the plasma science instrument on Mariner 10. Science **185**, 145–150 (1974)

K.W. Ogilvie, J.D. Scudder, V.M. Vasyliunas, R.E. Hartle, G.L. Siscoe, Observations at the planet Mercury by the plasma electron experiment—Mariner 10. J. Geophys. Res. **82**, 1807–1824 (1977). doi:10.1029/JA082i013p01807

S. Ohtani, M.A. Shay, T. Mukai, Temporal structure of the fast convective flow in the plasma sheet: comparison between observations and two-fluid simulations. J. Geophys. Res. **109**(A18), A03210 (2004). doi:10.1029/2003JA010002

M. Oieroset et al., THEMIS multi-spacecraft observations of magnetosheath plasma penetration deep into the dayside low-latitude magnetosphere for northward and strong B_y IMF. Geophys. Res. Lett. **35**(17), L17S11 (2008)

E.N. Parker, Interaction of the solar wind with the geomagnetic field. Phys. Fluids **1**, 171 (1958a). doi:10.1063/1.1724339

E.N. Parker, Dynamics of the interplanetary magnetic field. Astrophys. J. **128**, 664 (1958b)

G.K. Parks, J.R. Winckler, Acceleration of energetic electrons observed at the synchronous altitude during magnetospheric substorms. J. Geophys. Res. **73**, 5786 (1968)

G.K. Parks, M. McCarthy, R.J. Fitzenreiter, K.W. Ogilvie, J. Etcheto, K.A. Anderson, R.P. Lin, R.R. Anderson, T.E. Eastman, L.A. Frank, Particle and field characteristics of the high-latitude plasma sheet boundary layer. J. Geophys. Res. **89**, 8885–8906 (1984). doi:10.1029/JA089iA10p08885

A.A. Petrukovich, A.V. Artemyev, H.V. Malova, V.Y. Popov, R. Nakamura, L.M. Zelenyi, Embedded current sheets in the Earth's magnetotail. J. Geophys. Res. **116**, A00I25 (2011). doi:10.1029/2010JA015749

J.H. Piddington, Geomagnetic storm theory. J. Geophys. Res. **65**(1), 93–106 (1960). doi:10.1029/JZ065i001p00093

C.J. Pollock et al., The role and contributions of energetic neutral atom (ENA) imaging in magnetospheric substorm research. Space Sci. Rev. **109**, 155–182 (2003)

J.D.H. Pontius, R.A. Wolf, Transient flux tubes in the terrestrial magnetosphere. Geophys. Res. Lett. **17**, 49–52 (1990)

T.I. Pulkkinen, D.N. Baker, C.J. Owen, J.T. Gosling, N. Murphy, Thin current sheets in the deep geomagnetic tail. Geophys. Res. Lett. **20**, 2427 (1993)

A. Radioti, J. Woch, E.A. Kronberg, N. Krupp, A. Lagg, K.-H. Glassmeier, M.K. Dougherty, Energetic ion composition during reconfiguration events in the Jovian magnetotail. J. Geophys. Res. **112**, A06221 (2007). doi:10.1029/2006JA012047

A. Radioti, D. Grodent, J.-C. Gérard, B. Bonfond, J.T. Clarke, Auroral polar dawn spots: signatures of internally driven reconnection processes at Jupiter's magnetotail. Geophys. Res. Lett. **35**, L03104 (2008). doi:10.1029/2007GL032460

A. Radioti, D. Grodent, J.-C. Gérard, B. Bonfond, Auroral signatures of flow bursts released during magnetotail reconnection at Jupiter. J. Geophys. Res. **115**, A07214 (2010). doi:10.1029/2009JA014844

A. Radioti, D. Grodent, J.-C. Gérard, M.F. Vogt, M. Lystrup, B. Bonfond, Nightside reconnection at Jupiter: auroral and magnetic field observations from 26 July 1998. J. Geophys. Res. **116**, A03221 (2011). doi:10.1029/2010JA016200

A. Radioti, E. Roussos, D. Grodent, J.-C. Gérard, N. Krupp, D.G. Mitchell, J. Gustin, B. Bonfond, W. Pryor, Signatures of magnetospheric injections in Saturn's aurora. J. Geophys. Res. Space Sci. **118**, 1922–1933 (2013). doi:10.1002/jgra.50161

J.M. Raines, D. Schriver, S.C. Solomon, R.D. Starr, P. Trávníček, T.H. Zurbuchen, Mercury's magnetosphere after MESSENGER's first flyby. Science **321**, 85–89 (2008). doi:10.1126/science.1159040

J.M. Raines, J.A. Slavin, T.H. Zurbuchen, G. Gloeckler, B.J. Anderson, D.N. Baker, H. Korth, S.M. Krimigis, R.L. McNutt Jr., MESSENGER observations of the plasma environment near Mercury. Planet. Space Sci. **59**, 2004–2015 (2011). doi:10.1016/j.pss.2011.02.004

A. Raj, T. Phan, R.P. Lin, V. Angelopoulos, Wind survey of high-speed bulk flows and field-aligned beams in the near-Earth plasma sheet. J. Geophys. Res. **107**(A12), 1419 (2002). doi:10.1029/2001JA007547

L.C. Ray, Y.-J. Su, R.E. Ergun, P.A. Delamere, F. Bagenal, Current-voltage relation of a centrifugally confined plasma. J. Geophys. Res. **114**, A04214 (2009). doi:10.1029/2008JA013969

P.H. Reiff, J.L. Burch, T.W. Hill, Solar wind plasma injection at the dayside magnetospheric cusp. J. Geophys. Res. **82**, 479–491 (1977). doi:10.1029/JA082i004p00479

P.H. Reiff, R.W. Spiro, T.W. Hill, Dependence of polar cap potential drop on interplanetary parameters. J. Geophys. Res. **86**, 7639–7648 (1981)

E.C. Roelof, D.G. Sibeck, Magnetopause shape as a bivariate function of interplanetary magnetic field B_z and solar wind dynamic pressure. J. Geophys. Res. **98**(A12), 21421–21450 (1993). doi:10.1029/93JA02362

E.C. Roelof et al., Energetic neutral atom image of a storm-time ring current. Geophys. Res. Lett. **14**, 652–655 (1997)

H. Rosenbauer, H. Gruenwaldt, M.D. Montgomery, G. Paschmann, N. Sckopke, Heos 2 plasma observations in the distant polar magnetosphere—the plasma mantle. J. Geophys. Res. **80**, 2723–2737 (1975). doi:10.1029/JA080i019p02723

A. Runov, R. Nakamura, W. Baumjohann, T.L. Zhang, M. Volwerk, H.-U. Eichelberger, A. Balogh, Cluster observation of a bifurcated current sheet. Geophys. Res. Lett. **30**, 1036 (2003a)

A. Runov et al., Current sheet structure near magnetic X-line observed by Cluster. Geophys. Res. Lett. **30**(11), 1579 (2003b). doi:10.1029/2002GL016730

A. Runov, V.A. Sergeev, R. Nakamura, W. Baumjohann, T.L. Zhang, Y. Asano, M. Volwerk, Z. Vörös, A. Balogh, H. Rème, Reconstruction of the magnetotail current sheet structure using multi-point Cluster measurements. Planet. Space Sci. **53**, 237–243 (2005a)

A. Runov, V.A. Sergeev, W. Baumjohann, R. Nakamura, S. Apatenkov, Y. Asano, M. Volwerk, Z. Voros, T.L. Zhang, A. Petrukovich, A. Balogh, J.-A. Sauvaud, B. Klecker, H. Reme, Electric current and magnetic field geometry in flapping magnetotail current sheets. Ann. Geophys. **23**, 1391–1403 (2005b)

A. Runov, V. Angelopoulos, M.I. Sitnov, V.A. Sergeev, J. Bonnell, J.P. McFadden, D. Larson, K.-H. Glassmeier, U. Auster, THEMIS observations of an earthward-propagating dipolarization front. Geophys. Res. Lett. **36**, L14106 (2009). doi:10.1029/2009GL038980

A. Runov et al., Dipolarization fronts in the magnetotail plasma sheet. Planet. Space Sci. **59**, 517 (2010)

A. Runov, V. Angelopoulos, X.-Z. Zhou, X.-J. Zhang, S. Li, F. Plaschke, J. Bonnell, A THEMIS multicase study of dipolarization fronts in the magnetotail plasma sheet. J. Geophys. Res. **116**(A15), A05216 (2011). doi:10.1029/2010JA016316

C.T. Russell, The dynamics of planetary magnetospheres. Planet. Space Sci. **49** (2001). doi:10.1016/S0032-0633(01)00017-4

C.T. Russell, K.I. Brody, Some remarks on the position and shape of the neutral sheet. J. Geophys. Res. **72**(23), 6104–6106 (1967). doi:10.1029/JZ072i023p06104

C.T. Russell, D.N. Baker, J.A. Slavin, The magnetosphere of Mercury, in *Mercury*, ed. by F. Vilas, C.R. Chapman, M.S. Matthews (Univ. of Arizona Press, Tucson, 1988), pp. 514–561

C.T. Russell, C.M. Jackman, H.Y. Wei, C. Bertucci, M.K. Dougherty, Titan's influence on Saturnian substorm occurrence. Geophys. Res. Lett. **35**, L12105 (2008). doi:10.1029/2008GL034080

D.V. Sarafopoulos, E.T. Sarris, V. Angelopoulos, T. Yamamoto, S. Kokubun, Spatial structure of the plasma sheet boundary layer at distances greater than 180 R_E as derived from energetic particle measurements on GEOTAIL. Ann. Geophys. **15**, 1246–1256 (1997). doi:10.1007/s00585-997-1246-0

F.L. Scarf, I.M. Green, G.L. Siscoe, D.S. Intriligator, D.D. McKibbin, J.H. Wolfe, Pioneer 8 electric field measurements in the distant geomagnetic tail. J. Geophys. Res. **75**(16), 3167–3179 (1970). doi:10.1029/JA075i016p03167

F.L. Scarf, D.A. Gurnett, W.S. Kurth, R.L. Poynter, Voyager 2 plasma wave observations at Saturn. Science **215**, 587 (1982)

K. Schindler, A selfconsistent theory of the tail of the magnetosphere, in *Earth's Magnetospheric Processes*, ed. by B.M. McCormac (D. Reidel, Dordrecht, 1972), p. 200

K. Schindler, A theory of the substorm mechanism. J. Geophys. Res. **79**, 2803 (1974)

K. Schindler, J. Birn, Models of two-dimensional embedded thin current sheets from Vlasov theory. J. Geophys. Res. **107**(A8), 1193 (2002). doi:10.1029/2001JA000304

D. Schmid, M. Volwerk, R. Nakamura, W. Baumjohann, M. Heyn, A statistical and event study of magnetotail dipolarization fronts. Ann. Geophys. **29**(9), 1537–1547 (2011). doi:10.5194/angeo-29-1537-2011

N. Sckopke, G. Paschmann, The plasma mantle. A survey of magnetotail boundary layer observations. J. Atmos. Terr. Phys. **40**(3), 261–278 (1978). doi:10.1016/0021-9169(78)90044-2

J.D. Scudder, E.C. Sittler Jr., H.S. Bridge, A survey of the plasma electron environment of Jupiter: a view from Voyager. J. Geophys. Res. **86**(A10), 8157–8179 (1981). doi:10.1029/JA086iA10p08157

L. Scurry, C.T. Russell, Proxy studies of energy transfer to the magnetosphere. J. Geophys. Res. **96**, 9541–9548 (1991)

K. Seki, T. Terasawa, M. Hirahara, T. Mukai, Quantification of tailward cold O^+ beams in the lobe/mantle regions with geotail data: constraints on polar O^+ outflows. J. Geophys. Res. **103**, 29371–29382 (1998). doi:10.1029/98JA02463

V.A. Sergeev, D.G. Mitchell, C.T. Russel, D.J. Williams, Structure of the tail plasma/current sheet at 11 R_E and its changes in the course of a substorm. J. Geophys. Res. **98**, 17345–17365 (1993)

V.A. Sergeev, T.I. Pulkkinen, R.J. Pellinen, Coupled-mode scenario for the magnetospheric dynamics. J. Geophys. Res. **101**, 13047–13065 (1996a)

V.A. Sergeev, V. Angelopoulos, J.T. Gosling, C.A. Cattell, C.T. Russell, Detection of localized, plasma-depleted flux tubes or bubbles in the midtail plasma sheet. J. Geophys. Res. **101**, 10817–10826 (1996b). doi:10.1029/96JA00460

V. Sergeev, V. Angelopoulos, C. Carlson, P. Sutcliffe, Current sheet measurements within a flapping plasma sheet. J. Geophys. Res. **103**, 9177–9188 (1998)

V.A. Sergeev, K. Liou, C.-I. Meng, P.T. Newell, M. Brittnacher, G. Parks, G.D. Reeves, Development of auroral streamers in association with localized impulsive injections to the inner magnetotail. Geophys. Res. Lett. **26**(3), 417–420 (1999). doi:10.1029/1998GL900311

V. Sergeev, A. Runov, W. Baumjohann, R. Nakamura, T.L. Zhang, M. Volwerk, A. Balogh, H. Reme, J.A. Sauvaud, M. Andre, B. Klecker, Current sheet flapping motion and structure observed by Cluster. Geophys. Res. Lett. **30**, 1327 (2003)

V.A. Sergeev, V. Angelopoulos, S. Apatenkov, J. Bonnell, R. Ergun, R. Nakamura, J. McFadden, D. Larson, A. Runov, Kinetic structure of the sharp injection/dipolarization front in the flow-braking region. Geophys. Res. Lett. **36**, L21105 (2009). doi:10.1029/2009GL040658

V. Sergeev, Y. Nishimura, M. Kubyshkina, V. Angelopoulos, R. Nakamura, H. Singer, Magnetospheric location of the equatorward prebreakup arc. J. Geophys. Res. **117**, A01212 (2012a). doi:10.1029/2011JA017154

V.A. Sergeev, V. Angelopoulos, R. Nakamura, Recent advances in understanding substorm dynamics. Geophys. Res. Lett. **39**, L05101 (2012b). doi:10.1029/2012GL050859

S. Sharma, R. Nakamura, A. Runov, E.E. Grigorenko, H. Hasegawa, M. Hoshino, P. Louarn, C.J. Owen, A. Peturkovich, J.-A. Sauvaud, V.S. Semenov, V.A. Sergeev, J.A. Slavin, B.U.O. Sonnerup, L.M. Zelenyi, G. Fruit, S. Haaland, H. Malova, K. Snekvik, Transient and localized processes in the magnetotail: a review. Ann. Geophys. **26**, 955–1006 (2008)

J.K. Shi, Z.W. Cheng, T.L. Zhang, M. Dunlop, Z.X. Liu, K. Torkar, A. Fazakerley, E. Lucek, H. Rème, I. Dandouras, A.T.Y. Lui, Z.Y. Pu, A.P. Walsh, M. Volwerk, A.D. Lahiff, M.G.G.T. Taylor, A. Grocott, L.M. Kistler, M. Lester, C. Mouikis, C. Shen, South-north asymmetry of field-aligned currents in the magnetotail observed by Cluster. J. Geophys. Res. **115**(A14), A07228 (2010). doi:10.1029/2009JA014446

J.H. Shue, J.K. Chao, H.C. Fu, C.T. Russell, P. Song, K.K. Khurana, H.J. Singer, A new functional form to study the solar wind control of the magnetopause size and shape. J. Geophys. Res. **102**(A5), 9497–9511 (1997)

D.G. Sibeck, G.L. Siscoe, J.A. Slavin, E.J. Smith, S.J. Bame, F.L. Scarf, Magnetotail flux ropes. Geophys. Res. Lett. **11**, 1090 (1984)

D.G. Sibeck, R.E. Lopez, E.C. Roelof, Solar wind control of the magnetopause shape, location, and motion. J. Geophys. Res. **96**(A4), 5489–5495 (1991). doi:10.1029/90JA02464

S. Simon, A. Wennmacher, F.M. Neubauer, C.L. Bertucci, H. Kriegel, J. Saur, C.T. Russell, M.K. Dougherty, Titan's highly dynamic magnetic environment: a systematic survey of Cassini magnetometer observations from flybys TA-T62. Planet. Space Sci. **58**, 1230–1251 (2010). doi:10.1016/j.pss.2010.04.021

G. Siscoe, L. Christopher, Variations in the solar wind stand-off distance at Mercury. Geophys. Res. Lett. **2**, 158 (1975)

G.L. Siscoe, T.S. Huang, Polar cap inflation and deflation. J. Geophys. Res. **90**, 543–547 (1985). doi:10.1029/JA090iA01p00543

G.L. Siscoe, N.F. Ness, C.M. Yeates, Substorms on Mercury? J. Geophys. Res. **80**(31), 4359–4363 (1975). doi:10.1029/JA080i031p04359

G.L. Siscoe, N.U. Crooker, K.D. Siebert, Transpolar potential saturation: roles of region 1 current system and solar wind ram pressure. J. Geophys. Res. **107**(A10), 1321 (2002). doi:10.1029/2001JA009176

G. Siscoe, J. Raeder, A.J. Ridley, Transpolar potential saturation models compared. J. Geophys. Res. **109**, A09203 (2004). doi:10.1029/2003JA010318

M.I. Sitnov, L.M. Zelenyi, H.V. Malova, A.S. Sharma, Thin current sheet embedded within a thicker plasma sheet: self-consistent kinetic theory. J. Geophys. Res. **105**(A6), 13029–13043 (2000). doi:10.1029/1999JA000431

M.I. Sitnov, P.N. Guzdar, M. Swisdak, On the formation of a plasma bubble. Geophys. Res. Lett. **32**, L16103 (2005). doi:10.1029/2005GL023585

M.I. Sitnov, M. Swisdak, A.V. Divin, Dipolarization fronts as a signature of transient reconnection in the magnetotail. J. Geophys. Res. **114**(A13), A04202 (2009). doi:10.1029/2008JA013980

J.A. Slavin, Mercury's magnetosphere, comparative magnetospheres. Adv. Space Res. **33**(11), 1859–1874 (2004), ed. by X. Blanco-Cano, C.T. Russell

J.A. Slavin, B.T. Tsurutani, E.J. Smith, D.E. Jones, D.G. Sibeck, Average configuration of the distant (<220 R_e) magnetotail: initial ISEE-3 magnetic field results. Geophys. Res. Lett. **10**(10), 973–976 (1983). doi:10.1029/GL010i010p00973

J.A. Slavin, E.J. Smith, B.T. Thomas, Large scale temporal and radial gradients in the IMF: Helios 1, 2, ISEE-3, and Pioneer 10, 11. Geophys. Res. Lett. **11**, 279 (1984a)

J.A. Slavin, E.J. Smith, B.T. Tsurutani, D.G. Sibeck, H.J. Singer, D.N. Baker, J.T. Gosling, E.W. Hones Jr., F.L. Scarf, Substorm-associated traveling compression regions in the distant tail: ISEE 3 geotail observations. Geophys. Res. Lett. **11**, 657 (1984b)

J.A. Slavin, E.J. Smith, J.R. Spreiter, S.S. Stahara, Solar wind flow about the outer planets: gas dynamic modeling of the Jupiter and Saturn bow shocks. J. Geophys. Res. **90**(A7), 6275–6286 (1985a)

J.A. Slavin, E.J. Smith, D.G. Sibeck, D.N. Baker, R.D. Zwickl, S.-I. Akasofu, An ISEE-3 study of average and substorm conditions in the distant magnetotail. J. Geophys. Res. **90**, 10875 (1985b)

J.A. Slavin et al., CDAW-8 observations of plasmoid signatures in the geomagnetic tail: an assessment. J. Geophys. Res. **94**, 15153 (1989)

J.A. Slavin, M.F. Smith, E.L. Mazur, D.N. Baker, E.W. Hones Jr., T. Iyemori, E.W. Greenstadt, ISEE 3 observations of traveling compression regions in the Earth's magnetotail. J. Geophys. Res. **98**(A9), 15425–15446 (1993). doi:10.1029/93JA01467

J.A. Slavin, C.J. Owen, M.M. Kuznetsova, M. Hesse, ISEE 3 observations of plasmoids with flux rope magnetic topologies. Geophys. Res. Lett. **22**(15), 2061–2064 (1995)

J.A. Slavin, R.P. Lepping, J. Gjerloev, D.H. Fairfield, M. Hesse, C.J. Owen, M.B. Moldwin, T. Nagai, A. Ieda, T. Mukai, Geotail observations of magnetic flux ropes in the plasma sheet. J. Geophys. Res. **108**(A1), 1015 (2003). doi:10.1029/2002JA009557

J.A. Slavin, E.I. Tanskanen, M. Hesse, C.J. Owen, M.W. Dunlop, S. Imber, E.A. Lucek, A. Balogh, K.-H. Glassmeier, Cluster observations of traveling compression regions in the near-tail. J. Geophys. Res. **110**, A06207 (2005). doi:10.1029/2004JA010878

J.A. Slavin, S.M. Krimigis, M.H. Acuña, B.J. Anderson, D.N. Baker, P.L. Koehn, H. Korth, S. Livi, B.H. Mauk, S.C. Solomon, T.H. Zurbuchen, MESSENGER: exploring Mercury's magnetosphere. Space. Sci. Rev. (2007). doi:10.1007/s11214-007-9154-x

J.A. Slavin, M.H. Acuna, B.J. Anderson, D.N. Baker, M. Benna, G. Gloeckler, R.E. Gold, G.C. Ho, R.M. Killen, H. Korth, S.M. Krimigis, R.L. McNutt Jr., L.R. Nittler, J.M. Slavin et al., MESSENGER observations of magnetic reconnection in Mercury's magnetosphere. Science **324**, 606–610 (2009). doi:10.1126/science.1172011

J.A. Slavin et al., MESSENGER observations of extreme loading and unloading of Mercury's magnetic tail. Science **329**, 665–668 (2010). doi:10.1126/science.1188067

J.A. Slavin et al., MESSENGER and Mariner 10 flyby observations of magnetotail structure and dynamics at Mercury. J. Geophys. Res. **117**, A01215 (2012a). doi:10.1029/2011JA016900

J.A. Slavin, S.M. Imber, G.A. DiBraccio, T. Sundberg, S.A. Boardsen, B.J. Anderson, H. Korth, D.N. Baker, R.L. McNutt, S.C. Solomon, MESSENGER observations of magnetotail dynamics at Mercury. Geophys. Res. Abstr. **14**, EGU2012-3817-3 (2012b)

E.J. Smith, Radial gradients in the interplanetary magnetic field between 1.0 and 4.3 AU: Pioneer 10, in *Solar Wind Three*, ed. by C.T. Russell (University of California Press, Los Angeles, 1974)

K. Snekvik, S. Haaland, N. Østgaard, H. Hasegawa, R. Nakamura, T. Takada, L. Juusola, O. Amm, F. Pitout, H. Rème, B. Klecker, E.A. Lucek, Cluster observations of a field aligned current at the dawn flank of a bursty bulk flow. Ann. Geophys. **25**(6), 1405–1415 (2007). doi:10.5194/angeo-25-1405-2007

K. Snekvik, E. Tanskanen, N. Østgaard, L. Juusola, K. Laundal, E.I. Gordeev, A.L. Borg, Changes in the magnetotail configuration before near-Earth reconnection. J. Geophys. Res. **117**, A02219 (2012). doi:10.1029/2011JA017040

S.C. Solomon et al., The MESSENGER mission to Mercury: scientific objectives and implementation. Planet. Space Sci. **49**, 1445–1465 (2001). doi:10.1016/S0032-0633(01)00085-X

D.J. Southwood, M.G. Kivelson, Magnetospheric interchange instability. J. Geophys. Res. **92**(A1), 109–116 (1987). doi:10.1029/JA092iA01p00109

D.J. Southwood, M.G. Kivelson, Magnetospheric interchange motions. J. Geophys. Res. **94**(A1), 299–308 (1989). doi:10.1029/JA094iA01p00299

T.W. Speiser, Particle trajectories in model current sheets: 1. Analytical solutions. J. Geophys. Res. **70**, 4219–4226 (1965)

T.S. Stallard, S. Miller, S.W.H. Cowley, E.J. Bunce, Jupiter's polar ionospheric flows: measured intensity and velocity variations poleward of the main auroral oval. Geophys. Res. Lett. **30**(5), 1221 (2003). doi:10.1029/2002GL016031

Š. Štverák, M. Maksimovic, P.M. Trávníček, E. Marsch, A.N. Fazakerley, E.E. Scime, Radial evolution of nonthermal electron populations in the low-latitude solar wind: Helios, Cluster, and Ulysses observations. J. Geophys. Res. **114**, A05104 (2009). doi:10.1029/2008JA013883

T. Sundberg, S.A. Boardsen, J.A. Slavin, B.J. Anderson, H. Korth, T.H. Zurbuchen, J.M. Raines, S.C. Solomon, MESSENGER orbital observations of large-amplitude Kelvin-Helmholtz waves at Mercury's magnetopause. J. Geophys. Res. **117**, A04216 (2012a). doi:10.1029/2011JA017268

T. Sundberg et al., MESSENGER observations of dipolarization events in Mercury's magnetotail. J. Geophys. Res. **117**, A00M03 (2012b). doi:10.1029/2012JA017756

W.-L. Teh, R. Nakamura, H. Karimabadi, W. Baumjohann, T.L. Zhang, Correlation of core field polarity of magnetotail flux ropes with the IMF B_y: reconnection guide field dependency. J. Geophys. Res. **119**, 2933–2944 (2014). doi:10.1002/2013JA019454

N. Thomas, F. Bagenal, T.W. Hill, J.K. Wilson, The Io neutral clouds and plasma torus, in *Jupiter: Planet, Satellites, Magnetosphere*, ed. by Bagenal, Dowling, McKinnon (Cambridge University Press, Cambridge, 2004)

M.F. Thomsen, R.J. Wilson, R.L. Tokar, D.B. Reisenfeld, C.M. Jackman, Cassini/CAPS observations of duskside tail dynamics at Saturn. J. Geophys. Res. **118**, 5767–5781 (2013). doi:10.1002/jgra.50552

P.M. Travnicek et al., Mercury's magnetosphere-solar wind interaction for northward and southward interplanetary magnetic field: hybrid simulation results. Icarus **209**(1), 11–22 (2010). doi:10.1016/j.icarus.2010.01.008

N.A. Tsyganenko, D.H. Fairfield, Global shape of the magnetotail current sheet as derived from geotail and polar data. J. Geophys. Res. **109**, A03218 (2004). doi:10.1029/2003JA010062

V.M. Vasyliunas, Plasma distribution and flow, in *Physics of the Jovian Magnetosphere*, ed. by A.J. Dessler (Cambridge Univ. Press, Cambridge, 1983), pp. 395–453

M.F. Vogt, M.G. Kivelson, K.K. Khurana, S.P. Joy, R.J. Walker, Reconnection and flows in the Jovian magnetotail as inferred from magnetometer observations. J. Geophys. Res. **115**, A06219 (2010). doi:10.1029/2009JA015098

M.F. Vogt, M.G. Kivelson, K.K. Khurana, R.J. Walker, B. Bonfond, D. Grodent, A. Radioti, Improved mapping of Jupiter's auroral features to magnetospheric sources. J. Geophys. Res. **116**, A03220 (2011). doi:10.1029/2010JA016148

M.F. Vogt, C.M. Jackman, J.A. Slavin, E.J. Bunce, S.W.H. Cowley, M.G. Kivelson, K.K. Khurana, Structure and statistical properties of plasmoids in Jupiter's magnetotail. J. Geophys. Res. **119**, 821–843 (2014). doi:10.1002/2013JA019393

M. Volwerk, J. Berchem, Y.V. Bogdanova, O.D. Constantinescu, M.W. Dunlop, J.P. Eastwood, P. Escoubet, A.N. Fazakerley, H. Frey, H. Hasegawa, B. Lavraud, E.V. Panov, C. Shen, J.K. Shi, M.G.G.T. Taylor, J. Wang, J.A. Wild, Q.H. Zhang, O. Amm, J.M. Weygand, Interplanetary magnetic field rotations followed from L1 to the ground: the response of the Earth's magnetosphere as seen by multi-spacecraft and ground-based observations. Ann. Geophys. **29**, 1549–1569 (2011)

M. Volwerk, N. André, C.S. Arridge, C.M. Jackman, X. Jia, S.E. Milan, A. Radioti, M.F. Vogt, A.P. Walsh, R. Nakamura, A. Masters, C. Forsyth, Comparative magnetotail flapping: an overview of selected events at Earth, Jupiter and Saturn. Ann. Geophys. **31**, 817–833 (2013). doi:10.5194/angeo-31-817-2013

G.R. Voots, D.A. Gurnett, S.-I. Akasofu, Auroral kilometric radiation as an indicator of auroral magnetic disturbances. J. Geophys. Res. **82**, 2259–2266 (1977)

A.P. Walsh, C. Forsyth, Cluster observations of plasma bubbles, BBFs and their wakes, in *The Dynamic Magnetosphere*, ed. by W. Liu, M. Fujimoto. IAGA Special Sopron Book Series, vol. 3 (Springer, Dordrecht, 2011), pp. 117–124. doi:10.1007/978-94-007-0501-2_6

A.P. Walsh, A.N. Fazakerley, A.D. Lahiff, M. Volwerk, A. Grocott, M. Dunlop, T. Lui, L. Kistler, M. Lester, C. Mouikis, Z. Pu, C. Shen, J. Shi, M.G. Taylor, E. Lucek, T.L. Zhang, I. Dandouras, Cluster and Double Star multipoint observations of a plasma bubble. Ann. Geophys. **27**, 725–743 (2009). doi:10.5194/angeo-27-725-2009

A.P. Walsh, A.N. Fazakerley, C. Forsyth, C.J. Owen, M.G.G.T. Taylor, I.J. Rae, Sources of electron pitch angle anisotropy in the magnetotail plasma sheet. J. Geophys. Res. **118** (2013a). doi:10.1002/jgra.50553

A.P. Walsh, C.S. Arridge, A. Masters, G.R. Lewis, A.N. Fazakerley, G.H. Jones, C.J. Owen, A.J. Coates, An indication of the existence of a solar wind strahl at 10 AU. Geophys. Res. Lett. **40**, 2495–2499 (2013b). doi:10.1002/grl.50529

Y.C. Wang, J. Mueller, U. Motschmann, W.H. Ip, A hybrid simulation of Mercury's magnetosphere for the MESSENGER encounters in year 2008. Icarus **209**(1), 46–52 (2010). doi:10.1016/j.icarus.2010.05.020

H. Wiechen, K. Schindler, Quasi-static theory of the Earth's magnetotail, including the far tail. J. Geophys. Res. **93**, 5922 (1988)

S. Wing, J.R. Johnson, P.T. Newell, C.-I. Meng, Dawn-dusk asymmetries, ion spectra, and sources in the northward interplanetary magnetic field plasma sheet. J. Geophys. Res. **110**, A08205 (2005). doi:10.1029/2005JA011086

R.M. Winglee, E.M. Harnett, A. Kidder, D. Snowden, Supplying the Io plasma torus: local versus extended plasma sources, Fall AGU Abstract SM11C-03, 2009

J.D. Winningham, W.J. Heikkila, Polar cap auroral electron fluxes observed with Isis 1. J. Geophys. Res. **79**, 949–957 (1974). doi:10.1029/JA079i007p00949

R.M. Winslow, B.J. Anderson, C.L. Johnson, J.A. Slavin, H. Korth, M.E. Purucker, D.N. Baker, S.C. Solomon, Mercury's magnetopause and bow shock from MESSENGER magnetometer observations. J. Geophys. Res. **118**, 2213–2227 (2013). doi:10.1002/jgra.50237

J. Woch, N. Krupp, A. Lagg, Particle bursts in the Jovian magnetosphere: evidence for a near-Jupiter neutral line. Geophys. Res. Lett. **29**(7), 1138 (2002). doi:10.1029/2001GL014080

R.A. Wolf, Y. Wan, X. Xing, J.-C. Zhang, S. Sazykin, Entropy and plasma sheet transport. J. Geophys. Res. **114**(A13), A00D05 (2009). doi:10.1029/2009JA014044

R.A. Wolf, C.X. Chen, F.R. Toffoletto, Thin filament simulations for Earth's plasma sheet: interchange oscillations. J. Geophys. Res. **117**(A16), A02215 (2012a). doi:10.1029/2011JA016971

R.A. Wolf, C.X. Chen, F.R. Toffoletto, Thin filament simulations for Earth's plasma sheet: tests of validity of the quasi-static convection approximation. J. Geophys. Res. **117**(A16), A02216 (2012b). doi:10.1029/2011JA016972

C.S. Wu, L.C. Lee, A theory of the terrestrial kilometric radiations. Astrophys. J. **230**, 621–626 (1979)

J.R. Wygant, R.B. Torbert, F.S. Mozer, Comparison of S3-3 polar cap potential with the interplanetary magnetic field and models of magnetospheric reconnection. J. Geophys. Res. **88**, 5727–5735 (1983)

J.N. Yates, N. Achilleos, P. Guio, Response of the Jovian thermosphere to a transient 'pulse' in solar wind pressure. Planet. Space Sci. **91**, 27–44 (2014). doi:10.1016/j.pss.2013.11.009

D. Young, Ion and neutral mass spectrometry, in *Encyclopedia of Planetary Sciences*, ed. by J.A. Shirley, R.W. Fairbridge (Van Nostrand Reinhold, New York, 1997a)

D. Young, Space plasma particle instrumentation and the new paradigm: faster, cheaper, better, in *Measurement Techniques in Space Plasmas: Particles*, ed. by D.T. Young, R.F. Pfaff, J.E. Borovsky. AGU Monograph, vol. 102 (American Geophysical Union, Washington, 1997b)

P. Zarka, Auroral radio emissions at the outer planets: observations and theories. J. Geophys. Res. **103**(E9), 20159–20194 (1998). doi:10.1029/98JE01323

P. Zarka, L. Lamy, B. Cecconi, R. Prangé, H.O. Rucker, Modulation of Saturn's radio clock by solar wind speed. Nature **450**, 265–267 (2007)

L.M. Zelenyi, H.V. Malova, V.Y. Popov, D. Delcourt, A.S. Sharma, Nonlinear equilibrium structure of thin currents sheets: influence of electron pressure anisotropy. Nonlinear Process. Geophys. **11**, 579–587 (2004)

E. Zesta, Y. Shi, E. Donovan, E. Spanswick, L.R. Lyons, V. Angelopoulos, J.P. McFadden, C.W. Carlson, H.-U. Auster, S. Mende, M.A. McCready, C.J. Heinselman, E. Kendall, R. Doe, Ionospheric convection signatures of tail fast flows during substorms and poleward boundary intensifications (PBI). Geophys. Res. Lett. **38**, L08105 (2011). doi:10.1029/2011GL046758

T.L. Zhang, W. Baumjohann, R. Nakamura, A. Balogh, K.-H. Glassmeier, A wavy twisted neutral sheet observed by Cluster. Geophys. Res. Lett. **29**, 1899 (2002). doi:10.1029/2002GL015544

T.L. Zhang, W. Baumjohann, R. Nakamura, A. Runov, M. Volwerk, Y. Asano, Z. Vörös, H.-U. Eichelberger, V. Sergeev, J.K. Shi, A. Balogh, A statistical survey of the magnetotail current sheet. Adv. Space Res. **38**, 1834–1837 (2006)

M. Zhou et al., Observation of waves near lower hybrid frequency in the reconnection region with thin current sheet. J. Geophys. Res. **114**, A02216 (2009). doi:10.1029/2008JA013427

X.-Z. Zhou, V. Angelopoulos, V.A. Sergeev, A. Runov, Accelerated ions ahead of earthward propagating dipolarization fronts. J. Geophys. Res. **115**(A14), A00I03 (2010). doi:10.1029/2010JA015481

X.-Z. Zhou, V. Angelopoulos, V.A. Sergeev, A. Runov, On the nature of precursor flows upstream of advancing dipolarization fronts. J. Geophys. Res. **116**(A15), A03222 (2011). doi:10.1029/2010JA016165

X.-Z. Zhou, V. Angelopoulos, A. Runov, J. Liu, Y.S. Ge, Emergence of the active magnetotail plasma sheet boundary from transient, localized ion acceleration. J. Geophys. Res. **117**, A10216 (2012). doi:10.1029/2012JA018171

B. Zieger, K.C. Hansen, T.I. Gombosi, D.L. DeZeeuw, Periodic plasma escape from the mass-loaded Kronian magnetosphere. J. Geophys. Res. **115** (2010). doi:10.1029/2009JA014951

T.H. Zurbuchen, J.M. Raines, G. Gloeckler, S.M. Krimigis, J.A. Slavin, P.L. Koehn, R.M. Killen, A.L. Sprague, R.L. McNutt Jr., S.C. Solomon, MESSENGER observations of the compositions of Mercury's ionized exosphere and plasma environment. Science **321**, 90–92 (2008)

T.H. Zurbuchen, J.M. Raines, J.A. Slavin, D.J. Gershman, J.A. Gilbert, G. Gloeckler, B.J. Anderson, D.N. Baker, H. Korth, S.M. Krimigis, M. Sarantos, D. Schriver, R.L. McNutt Jr., S.C. Solomon, MESSENGER observations of the spatial distribution of planetary ions near Mercury. Science **30**(333), 1862–1865 (2011). doi:10.1126/science.1211302